Research Report
KTC-99-16

Seismic Evaluation of the US41 Northbound Bridge over the Ohio River at Henderson, KY
(KYSPR 96-173)

by

Issam E. Harik
Professor of Civil Engineering and Head, Structures Section,
Kentucky Transportation Center

Chelliah Madasamy
Visiting Professor, Kentucky Transportation Center

Denglin Chen
Research Assistant, Dept. of Civil Engineering

K. Vasudevan
Visiting Professor, Kentucky Transportation Center

Leonong Zhou
Formerly Visiting Professor, Kentucky Transportation Center

Kevin Sutterer
Assistant Professor, Department of Civil Engineering

Ron Street
Assistant Professor, Department of Geological Sciences

and

David L. Allen
Transportation Engineer, Kentucky Transportation Center

Kentucky Transportation Center
College of Engineering, University of Kentucky

in cooperation with

Transportation Cabinet
Commonwealth of Kentucky

and

Federal Highway Administration
U.S. Department of Transportation

November 1999

Commonwealth of Kentucky
Transportation Cabinet
Frankfort, Kentucky 40622

James C. Codell, III
Secretary of Transportation

E. Jeffrey Mosley
Deputy Secretary

Paul E. Patton
Governor

December 20, 2000

Mr. Jose M. Sepulveda
Division Administrator
Federal Highway Administration
330 West Broadway
Frankfort, KY 40601

Subject:
- Implementation Statement for Final Report entitled "Seismic Evaluation of the US41 Northbound bridge over the Ohio River at Henderson, KY"
- Study number: KYSPR 96-173
- Study title: "Seismic Rating and Evaluation of Highway Structures"

Dear Mr. Sepulveda:

The objective of this study was to seismically evaluate the US41 Northbound bridge over the Ohio River at Henderson, KY for a projected 50-year earthquake event. The objective set forth has been achieved by conducting field-testing, computer modeling and dynamic analysis.

The results of this study show that the superstructure of the main bridge will withstand the 50-year earthquake event without any damage. All supports on the piers of the main bridge and thirteen out of forty-two supports having fixed bearings on both the approach spans require retrofit. This retrofit can be provided by additional anchor bolts in order to prevent shear failure of the existing anchor bolts, or by replacing those bearings with seismic isolation bearings.

Sincerely,

J. M. Yowell, P.E.
State Highway Engineer

JMY/JLC/dp

c: John Carr

Technical Report Documentation Page

1. Report No.	2. Government Accession No.	3. Recipient's Catalog No.
KTC-99-16		

4. Title and Subtitle

SEISMIC EVALUATION OF THE US41 NORTHBOUND BRIDGE OVER THE OHIO RIVER AT HENDERSON, KY

(KYSPR 96-173)

5. Report Date
November 1999

6. Performing Organization Code

7. Author(s): I.E. Harik, C.M. Madasamy, D. Chen, K. Vasudevan, L. Zhou, K. Sutterer, R. Street and D. Allen

8. Performing Organization Report No.
KTC-99-16

9. Performing Organization Name and Address

Kentucky Transportation Center
College of Engineering
University of Kentucky
Lexington, Kentucky 40506-0281

10. Work Unit No. (TRAIS)

11. Contract or Grant No.
KYSPR 96-173

13. Type of Report and Period Covered
Final

12. Sponsoring Agency Name and Address

Kentucky Transportation Cabinet
State Office Building
Frankfort, Kentucky 40622

14. Sponsoring Agency Code

15. Supplementary Notes

Prepared in cooperation with the Kentucky Transportation Cabinet and the U.S. Department of Transportation, Federal Highway Administration.

16. Abstract

This report presents the seismic evaluation of the US41 Northbound bridge over the Ohio River connecting Evansville, Indiana and Henderson, Kentucky. The main bridge is a four-span cantilever through-truss type. The approach bridge has 8 spans on the Evansville, IN side and 35 spans on the Henderson, KY side. Although this bridge has not yet been subjected to a moderate or major earthquake, it is situated within the influence of the New Madrid and Wabash Valley Seismic Zones.

The seismic evaluation program consisted of field testing and seismic response analysis. The modal properties of the main bridge were determined through field testing, and were used to calibrate a three dimensional finite element model. The finite element model was then subjected to time histories of the 50-year earthquake event. Stresses and displacements obtained were found to be within the acceptable limits. Analytical results indicate that the superstructure of the main bridge will survive the projected 50-year earthquake without any damage and no loss-of-span. However, all supports on the piers of the main bridge require additional anchor bolts or seismic isolation bearings.

The approach spans were analyzed using response spectrum method with simplified single-degree-of-freedom models. Thirteen out of forty-two supports having fixed bearings on both the Kentucky and Indiana approach spans require additional anchor bolts at the fixed bearings or seismic isolation bearings.

17. Key Words	18. Distribution Statement
Seismic Evaluation, Time-History, US41 Northbound Bridge, Field Testing, Finite Element Model, Response Spectra	Unlimited with approval of Kentucky Transportation Cabinet

19. Security Classif. (of this report)	20. Security Classif. (of this page)	21. No. of Pages	22. Price
Unclassified	Unclassified	152	

FormDOT 1700.7 (8-72)Reproduction of Completed Page Authorized

Executive Summary

Research Objectives

The main objective of this investigation is to assess the structural integrity of the Ohio River bridge (Figures E-1, E-3 and E-5) on US41 Northbound at Henderson, Kentucky, when subjected to a projected 50-year earthquake. The investigation considers both the main bridge and the approach spans. To achieve the objective, the scope of the work was divided into the following tasks: 1) Field testing of the main bridge; 2) Finite element modeling and calibration; 3)Time-history seismic response analysis; and 4) Seismic response of the approach bridges using the response spectrum method.

Background

The need for evaluating the seismic adequacy of the existing infrastructure has come into focus following the damage and collapse of numerous bridge structures due to the recent earthquakes. For example, the 1989 Loma Prieta earthquake and 1994 Northridge earthquake brought the seismic risk to bridges and elevated freeway structures to the attention of the public. In particular, the seismic rehabilitation of older bridges in regions of high seismicity, which were designed prior to the advent of modern seismic design codes, is a matter of growing concern. The US41 Northbound bridge at Henderson, Kentucky was built in according to earlier codes that had minimal provisions for earthquake loading.

Field Testing

The ambient vibration properties of the main bridge were determined through field testing under traffic- and wind-induced excitation. The purpose of measuring the ambient vibration properties was to determine the natural frequencies and their associated mode shapes. These vibration properties were subsequently used as the basis for calibrating the finite element model for seismic response analysis.

Finite Element Modeling

A three dimensional finite element model of the main bridge was used for free vibration and seismic response analyses. The model was calibrated by comparing the free vibration analysis results with the ambient vibration properties obtained from

field testing. After calibration, the model was used for seismic response analysis. The three dimensional model of the main bridge was subjected to the time histories of the projected 50-year earthquake to determine maximum displacements at joints, stresses in members, and forces on bearings.

Approach Spans

The approach spans were modeled using simplified single-degree-of-freedom systems. The seismic response was analyzed in the longitudinal direction using response spectrum method. For the approach spans, the seismic analysis dealt with the potential for loss-of-span due to excessive longitudinal displacements and bearing forces along the highway main line.

Recommendations

The seismic analysis indicates that the main bridge can resist the 50-year earthquake event without yielding or buckling of truss members and loss-of-span at supports. The analysis indicates a possibility for anchor bolt shear failure at all pier bearings. In order to avoid anchor bolt shear failure at all pier bearings, additional anchor bolts are required, or replacement of the existing bearings with seismic isolation bearings is suggested (Figure E-4). Chapter 5 presents the details for the proposed retrofit measures for the main bridge (Figures 5.9 through 5.13 and Table 5.16).

The approach spans on the Henderson, KY side have the potential for anchor bolt shear failure due to longitudinal seismic force at five out of thirty-four supports having fixed bearings. Therefore, retrofitting of the fixed bearings at those supports with additional anchor bolts or replacing the existing fixed bearings with seismic isolation bearings is recommended (Figure E-5). For all the expansion bearings, the bearing displacement Capacity/Demand ratio, is greater than 1.0 and hence loss-of-span cannot occur.

Similarly, the approach spans on the Evansville, IN side have the potential for anchor bolt shear failure due to longitudinal seismic force at all eight supports having fixed bearings. Therefore, retrofitting of the fixed bearings, at those eight supports on the approach spans, with additional anchor bolts, or replacing the existing fixed bearings with seismic isolation bearings is recommended (Figure E-6). For all the expansion bearings, the bearing displacement Capacity/Demand ratio, is greater than 1.0 and hence loss-of-span cannot occur. Chapter 6 presents the details of the proposed retrofit measures (Figures 6.7 through 6.16 and Tables 6.4 through 6.7) for the both approach spans.

Figure E.1 US41 Bridges over the Ohio River at Henderson, KY

Figure E-2 A View of Henderson, KY
Approach Bridge on the US41
Northbound Bridge

Figure E-3 The US 41 Northbound Approach Bridge at Evansville, IN
(Northbound on left side in the picture)

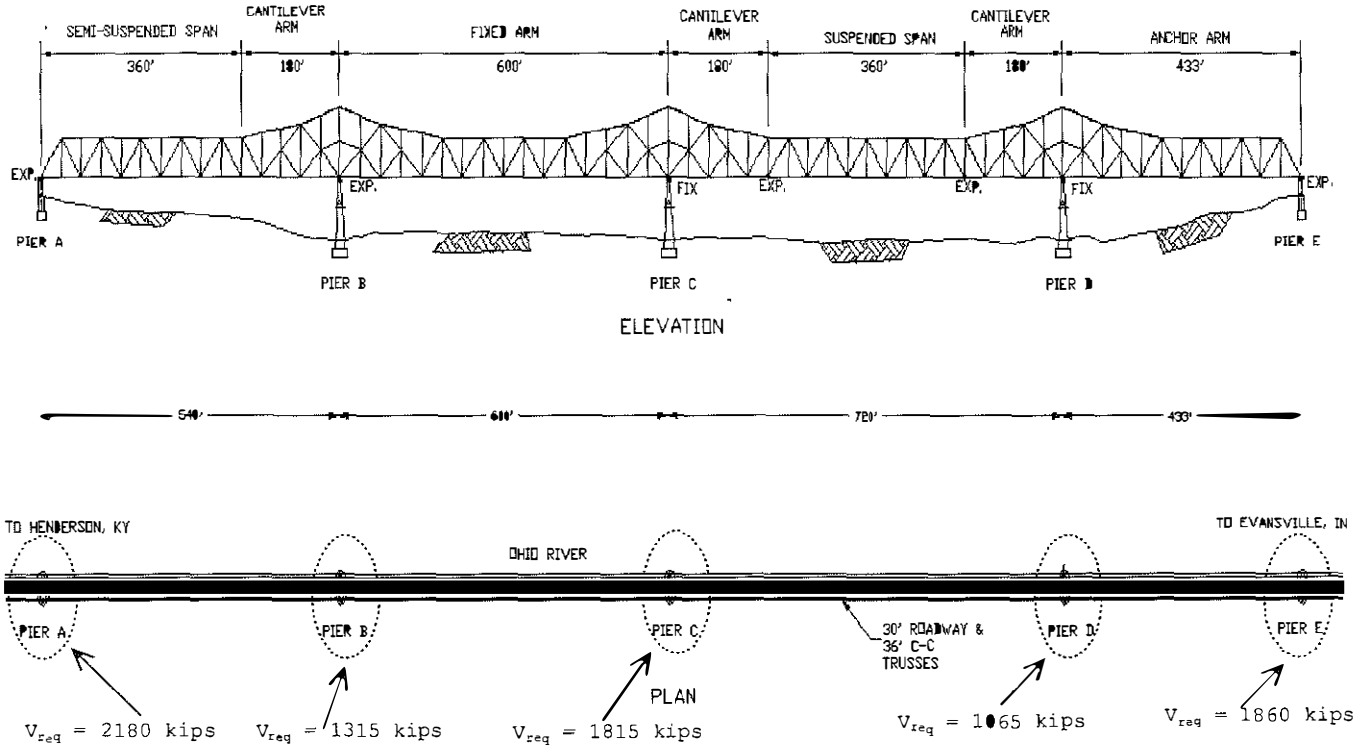

Figure E-4 Minimum Required Shear Capacity (V_{req}) to be Provided by Additional Anchor bolts at Pier Bearings for the US 41 Northbound Main Bridge

Note: Refer Figures 5.9 through 5.13 for the proposed retrofit details. Alternate retrofit would be to replace the existing fixed bearings with seismic isolation bearings

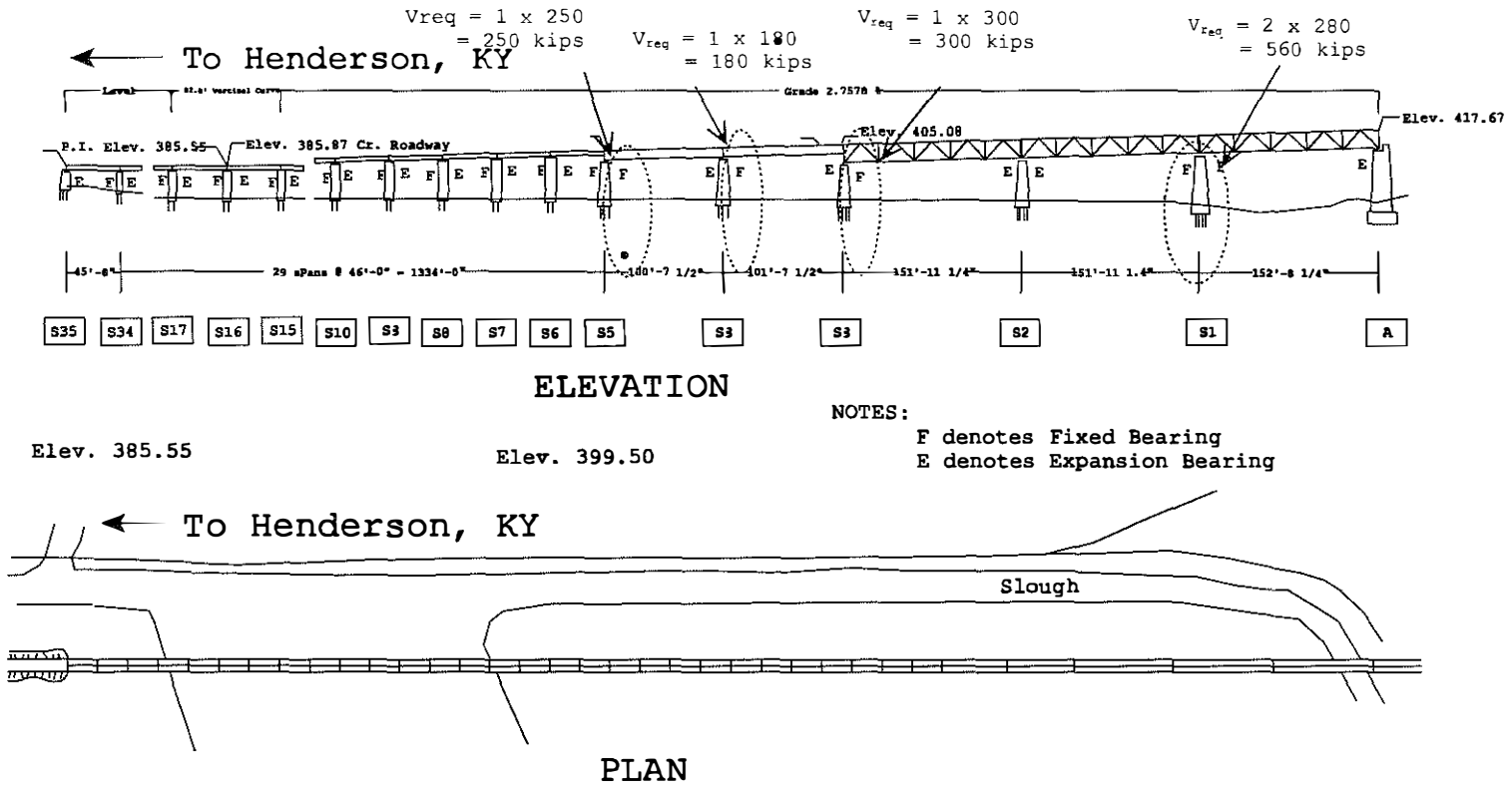

Figure E-5 Minimum Required Shear Capacity (V_{req}) to be Provided by Additional Anchor Bolts at Fixed Bearings on the Henderson, KY Approach of the US41 Northbound Bridge

Note: Refer Figures 6.13 through 6.16 for the proposed retrofit details. Alternate retrofit would be to replace the existing fixed bearings with seismic isolation bearings

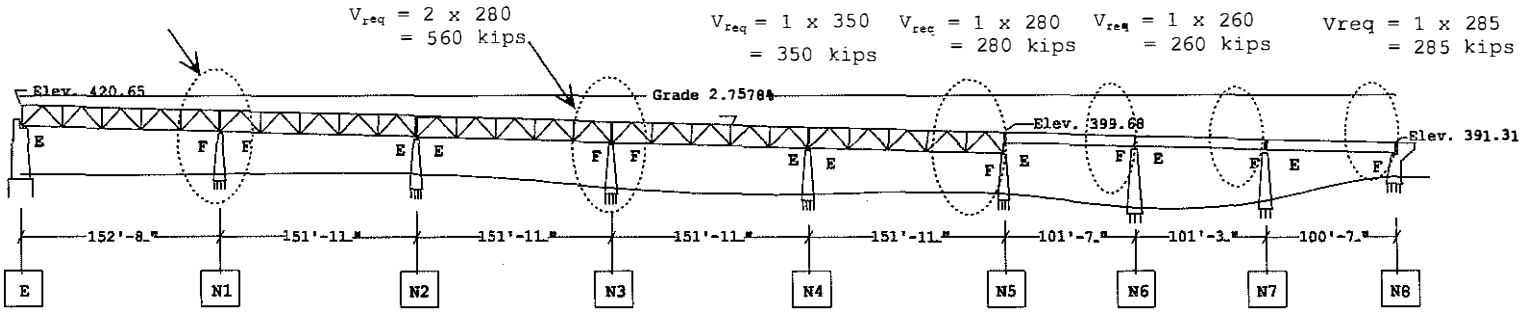

ELEVATION

NOTES:

F denotes Fixed Bearing
E denotes Expansion Bearing

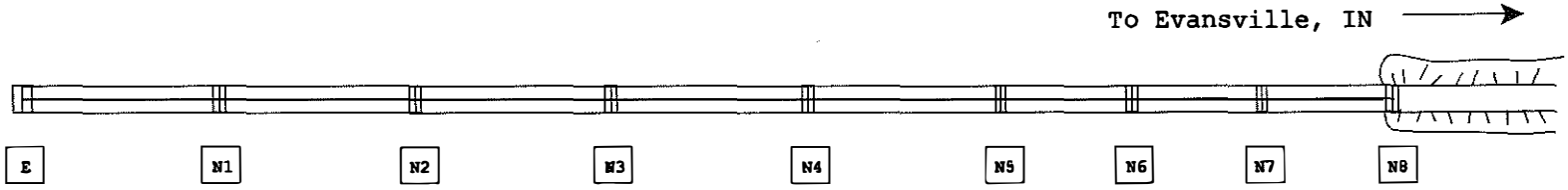

PLAN

ACKNOWLEDGMENTS

The financial support for this project was provided by the Kentucky Transportation Cabinet and Federal Highway Administration. The help of John Flekenstein and Clark Graves in coordinating and conducting the bridge testing is especially noteworthy. The authors would like to acknowledge the cooperation, suggestions, and advice of the members of the study advisory committee: Donald Herd (committee chairperson), Glenn Givan, Ray Greer, David Moses, Ted Noe, N.B. Shah, and David Steele.

The authors would also like to acknowledge the partial support for equipment by the National Science Foundation under grant CMS-9601674-ARI Program.

Table of Contents

Description **Page**

Implementation Letter i

Technical Report Documentation Page ii

EXECUTIVE SUMMARY iii

ACKNOWLEDGMENTS xi

TABLE OF CONTENTS xii

LIST OF TABLES xiv

LIST OF FIGURES xvi

1. INTRODUCTION 1

    1.1 General 1
    1.2 Field Testing 2
    1.3 Earthquake Background 2
    1.4 Scope of the work 3

2. THE US41 NORTHBOUND BRIDGE OVER THE OHIO RIVER AT HENDERSON, KENTUCKY 5

    2.1 General 5
    2.2 Bridge Superstructure 5
    2.3 Fixed and Expansion Bearings 6
    2.4 Bridge Substructure 7

3. FIELD TESTING 8
    3.1 General 8
    3.2 Instrumentation 8
    3.3 Testing Procedure 9
    3.4 Data Analysis 9
    3.5 Finite Element Model Calibration 11

4. FINITE ELEMENT MODELING AND FREE VIBRATION ANALYSIS.....15

4.1 General.....15
4.2 Finite Element Model.....15
4.3 Free Vibration Analysis.....16

5. SEISMIC RESPONSE ANALYSIS.....20

5.1 General.....20
5.2 Seismic Response.....21
5.3 Capacity/Demand Ratios.....25
5.4 Retrofit for the Main Bridge.....26

6. APPROACH BRIDGE.....27

6.1 General.....27
6.2 Structural Modeling.....27
6.3 Seismic Response Analysis.....28
6.4 Capacity/Demand Ratios.....29
6.5 Retrofit for the Approach Bridge.....30

7. CONCLUSIONS AND RECOMMENDATIONS.....31

7.1 General.....31
7.2 Main Bridge.....31
7.3 Approach Bridge.....32

REFERENCES.....33

LIST OF TABLES

Table No.	Description	Page No.
3.1a	US41 Northbound bridge testing details - Moving station on right lane	36
3.1b	US41 Northbound bridge testing details - Base station on right lane	37
3.2a	US41 Northbound bridge testing details - Moving station on left lane	38
3.2b	US41 Northbound bridge testing details - Base station on left lane	39
3.3	Frequency identification from the field test data	40
4.1	Natural frequencies and mass participation of the main bridge (Exact eigen system)	42
4.2	Natural frequencies and mass participation of the main bridge (Ritz vector based)	43
5.1	Description of seismic excitation cases	44
5.2	Cross sectional properties of members for stress calculation	45
5.3	Stresses (ksi) in members due to seismic excitation case L1T2V3, dead load and temperature	46
5.4	Stresses (ksi) in members due to seismic excitation case L2T1V3, dead load and temperature	47
5.5	Stresses (ksi) in members due to seismic excitation case LL11	48
5.6	Stresses (ksi) in members due to seismic excitation case LL22	49
5.7	Stresses (ksi) in members due to seismic excitation case TT11	50
5.8	Stresses (ksi) in members due to seismic excitation case TT22	51
5.9	Stresses (ksi) in members due to temperature of 90°F	52
5.10	Self-weight induced stresses (ksi)	53
5.11	Stress requirement based on AASHTO Equations for L1T2V3 earthquake	54
5.12	Stress requirement based on AASHTO Equations for L2T1V3 earthquake	55
5.13	Displacements (in) due to seismic excitation of the 50-year earthquake event	56
5.14	Displacements (in) due to self-weight and temperature	57
5.15	Maximum and minimum base shears from modal time-history for the 50-year earthquake	58
5.16	Bearing force capacity/demand ratios of the main bridge without site soil coefficients for the 50-year earthquake	59
6.1a	Calculation of superstructure weights for 150' truss spans	60
6.1b	Calculation of superstructure weights for 100' truss spans	60

6.1c	Calculation of superstructure weights for 46' girder span	61
6.2	Calculation of pier stiffness and pier mass of SDOF systems	62
6.3	Calculation of seismic response	63
6.4	Bearing force C/D ratios for the fixed bearings on the Evansville, IN approach spans	64
6.5	Displacement C/D ratios for expansion bearings on the Evansville, IN approach spans	65
6.6	Bearing force C/D ratios for the fixed bearings on the Henderson, KY approach spans	66
6.7	Displacement C/D ratios for expansion bearings on the Henderson, KY approach spans	67

LIST OF FIGURES

Fig. No.	Description	Page No.
2.1a	US41 bridges over the Ohio river at Henderson, KY - Entrance View	68
2.1b	Side views of the US41 bridges over the Ohio river	68
2.1c	End portal of the US41 bridges	69
2.1d	Typical hinge location on US41 bridges	69
2.1e	Inside view showing portals, cross bracings, etc	70
2.2	Plan and elevation views of the US41 northbound bridge over the Ohio river	71
2.3	Elevation view of the first span A-B	72
2.4	Elevation view of the second span B-C	73
2.5	Elevation view of the third span C-D	74
2.6	Elevation view of the fourth span D-E	75
2.7	Transverse cross section of the US51 main bridge	76
2.8a	Plan view of pier A and E	77
2.8b	Elevation views of pier A and E	77
2.9a	Plan view of pier B, C, and D	78
2.9b	Elevation views of pier B, C, and D	78
3.1a	Triaxial accelerometer block	79
3.1b	Accelerometer positions on the bridge	79
3.1c	Accelerometer placement on the deck	80
3.2a	Transverse acceleration time-history obtained from field testing at moving station 6	81
3.2b	FFT of transverse acceleration time-history at moving station 6	81
3.2c	Vertical acceleration time-history obtained from field testing at moving station 6	82
3.2d	FFT of vertical acceleration time-history at moving station 6	82
3.2e	Longitudinal acceleration time-history obtained from field testing at moving station 6	83
3.2f	FFT of longitudinal acceleration time-history at moving station 6	83
3.3a	First transverse mode	84
3.3b	Peak comparison for the first transverse mode	84
3.4a	First vertical mode	85
3.4b	Peak comparison for the first vertical mode	85
3.5a	First longitudinal mode	86
3.5b	Peak comparison for the first longitudinal mode	86
3.6a	Second transverse mode	87
3.6b	Peak comparison for the second transverse mode	87

3.7a	Second vertical mode	88
3.7b	Peak comparison for the second vertical mode	88
3.8a	Third transverse mode	89
3.8b	Peak comparison for the third transverse mode	89
3.9a	Third vertical mode	90
3.9b	Peak comparison for the third vertical mode	90
4.1	3D finite element model of the US41 Northbound bridge (a) isometric view, (b) elevation view, and (c) plan view	91
4.2	Mode shape of the first natural frequency (0.534 Hz) (a) isometric view, and (b) plan view	92
4.3	Mode shape of the second natural frequency (0.674 Hz) (a) isometric view, and (b) plan view	93
4.4	Mode shape of the third natural frequency (0.781 Hz) (a) isometric view, and (b) plan view	94
4.5	Mode shape of the fourth natural frequency (0.821 Hz) (a) isometric view, (b) elevation view, and (c) plan view	95
4.6	Mode shape of the fifth natural frequency (0.891 Hz) (a) isometric view, and (b) plan view	96
4.7	Mode shape of the sixth natural frequency (1.022 Hz) (a) isometric view, and (b) plan view	97
4.8	Mode shape of the seventh natural frequency (1.065 Hz) (a) isometric view, (b) elevation view, and (c) plan view	98
4.9	Mode shape of the eighth natural frequency (1.126 Hz) (a) isometric view, (b) elevation view, and (c) plan view	99
4.10	Mode shape of the ninth natural frequency (1.174 Hz) (a) isometric view, and (b) plan view	100
4.11	Mode shape of the tenth natural frequency (1.375 Hz) (a) isometric view, (b) elevation view, and (c) plan view	101
4.12	Mode shape of the eleventh natural frequency (1.456 Hz) (a) isometric view, (b) elevation view, and (c) plan view	102
4.13	Mode shape of the twelveth natural frequency (1.539 Hz) (a) isometric view, and (b) plan view	103
4.14	Mode shape of the thirteenth natural frequency (1.637 Hz) (a) isometric view, (b) elevation view, and (c) plan view	104
4.15	Mode shape of the fourteenth natural frequency (1.64 Hz) (a) isometric view, (b) elevation view, and (c) plan view	105
4.16	Mode shape of the fifteenth natural frequency (1.751 Hz) (a) isometric view, (b) elevation view, and (c) plan view	106
5.1	Time-history and response spectra identification map for the Commonwealth of Kentucky	107
5.2	Acceleration-time history of the horizontal component of the 50-year earthquake	108

5.3	Acceleration-time history of the vertical component of the 50-year earthquake	108
5.4	Acceleration-time history of the transverse component of the 50-year earthquake	109
5.5	Displacement-time history in the transverse direction at node 44 under the L1T2V3 excitation case	109
5.6	Displacement-time history in the vertical direction at node 44 under the L1T2V3 excitation case	110
5.7	Displacement-time history in the longitudinal direction at node 44 under the L1T2V3 excitation case	110
5.8	Axial force-time history of member 1 under L1T2V3 excitation case	111
5.9	Minimum required shear capacity for Pier A on the main bridge	112
5.10	Minimum required shear capacity for Pier B on the main bridge	113
5.11	Minimum required shear capacity for Pier C on the main bridge	114
5.12	Minimum required shear capacity for Pier D on the main bridge	115
5.13	Minimum required shear capacity for Pier E on the main bridge	116
6.1a	Truss spans in Evansville, IN approach bridge	117
6.1b	Girder spans in Evansville, IN approach bridge	117
6.1c	View of Evansville, IN approach bridge	118
6.1d	View of Henderson, KY approach bridge	118
6.2	Plan and elevation views of Evansville, IN approach bridge on the US41 northbound bridge	119
6.3	Plan and elevation views of Henderson, KY approach bridge on the US41 southbound bridge	120
6.4	Single degree of freedom system models for Evansville, IN approach	121
6.5	Single degree of freedom system models for Henderson, KY approach	122
6.6	Response spectra for the 50-year event for Henderson, KY (0.15g-2 from fig. 5.1) Damping ratio = 0.05	123
6.7	Arrangement of additional anchor bolts on pier N1	124
6.8	Arrangement of additional anchor bolts on pier N3	125
6.9	Arrangement of additional anchor bolts on pier N5	126
6.10	Arrangement of additional anchor bolts on pier N6	127
6.11	Arrangement of additional anchor bolts on pier N7	128
6.12	Arrangement of additional anchor bolts on pier N8	129
6.13	Arrangement of additional anchor bolts on pier S1	130
6.14	Arrangement of additional anchor bolts on pier S3	131
6.15	Arrangement of additional anchor bolts on pier S4	132
6.16	Arrangement of additional anchor bolts on pier S5	133

1. INTRODUCTION

1.1 General

The need for evaluating the seismic adequacy of existing infrastructure has come into focus, following the damage and collapse of numerous structures during recent earthquakes. In particular, the seismic rehabilitation of older bridges which were designed prior to the advent of modern seismic design codes is a matter of growing concern in regions of high seismicity. Bridge failures from earthquakes have so far only occurred in California and Alaska. The 1989 Loma Prieta earthquake [EERI 1990] and 1994 Northridge earthquake [EERI 1995], have brought the seismic risk to bridges and elevated freeway structures to the attention of the public. The partial collapse of the San Francisco - Oakland Bay Bridge and the Cypress Viaduct portion of Interstate 880 not only caused the loss of life but created considerable problems to the transportation infrastructure. The Bay bridge was unusable for a month and transbay commuters were forced to commute on ferries or the crowded Bay Area Rapid Transit System. Following the Loma Prieta earthquake, the Federal Highway Administration commissioned the seismic evaluation of bridges located in seismically active regions.

After seismic evaluation, if the bridge is found to be deficient, not all bridges in highway system has to be retrofitted simultaneously; instead, only those bridges with the highest priority should be retrofitted first. It should always be remembered that seismic retrofitting is one of several possible courses of action. Other possible actions are closing the bridge, replacing the bridge, taking no action at all, and accepting the risk of seismic damage.

Seismic design of bridges throughout the United States is governed by AASHTO's Standard Specifications for Highway Bridges, Division I-A (1996). Use of the AASHTO specifications is intended: (1) to allow the structure to yield during a major earthquake, (2) to allow damage (yielding) only in areas that are accessible (visible) and repairable, and (3) to prevent collapse even during very large earthquakes (NHI 1996). There are many bridges in the Commonwealth of Kentucky which were designed before the seismic provisions were introduced into the AASHTO Code. Recently, the Brent-Spence bridge on Interstate 75 connecting Covington, Kentucky to Cincinnati, Ohio, a double-deck through-truss bridge, was evaluated for seismic excitation [Harik et al.(1997a,b)]. There are many long-span through-truss bridges in Kentucky which require seismic evaluation. The present work concentrates on the seismic evaluation of the US41 Northbound Bridge over the Ohio River. This bridge connects US41 across the Ohio River between Henderson, KY and Evansville, IN.

1.2 Field Testing

Nowadays, field testing of bridges has become an integral part of the seismic evaluation process in order to eliminate the uncertainties and assumptions involved in analytical modeling. Full-scale dynamic tests on structures can be performed in a number of ways. Hudson (1977) describes the different types of testing as: (1) free vibration tests, including (i) initial displacement as in the pullback, quick-release test, and (ii) initial velocity from impacts; (2) forced vibration tests, including (i) steady-state resonance testing, (ii) variable frequency excitation including sweep, rundown, random and pulse sequences, and (iii) transient excitations including earthquakes, wind, traffic, and explosions. Shelley (1995b) provides a very informative discussion of the advantages and disadvantages of the various test methods used on highway bridges.

An alternative technique used to dynamically test bridges measures the bridge's response under normal traffic and wind. In this method no equipment is required to excite the structure, instead equipment is required only to record the vibrations. This technique has been used by a number of researchers (Abdel-ghaffer and Scanlan, 1985a,b, Alampalli and Fu 1994, Buckland et al. 1979, Doll 1994, Farrar et al. 1995, Paultre et al. 1995, Saiidi et al. 1994, Shahawy 1995, Ventura et al. 1994, Wendichansky et al. 1995). Harik et. al. used this method with success to identify the vibration mode shapes and frequencies of the Brent-Spence Bridge at Covington, KY (Harik et al. 1997a,b) and US51 Bridge at Wickliffe, KY (Harik et al. 1998).

1.3 Earthquake Background

The test bridge is located in Henderson County, Kentucky, in the Wabash Valley Seismic Zone. The two largest earthquakes known to have occurred in this zone were in 1891 and 1968. Street et al. (1996) calculated an $m_{b.Lg}$ of 5.5 to 5.8 for the September 27, 1891, event. This earthquake was centered near Mt. Vernon, Illinois, where several chimneys were shaken down and a church was damaged. The November 9, 1968, earthquake was more damaging than the 1891 one since the area was much more denseley settled and more vulnerable to damage. Stover and Coffman (1993) estimated the $m_{b.Lg}$ of the two events as 5.2 and 5.5, respectively.

The most significant recent earthquake in the Wabash Valey Seismic Zone was on June 10, 1987. Taylor et al. (1989) estimated the $m_{b\,Lg}$ of this event at 5.2 and described it as a predominantly strike-slip event with a focal depth of 10 km.

Nuttli and Herrmann (1978) estimated a maximum credible earthquake of 6.6 $m_{b,Lg}$ for the Wabash Valley Seismic Zone. More recently, Obermeier et al. (1992) found evidence of one or more strong earthquakes centered near Vincennes, IN. Based on the areal extent of liquefaction features (dikes), Obermeier et al. (1992) concluded that if all the dikes are from a single event, the level of shaking would have been on the order of 6.7 $m_{b,Lg}$, a magnitude that is in close agreement with Nuttli and Herrmann's (1978) maximum credible earthquake.

With increasing recognition of potential damage from a large Wabash Valley earthquake, or other less severe quake, the Kentucky Transportation Cabinet funded the research project *Evaluation and Analysis of Innovative Concepts for Bridge Seismic Retrofit*. Research was conducted by the Kentucky Transportation Center at the University of Kentucky. Fundamental to this research project was the characterization of the seismic potential affecting Kentucky from known seismic zones as well as unknown "local" events. Results from this seismological assessment of Kentucky were published in *Source Zones, Recurrence Rates, and Time Histories for Earthquakes Affecting Kentucky* (Street et al., 1996). In this report, three main tasks were covered: (1) definition and evaluation of earthquakes in seismic zones that have the potential to generate damaging ground motions in Kentucky, (2) specification of the source characteristics, accounting for the spreading and attenuation of the ground motions to top-of-bedrock at sites in Kentucky, and (3) determination of seismic zoning maps for the Commonwealth based on peak-particle accelerations, response spectra, and time-histories.

Time-histories generated in the aforementioned report were used in the seismic evaluation of the US41 northbound bridge. Effects of these artificial earthquakes were calculated for bedrock elevation at the county seat of each Kentucky county. These acceleration time-histories were derived through the use of random vibration analysis and take into consideration the probability of earthquakes from nearby seismic zones, the attenuation of ground motions with distance in the Central United States, and the possibility of a random event occurring outside of the generally recognized seismic zones (Street et al., 1996).

1.4 Scope of the Work

The primary aim of this study is to assess the structural integrity of the US41 northbound bridge when subjected to a 50-year earthquake event at Henderson Co., Kentucky. To achieve this the scope of work was divided into four tasks: 1) Field testing of the main bridge, 2) finite element modeling, 3) time history seismic response analysis of the main bridge, and 4) seismic response of the approach bridge.

The ambient vibration properties of the main bridge were determined through field testing under traffic and wind induced excitation. The purpose of measuring the ambient vibration properties is to determine the mode shapes and the associated natural frequencies. Full scale ambient or forced vibration tests have been used extensively in the past to determine the dynamic characteristics of highway bridges (Abdel-ghaffer and Scanlan, 1985a,b).

A three dimensional finite element model of the main bridge is used for free vibration and seismic response analyses. The model is first calibrated by comparing the free vibration analysis results with ambient vibration properties from field testing. After the calibration, the model is used for seismic response analysis to determine the maximum displacements, stresses in truss members, and forces on bearings.

The approach spans are modeled using simplified single-degree-of-freedom (SDOF) systems. The superstructure mass is lumped at the top of the piers. For the approach spans the seismic analysis dealt only with the potential for loss-of-span due to longitudinal displacement and forces on the bearings. Seismic response is analyzed in the longitudinal direction only using the response spectrum method to determine the maximum displacements and forces.

2. The US41 Northbound Bridge over the Ohio River at Henderson, Kentucky: Main Bridge

2.1 General

The Ohio River bridge on US41 northbound, shown in figures 2.1(a)-(e), is a cantilever through-truss bridge, a bridge type commonly employed for spans of 600' (183 m) to 1500' (457 m) through the mid 1970's. This bridge was originally designed by Modjeski and Masters Engineers in 1929. Figures 2.1(a)-(e) show the different views of the main bridge. The total length of the bridge including approach spans is 5395' 2.5". The length of the four-span main bridge is 2293' 1.5". The plan and elevation of the main bridge are shown in Figure 2.2. The superstructure truss members are made of structural steel, while the substructure piers are made of reinforced concrete. The details of approach bridges and their seismic evaluation are discussed separately in Chapter 6.

2.2 Bridge Superstructure

The superstructure is described in terms of the vertical truss system, the lateral truss system and the floor system. The lateral truss is a combination of lateral bracing, sway and portal bracings. The bridge is a through-truss type with suspended spans, fixed spans, anchor arms and cantilever arms.

As seen from Figure 2.2, the height of the vertical truss near each midspan is 55', and at each internal support is 75'.

The vertical truss system, shown in Figure 2.2, consists of a semi-suspended span of 360' between piers A and B, which is supported over pier A and a cantilever arm 'B' of 180', as shown in Figure 2.3. 'B-C' is a fixed span (Figure 2.4), between piers B and C, spanning 600'. In span C-D (Figure 2.5), there are two cantilever arms, spanning 180' each. Furthermore, 'C' and 'D' support a suspended span of 360' as shown in Figure 2.2. The span between piers D and E (Figure 2.6) is provided with an anchor arm 'D-E' spanning 432' 7" . The lengths of span AB, BC, CD and DE are 540' 6.5", 600', 720' and 432' 7" respectively.

The vertical truss members were made of medium carbon steel or silicon steel. Shop rivets of 1" dia. were used for main truss members; 7/8" dia. were used for verticals, floor beams, stringers, laterals and sway bracing. Field rivets of 1" dia. were used for all truss members and floor beam connections; 7/8" dia were used for stringer connections, laterals and sway bracings. Except for a very few 16" CB sections for verticals, all other members were made of built-up sections using channels, angles and web plates. Many vertical truss members in the tapered portion near the pier support are connected by pins of 10" dia.

The lateral truss system consists of lateral bracing members in the top and bottom chord planes combined with portals and sway bracing between the two vertical trusses as shown in Figure 2.1. At the hinge locations, longitudinal sliding joints in both the top and bottom chords are designed for free thermal expansion.

The floor system consists of a 7" thick concrete slab supported by longitudinal WF stringers which are carried by transverse built-up floor beams as shown in Figure 2.7. The width of the roadway is 30'. The longitudinal stringers are spaced at 4' 9". The floor beams span 36' between the vertical trusses and are attached to the truss verticals. Three handrails are attached to the truss members on either of the deck.

2.3 Fixed and Expansion Bearings

The superstructure is supported by expansion roller bearings on piers A , B and E, and fixed bearings on piers C and D. The expansion bearings on piers A and E permit longitudinal translation and longitudinal rotation. The expansion bearing on pier B allows only longitudinal translation. The fixed bearings do not allow longitudinal rotation and translation.

The fixed bearings consist of three layers of built-up sections bolted together. The bottom of the bearing is connected to the pier through anchor bolts. The size of the bearing is 7' 6" in length and 5' wide. There are a total of four 2" dia. anchor bolts running 4' into the pier concrete. The anchor bolts are spaced at 4' 9" in length direction and 5' in width direction.

The expansion bearings on pier A and E consist of pin and roller combinations to allow rotation and translation. The top shoe of this bearing is connected to the bottom chord of the vertical truss, and the bottom shoe is connected to the pier through anchor bolts. There are a total of four 2" dia. anchor bolts running 4' into the pier concrete. The size of the bearing is 4' 6" in length and 4' wide.

The expansion bearings on pier B consist of three layers of built-up sections bolted together. The top layer is bolted to the bottom chord of the vertical truss, and

the bottom layer is connected to the pier through anchor bolts. The middle layer consists of rollers to allow longitudinal translation. There are a total of four 2" dia. anchor bolts running 4' into the concrete. The size of the bearing is 7' 6" in length and 6' wide.

2.4 Bridge Substructure

The main bridge is supported on piers A, B, C, D and E, which are of tapered wall type piers with a batter of ½" per ft. All the piers are supported on caisson foundations. The heights of the caisson foundations for piers A and E are 101.5' and 104.57'. The heights of pier A and E above the caisson foundations are 46' 7(1/4)" and 49' 7". The plan and side elevations of the pier A and E are shown in figure 2.8a-b. The change in the cross section in these piers near the top is mainly to accommodate the deck-truss type approach spans. Plan and side elevation and plan view of the piers B, C and D are shown in Figures 2.9a-b. The heights of the caisson foundations of pier B, C and D are 73', 71.5' and 69'. The heights of pier B, C and D above the caisson are 101' 7/8", 102' 6(1/8)" and 101' 7/8". All the piers are constructed with reinforced concrete class 'D'. The reinforcement in the pier consists of 3/4" dia. rebar running horizontally and vertically at 2' c/c. The center to center distance between bearings is 36'

3. Field Testing

3.1 General

Field testing of a bridge provides an accurate and reliable description of its actual dynamic characteristics. Field testing was conducted on the US41 northbound main bridge. Testing was conducted on right and left lanes. Since there is no symmetry in the longitudinal direction of the bridge, the full bridge was tested. All measurements were taken by placing the instruments on the pavement due to the limited access to the actual floor beams and the time constraints involved. Each instrument was placed with its longitudinal axis aligned parallel to the longitudinal direction of the bridge. Ambient vibration measurements under traffic and wind induced excitations were recorded at 25 locations beginning from pier A to pier E.

3.2 Instrumentation

The equipment used to measure the acceleration-time histories consisted of a triaxial accelerometer (Figure 3.1a) in conjunction with its own data acquisition system. The system consisted of Kinemetrics SSA-2 digital recording strong motion accelerograph. Two of the units contained internal accelerometers, and the remaining two were connected to Kinemetrics FBA-23 force balance accelerometers. Each of the accelerometers was capable of measuring accelerations of ±2g's with a frequency response of DC-50 Hz. All data were sampled using a 1002 Hz sampling rate and stored internally on the SSA-2, then downloaded to a personal computer. Each of these units was triggered simultaneously using laptop personal computers connected to each SSA-2. A nominal 30 sec record was obtained at each location. Accelerometers were mounted in order to measure vibrations in three orthogonal directions. To ensure the blocks were placed in level, adjustable feet and a carpenter's level were attached to each block. Accelerometers were connected to the data acquisition system by shielded cables.

Sets of three accelerometers were mounted to aluminum blocks in orthogonal directions. A block was positioned at each location with the accelerometers oriented in the vertical, transverse and longitudinal directions. To prevent any shifting of the accelerometers during testing, 25-pound bags of lead shot were laid on top of the accelerometer blocks once in position. During ambient vibration tests, traffic was allowed to cross at normal highway speed.

3.3 Testing Procedure

A reference location, hereinafter called the base station, was selected based on the mode shapes from the preliminary finite element model at location 14 as shown in Figure 3.1b. Two of the accelerometers, one at each side of the roadway width (Figure 3.1c), remained at the base station 14 throughout the testing sequence. Five triaxial accelerometers were used at moving station locations. From the preliminary finite element analysis, 25 locations were identified to be measured to represent the dynamic behavior of the bridge. In total there were five sets of moving station data with each set having 5 moving station locations. Tables 3.1a and 3.1b describe the designations of moving and base station accelerometer on the right lane. Tables 3.2a and 3.2b detail the designations of moving and base station accelerometers on the left lane. First five stations, 2 through 6 were placed in span A-B; stations 8 through 12 were placed in span B-C; stations 14 through 20 were placed in span C-D; and stations 22 through 25 were placed in span D-E. Data collection began from pier A to pier E on the right lane. The same procedure was repeated for the left lane also without altering the base station. Stations 1, 7, 13, 21, and 25 were placed just above the piers A, B, C, D and E respectively.

One set of measurements consisted of recording acceleration-time history on two base stations and five moving stations simultaneously. After collecting the data, the moveable stations were shifted to the next locations while the base stations remained stationary. This sequence was repeated five times to get measurements on all stations on the northbound lane.

3.4 Data Analysis

Once the data have been downloaded from the field test, a Fast Fourier Transform (FFT) was performed on each acceleration-time history using the DADiSP software. The program DADiSP (Data Analysis and Display Software) by DSP Development Corporation, Cambridge, Massachusetts, (DADiSP 1995) was used to view and analyze the large amount of data. The program has the ability to quickly access and display the large records of 30,000 data points. Also, the program has an extensive data handling and analysis library which was needed for this research. Fast Fourier transformation of the acceleration histories was possible in a few seconds. The speed of the program made analyzing and viewing such a huge amount of data manageable.

Acceleration records were transformed from the time domain to the frequency domain through the use of the Fourier transform. Equations 3.1 and 3.2 are the mathematical definitions of the Fourier transform pair. Equation 3.1 is referred to as the Fourier transform of $f(t)$ and the equation 3.2 as the inverse Fourier transform

(Pressetal.1992,ChapraandCanale 1988).

$$F(\omega) = \int_{-\infty}^{\infty} f(t)\, e^{i\omega t}\, dt \tag{3.1}$$

$$f(t) = \frac{1}{2\pi} \int_{-\infty}^{\infty} F(\omega)\, e^{-i\omega t}\, d\omega \tag{3.2}$$

where **f(t)** = a function of time, **F(ω)** = amplitude as a function of frequency, and ω = circular frequency (radians per second).

From equations 3.1 and 3.2, a time function can be derived from a frequency function or vice versa. The problem with using equations 3.1 and 3.2 lies in the fact that a continuous function is required. For discretely sampled data, such as a dynamic bridge test, a different form of the Fourier transform is needed. A form of equation 3.1, known as the Discrete Fourier Transform (DFT), is used when points of data are known at evenly spaced intervals. Equations 3.3 and 3.4 are the discrete forms of the Fourier transform pair.

$$F_n = \sum_{k=0}^{N-1} f_k\, e^{2\pi i k n / N} \qquad \text{(for n=0 to N-1)} \tag{3.3}$$

$$f_k = \frac{1}{N} \sum_{n=0}^{N-1} F_n\, e^{-2\pi i k n / N} \qquad \text{(for k=0 to N-1)} \tag{3.4}$$

where N = number of sampled points and f_k = set of N sampled points.

The DFT as expressed in equation 3.3 is usually the most useful in civil engineering applications where frequency components are sought from discretely sampled (digitized) data. However, the direct application of equation 3.3 requires N^2 complex mathematical operations. This becomes prohibitively time-consuming even for modest length data records. Fortunately, there is a numerical operation that reduces computing time for the DFT substantially.

The method is called the Fast Fourier transform (FFT) and owes its efficiency to exploitation of the periodicity and symmetry of trigonometric functions. An FFT can be computed in approximately $N\log_2 N$ operations. For a set of 1000 data points, the FFT is approximately 100 times faster than the DFT. The first FFT is attributed to Gauss in 1805 but did not become widely known until the mid 1960's with the advent of the Cooley-Tukey algorithm. A more complete mathematical and numerical treatment of the FFT can be found in Press et al. (1992) and Chapra and Canale

(1988). Using the Fast Fourier Transform (FFT), natural frequencies in three orthogonal directions were determined. Additional processing into a Power Spectral Density (PSD) plot, which squares the FFT amplitudes and divides out the record length, was sometimes helpful in identifying natural frequencies.

Mode shapes were determined by plotting the ratios of accelerometer FFT magnitude to base station FFT magnitude at their respective locations along the bridge. Comparing the phase angle of an FFT frequency to the base-station FFT phase angle determined the sign of the magnitude to be plotted (in-phase or out-of-phase with the base station).

A typical ambient vibration acceleration-time history obtained in the transverse direction at the moving station 6 is shown in Figure 3.2a. Similar time histories are shown for the vertical (figure 3.2c) and longitudinal (figure 3.2e) directions at moving station 6. For the transverse direction, the FFT of the acceleration time-history of moving station 6 is shown in Figure 3.2b. Similar FFTs for vertical and longitudinal direction time-histories are shown in Figures 3.2d and 3.2f. By observing the peaks of all the stations, the natural frequencies were identified. These peaks do not always occur at exactly the same frequency at all locations. Therefore, the number of peaks of adjacent natural frequencies were calculated. Table 3.3 lists the distribution of frequencies from acceleration records obtained on longitudinal, transverse and vertical direction accelerometers. Then, the bridge natural frequency was identified as the one which has the maximum number of peaks. The frequency was also found to be based on the mode shape that follows closer to the preliminary finite element model results.

Table 3.3 also lists the comparison between the field tested natural frequency with that of the calibrated finite element model. They are discussed in the following section.

3.5 Finite Element Model Calibration

A logical next step to field testing in bridge evaluation is to create an analytical model which will correlate well to the measured dynamic properties. Many assumptions and modeling approximations must be made when creating a practical model of a bridge. For example, a finite element model requires input of the material properties which are inherently variable. This is one input where the analyst can only make a best estimate and later adjust to match the experimental results.

Using results from the eigenvalue analysis, generally, the bridge model has to be calibrated to experimentally determined mode shapes and frequencies. A perfectly calibrated model would match all experimentally determined mode shapes

and frequencies exactly. However, to hope for such a perfect calibration is not realistic. Therefore, only the most structurally significant modes and frequencies are used in the model calibration process. Namely, the first three transverse modes, first three vertical modes and the first longitudinal mode from field testing are selected as calibration targets.

Parameters which were used to correlate with the field test include the following: modulus of elasticity (E) of the frame elements, the bearing spring stiffness, and spring stiffnesses for the piers. Initial estimates of these parameters were obtained from the structural drawings. But the estimates do not account for (1) construction tolerances or errors that can make as-built dimensions different from design dimensions, or (2) actual strengths of materials such as the actual compressive strength of concrete, which affects its modulus of elasticity. Calibration is performed by adjusting the stiffnesses and masses of the bridge members until an acceptable match is observed in the natural frequency and mode shape.

Since the bridge does not have a symmetry along the vertical direction, it is not possible to observe pure transverse modes. Instead, transverse flexural-torsional modes are obtained. But pure vertical mode are obtained, because the bridge is symmetric in the transverse direction. Longitudinal modes are accompanied with little vertical bending mainly because of the unequal pier stiffnesses. For comparison purposes, only the transverse components from field testing are taken into consideration for the transverse flexural-torsional modes. All the transverse flexural-torsional modes are hereinafter referred as transverse modes, because they have major mass participation in the transverse direction.

The finite element results for the mode shapes are generated at the end nodes in the floor beams. On the other hand, due to the limited access to the actual floor beams, all measurements were taken by placing the instruments on the pavement just above the floor stringers.

Figure 3.3a shows the comparison of the mode shape obtained from the test and finite element model. Although this mode is not a pure transverse mode, Figure 3.3a compares only the transverse components. This mode has four half-waves along the length of the bridge. The distribution of fundamental natural frequency is given in Figure 3.3b. It can be seen from this figure that the peak in the magnitude varied from 0.4676 Hz to 0.6012 Hz, with a maximum number of peaks occurring at 0.5344 Hz. Therefore, 0.5344 Hz is identified as the fundamental frequency from the field test. The natural frequency from the finite element model is 0.5342 Hz, and the difference is only about 0.04%.

Figure 3.4a shows the first vertical mode with a natural frequency of 0.8016 Hz from the test. The distribution of natural frequency is shown in Figure 3.4b. The maximum number of peaks appears to be at 0.8016 Hz, and hence this is identified as the natural frequency from field testing. The finite element model frequency is 0.7807 Hz, and the difference is only about 2.7%. This mode is a pure vertical mode with 4 half-waves along the length of the bridge.

The traffic induced excitation can produce clear acceleration records in the vertical direction, and the traffic combined with wind excitations can produce in the transverse direction. Since there was no excitation along the longitudinal direction, clear acceleration records in the longitudinal direction were not obtained. Therefore, matching the frequencies is difficult for this mode. The first longitudinal mode shape is shown in Figure 3.5a. The natural frequency from the field test according to Figure 3.5b is 1.9372 Hz. Although the maximum number of peaks occurs at 1.9038 Hz, the mode shape corresponding to 1.9372 Hz matches well. The FE model frequency is 1.8537 Hz, and the difference is only about 2.7 %. Due to the difference in stiffness of the piers, pure longitudinal modes are not obtained. Therefore, longitudinal mode is accompanied by a small vertical modal deformation; however, the mass participation in this mode is mainly due to the longitudinal deformation of the piers.

Figure 3.6a shows the mode shape of the second transverse mode. The distribution of natural frequency is shown in Figure 3.6b, and the natural frequency is identified as 0.668 Hz. The natural frequency from the FE model is 0.674 Hz, and the difference with the test is only 0.878%. This is not a pure transverse mode. It is a transverse flexural-torsional mode with four half-waves.

The mode shape of the second vertical mode is shown in Figure 3.7a. Although the maximum number of peaks occurs at 1.0668 Hz, the frequency 1.1022 Hz is selected based on its closer match in mode shapes. The natural frequency from the test is 1.1022 Hz, whereas the FE model is 1.065 Hz and the difference with the test is 0.37%. Figure 3.7b shows the distribution of natural frequency of this mode. The mode shape consists of four half-waves along the length of the bridge.

Figure 3.8a shows the mode shape of the third transverse mode. This is a transverse flexural-torsional mode with the frequency of 0.8016 Hz from field testing and 0.7807 from FE model. The difference of FE model natural frequency with test is only 2.7%. There are four half-waves in the mode shape along the length of the bridge. Figure 3.8b shows the distribution of the natural frequency, and 0.8016 Hz is observed at 14 stations out of the total 25 stations.

Figure 3.9a shows the mode shape of the third vertical mode. The natural frequency of 1.3694 Hz is identified from the test and 1.375 from the FE model. The difference of FE model frequency with the test is 2.8%. The mode shape consists of five

half-waves along the length of the bridge. From Figure 3.9b it is seen that the maximum of number of peaks occurs at 1.336 Hz, but the mode shape corresponding to this frequency does not match well with the finite element model. The frequency 1.3694 is identified as the natural frequency, since the mode shape corresponding to this frequency matches better with the finite element model.

4. Finite Element Modeling and Free Vibration Analysis

4.1 General

Based on the general dynamic characteristics of cantilever truss bridges and the proximity and activity of the seismic zones, the main bridge model was expected to remain elastic, and displacements were anticipated to be small enough to neglect the material and geometric nonlinear effects. Hence, the consideration of linear elastic small displacement analysis is considered to be appropriate.

Free vibration analysis is a key process in the dynamic analysis of a structure; the resulting natural frequency and mode shapes succinctly describe the dynamic characteristics of a complex structure. The analytical model is calibrated by comparing free vibration analysis results with ambient vibration measurements.

4.2 Finite Element Model

A three dimensional linear elastic finite element model (Figure 4.1) of the main bridge was developed in SAP90 finite element analysis software (Wilson and Habibullah, 1992). Developed for both the free vibration analysis and earthquake response analysis, the model represents the structure in its current as-built configuration. All truss members of the superstructure are modeled using two noded frame (beam) elements which have three translational DOF and three rotational DOF at each node. Rotational degrees of freedom (DOF) of members are included in this bridge because the connections are of riveted type that could induce flexural stresses in addition to axial stresses. Based on the connection between the concrete deck and stringers, it is assumed that the deck and stringers will not contribute to the stiffness of the bridge. Wall type piers are idealized as frame elements with their gross cross-sectional properties.

The piers A, B and E are provided with expansion bearings, while the piers C and D are provided with fixed bearings. The fixed bearings were modeled by simply restraining both the rotational DOF that causes bending in the longitudinal direction and longitudinal translation. Piers and bearings are represented by a set of spring elements that simulate the actual behavior.

The expansion bearings at the piers A and E were modeled by establishing nodes in the bottom chord of the truss and the top of the pier at the bearing centers and coupling all DOF except the longitudinal translation and the vertical bending rotation (DOF: u_z and q_x). The coupled nodes provide direct output of the relative displacement between the top and bottom shoes of the bearings and thus indicate if the translation has exceeded the expansion capacity. At the expansion bearing of pier B, only the longitudinal translation is released.

While conducting free vibration analysis, it was found that the modeling of piers using frame elements resulted into less mass participation. This may be due to large differences in stiffness and masses of members in superstructure and piers of substructure. Therefore, the piers were replaced by springs at the bottom of bearings. The spring stiffnesses were obtained by applying unit displacement along the appropriate DOF.

4.3 Free vibration Analysis

An eigenvalue analysis is used to determine the undamped, free vibrations of the structure. The eigensolution results in the natural mode shapes and frequencies of the structure. Free vibration analysis is required first to calibrate the finite element model with the field ambient vibration test measurements. Secondly, to perform seismic response analysis using the modal time-history method, the natural frequencies and their associated mode shapes are required from free vibration. Free vibration analysis involves the solution of the following eigenvalue problem:

$$[M - \omega^2 K]u = 0 \qquad (4.1)$$

where **M** and **K** are system mass and stiffness matrices and **u** is modal displacement vector. The eigenvalue of a mode ($\mathbf{w^2}$) is the square of the circular frequency of that mode (**w**) and relates to the cyclical frequency (**f**) by the relation $\mathbf{f = \omega/2\pi}$, and relates to the period of vibration (**T**) by the equation $\mathbf{T = 1/f}$.

SAP90 uses an "accelerated subspace iteration" algorithm to solve the eigenvalue problem. The subspace iteration method was developed by Bathe in 1971 and a detailed discussion of the method and its fundamentals can be found in Bathe (1982). Various techniques have been used to accelerate the basic subspace iteration method, and the particular algorithm used in the SAP90/SAP2000 programs can be found in Wilson and Tetsuji (1983).

Traditionally, mode-superposition analysis was performed using a structure's eigenvectors as the basis for the analysis. Research (Wilson, Yuan, and Dickens, 1982) indicates that this is not the best basis for a mode-superposition time-history analysis.

Instead, a special set of load-dependent, orthogonal Ritz vectors yields more accurate results than the same number of natural mode shapes. Ritz vector analysis significantly reduces computing time and automatically includes the proven numerical techniques of static condensation, Guyan reduction, and static correction due to higher mode truncation.

The reason that Ritz vector analysis yields better results than an equal number of eigenvectors is that the Ritz vectors take into account the spatial distribution of dynamic loading. In fact, the spatial distribution of loading serves as a starting load vector to begin the process of finding appropriate Ritz vectors. Subsequent Ritz vectors are formed based on the preceding Ritz vector and the neglected inertial effects. In contrast, the eigenvectors are computed from the stiffness and mass matrices only and, therefore, cannot account for the spatial distribution of loading. Eigenvectors that are orthogonal to loading do not participate in the structural response even if they are at or near the forcing frequency.

For model calibration, the natural frequencies and their mode shapes have to be accurate; therefore exact eigenvalues(natural frequencies) have been extracted. All the frequencies may not participate in calculating the response under seismic excitation kind of loading. In order to get full participation, many modes have to be extracted. In this work, around 450 modes were tried to improve the mass participation. But there was no increase in the mass participation. Therefore, Ritz-vector based (which are load dependent) extraction of eigenvalues has been carried out. This method gives more than 90% participation in all the three directions.

The natural frequencies and mass participation for the lowest 20 modes are presented in Table 4.1. Some of the frequencies and their mode shapes have been compared with the field testing in the earlier chapter. The natural frequency of the bridge ranges from 0.534 Hz to 2.082 Hz for the first 20 modes, and the period ranges from 1.87 sec to 0.48 sec. The natural frequencies listed in Table 4.1 and their mode shapes are used only to calibrate the finite element model. They are not used for the seismic response analysis. It is seen from Table 4.1 that the mass participation of the first three modes are only in the transverse direction. Therefore, these three modes are treated as transverse modes based on the mass participation point of view, although there is some torsional and vertical displacement component as seen from Figure 4.2b.

Figures 4.2(a) and (b) show the first mode shape in isometric and plan views, respectively. The natural frequency of this mode is 0.534 Hz. The percentage of mass participation of this mode is about 3.6. This mode has a maximum modal displacement in the span C-D. Based on mass participation, this mode is identified as a transverse mode.

Figures 4.3(a) and (b) show the second mode shape with a frequency of 0.674 Hz in isometric and plan views, respectively. Contrary to the first mode, this mode has two adjacent spans having modal deformations in the same direction. The mass participation for this mode is 0.8% . Based on mass participation, the second mode is also observed as the transverse mode.

Figures 4.4(a) and (b) show the third mode shape with a frequency of 0.781 Hz in isometric and plan views, respectively. First two spans have modal deformation in the same direction, and the mass participation for this mode is 14.5%. Based on mass participation, this mode is a transverse mode. This is one of the very important modes that significantly contribute to the transverse seismic motion.

The fourth mode shape in isometric, elevation and plan views is shown in Figures 4.5(a), (b) and (c), respectively. The natural frequency of this mode is 0.821 Hz. Based on mass participation and from Figures 4.5(b) and (c), it is seen that this mode is a first vertical mode. The mass participation in the vertical direction is only 1.4%.

Figures 4.6(a) and (b) show the fifth mode shape with a frequency of 0.891 Hz, in the isometric and plan views, respectively. The mass participation for this mode is 0.11%. Based on mass participation, this mode is observed as a transverse mode.

The sixth mode shape in isometric and plan views is shown in Figures 4.7(a) and (b), respectively. The natural frequency of this mode is 1.022 Hz, and the mass participation is 5.9%. Based on mass participation, this mode is treated as a transverse mode. Figures 4.8(a), (b) and (c) show the seventh mode shape with a frequency of 1.065 Hz. The mass participation is only 0.38%. Based on Figures 4.8(b) and (c), this mode is mainly a vertical mode.

Figures 4.9(a), (b) and (c) show the eighth mode shape with a frequency of 1.126 Hz. Major mass participation 1.321% is in the transverse direction with a little participation of 0.2% in the vertical direction. Therefore, this mode is observed as a transverse mode. The ninth mode shape with a frequency of 1.174 Hz is shown in Figures 4.10(a) and (b). The mass participation is only 3.86% in the transverse direction. This mode is identified as a transverse mode.

The tenth mode with a frequency of 1.375 Hz is shown in Figures 4.11(a), (b) and (c). The mass participation for this mode is 13.1% in the vertical direction and 0.2% in the longitudinal direction. Hence, it is identified as a vertical mode.

Figures 4.12(a), (b) and (c) show the eleventh mode shape with a frequency of 1.456 Hz. The mass participation in transverse and vertical direction are 0.42% and 0.63%. This mode is a combination of vertical and transverse modes.

The twelve mode shape with a frequency of 1.539 Hz is shown in Figure 4.13(a) and (b). The mass participation for this mode is 0.22%. Based on the mode shape and mass participation, this mode is identified as a transverse mode with many half-waves. Figures 4.14(a), (b) and (c) show the thirteenth mode shape with a frequency of 1.637 Hz. The mass participation for this mode is 12.9%. Based on the mode shape and mass participation, it is observed that this mode is the second dominant mode to contribute significantly in the vertical direction.

Figures 4.15(a), (b) and (c) show the fourteenth mode shape with a frequency of 1.64 Hz. The mass participation for this mode is 5.35% in the vertical direction. Therefore, this mode is observed as a vertical mode with a little transverse bending. The fifteenth mode shape with a frequency of 1.751 Hz is shown in Figures 4.16(a), (b) and (c). The mass participation for this mode in the longitudinal direction is 2.357% and in the vertical direction is 0.37%. Therefore, this mode is the first dominant mode to contribute significantly in the longitudinal direction. Similar observations can be made for other modes from Table 4.1.

The mode shapes and natural frequencies discussed above consisted of all the system frequencies. For earthquake response analysis, all these frequencies and modes may not be excited, and therefore all the frequencies are not required. The Ritz-vector based method yields frequencies and mode shapes that provide significant participation in all directions. These frequencies and their mass participation are presented in Table 4.2. By comparing Tables 4.1 and 4.2, it is seen that the modes with very less mass participation in all the three directions are omitted by Ritz vector based eigenvalue extraction method. From Table 4.2, it is seen that the mass participation in all the three directions is more than 90%, and this indicates that model will give reasonable response under earthquake type loading.

5. Seismic Response Analysis

5.1 General

A number of different analytical methods have been developed for assessing the seismic vulnerability of existing bridges including elastic analysis, inelastic pushover analysis, capacity spectrum analysis and nonlinear dynamic analysis (Priestly et al. 1996). Each approach incorporates different assumptions and varies in complexity of application. The problem of an engineer assessing the seismic vulnerability of a bridge structure is to select the most appropriate and cost-effective method for performing the assessment. Under minor ground motions, a bridge will experience little inelastic behavior, and thus the linear elastic analysis is sufficient for bridge design and assessment for minor earthquakes. A limitation of the elastic analysis method is that the linear analysis offers little information regarding the inelastic response of the structure. Disadvantages of nonlinear dynamic time-history analysis are that the structural elements of nonlinear models are considerably more complex than that of their linear elastic counterparts, the numerical algorithms do not always ensure convergence to a physically valid solution, processing and evaluation of the output often require considerable effort, and the results can be extremely sensitive to input parameters and structural models.

In this work, modal time-history analysis is used because the bridge is assumed to behave elastically linear with small displacements under the expected earthquake loading. The Modal time-history method was used instead of the response spectrum method for the main bridge due to the importance of the bridge and also due to the lack of seismic considerations in its initial design. Time-history analysis is the most sophisticated analysis technique available to the structural analyst. Using this type of analysis affords the engineer a complete description of the behavior of a structure at all times throughout an earthquake. Since no strong earthquake records are available for the Eastern U.S., time-history analyses for Kentucky bridges were performed using artificial earthquake records characteristic of the New Madrid and other nearby seismic zones.

The Modal time-history method for the earthquake analysis involves the solution of the following equation of motion:

$$M\ddot{u} + C\dot{u} + Ku = -M\ddot{u}_g \qquad (5.1)$$

where **M,** C and **K** are the system mass, damping and stiffness matrices, respectively. $\ddot{u}$, $\dot{u}$ and **u** are the system nodal acceleration, velocity and displacement vectors. $\ddot{u}_g$ is the earthquake motion for which the bridge's response has to be calculated. The SAP90 software performs exact integration of the modal-response equations for a linear variation of the time-function between the input data time points. Therefore, the results are not dependent on the selection of a "time-integration interval" as in some other methods [Wislon and Habibullah, 1994]. Damping for all the modes is assumed to be 5%.

Time-histories representing the 50-year event and the 500-year event were generated for the vertical and two orthogonal horizontal directions in the report by Street et al. (1996). The 50-year event is defined as: the peak horizontal particle acceleration, at the top of rock, that has a 90% probability of not being exceeded in 50 years (i.e. 10% probability of exceedance). Likewise, the 500-year event has a 90% probability of not being exceeded in 500 years. A recurrence rate (return period) can be calculated for the earthquakes which would produce the 50- and 500-year events.

The 50-year event that has a 10% probability of exceedance corresponds to AASHTO's (1996) design earthquake for highway bridges. For low probability of exceedance, the recurrence rate is approximately (National Highway Institute, 1996) the ratio of time and return period. Actual return period for the 50-year event is 475 years (Mayes et al. 1992). Some states require even longer return periods for their design earthquake. For example, California's Department of Transportation (Caltrans) uses a 2400-year return period, which has a 10% probability of exceedance every 250 years.

For the seismic zones affecting Kentucky, the 50-year and 500-year events defined in Street et al. (1996) correspond to the AASHTO design earthquake and near the maximum credible earthquake, respectively. For the bridge location in this study, Henderson County, Kentucky, a time-history with peak horizontal acceleration of 15% gravity represents the AASHTO design earthquake. The time-history for the "near maximum credible earthquake" (500-year event) has a peak horizontal acceleration of 15% gravity in Henderson County.

5.2 Seismic Response

The seismic response of the US41 Northbound bridge is calculated for the 50-year earthquake. For the Henderson County bridge site, peak horizontal bedrock acceleration for this artificial earthquake is 15% gravity as mentioned in Street et al. (1996) (Figure 5.1). For comparison, AASHTO's map (1996) of peak horizontal acceleration places the Henderson County bridge site in, approximately, the 25% gravity contour for the same probability event. Earthquake duration is 2.6 seconds with data points at 0.005 second intervals. The input histories along longitudinal, transverse and vertical directions are presented in Figures 5.2-5.4, respectively. The peak ground accelerations along

horizontal, vertical and transverse directions are 56.3, 35.7 and 56 in/sec^2, respectively. Since the longitudinal direction of the earthquake may not coincide with the longitudinal direction of the bridge, it is necessary to analyze the bridge under different excitation cases as described in Table 5.1. Under LL11 excitation case, as mentioned in Table 5.1, the horizontal earthquake is applied along the longitudinal direction of the bridge, and vertical earthquake is applied along the vertical direction of the bridge. Similarly for other excitation cases, the vertical earthquake is considered to be acting in the vertical direction of the bridge. Only the horizontal and transverse earthquakes are reversed. On some excitation cases, all three direction earthquakes are applied simultaneously.

Time-history analysis produces a very large quantity of output. It is difficult to monitor the maximum forces for all the members and maximum displacements at all the joints in a modal time-history analysis for the seismic excitation kind of loading. Therefore, members and joints are selected based on their proximity to critical locations. From SAP90 software, forces and moments are obtained for selected members. Stresses are calculated externally using simple computer programs/spreadsheets. Table 5.2 presents the cross-sectional properties of members that are selected for stress calculation.

As an example, for the L1T2V3 (Table 5.1) earthquake, the time history plots of transverse, vertical and longitudinal displacements at joint 44 (Fig. 2.5) are presented in Figures 5.5-5.7, respectively. It is observed that the maximum transverse displacement of 0.41" occurs at 2.52 secs, maximum vertical displacement of 0.263" occurs at 0.705 secs, and the maimum in longitudinal direction is 0.27" at 1.76 secs. The axial force time history for member 1 (Fig. 2.6) is presented in Figure 5.8. The maximum axial force of 151 kips occurs at 1.01 secs.

For stress calculations, the axial stresses are calculated from P/A and bending stresses are calculated from M_{12}/Z_{13} and M_{13}/Z_{12}. M_{12} and M_{13} are the bending moments in the local 1-2 and 1-3 planes respectively. Z_{12} and Z_{13} are the section modulus about the 1-2 and 1-3 planes, respectively. Combined stresses are calculated as the sum of P/A, M_{12}/Z_{13}, M_{13}/Z_{12} with appropriate signs to get the maximum stresses.

Axial stress = σ_a = Axial force/Area
Bending stress in 1-2 plane at Ith joint = σ_{b12i} = Absolute(M_{12} at Node I / Z_{13})
Bending stress in 1-2 plane at Jth joint = σ_{b12j} = Absolute(M_{12} at Node J / Z_{13})
Bending stress in 1-3 plane at Ith joint = σ_{b13i} = Absolute(M_{13} at Node I / Z_{12})
Bending stress in 1-3 plane at Jth joint = σ_{b13j} = Absolute(M_{13} at Node J / Z_{12})

Combined axial and bending stress:

Stress at node I = $\sigma_a + \sigma_{b12i} + \sigma_{b13i}$
Stress at node J = $\sigma_a + \sigma_{b12j} + \sigma_{b13j}$

Shear stress is calculated from the shear forces in 1-2 and 1-3 plane, i.e.,

$$\text{Shear stress} = \tau = \{ \text{Square root of } [(SF_{12})^2 + (SF_{13})^2]\}/\text{Area}$$

The absolute maximum of stresses obtained from the maximum and minimum responses from time-history analysis are presented in tabular form and are discussed in the following. Table 5.3 lists the stresses at selected members (Figs. 2.3-2.7) due to seismic excitation case L1T2V3 (Table 5.1). Due to earthquake motion alone, the axial stresses are found to be larger than the bending stresses with a maximum of 1.69 ksi in member 1. Bending stresses are calculated and presented at nodes I and J of the member. Table 5.3 also presents the maximum of the combined stresses from the Dead load ± Earthquake load (EQ) ± Thermal load (90° F). Shear stress is found to be very low with a maximum of 2.5 ksi in member 175. The maximum of combined axial and bending stress is found to be 30.6 ksi in member 1, which is less than the yield strength of steel (36 ksi).

Table 5.4 lists the stresses at selected members (Figs. 2.3-2.7) when two of the excitation directions are reversed, i.e. under L2T1V3 (Table 5.1) case. Axial stresses due to seismic forces alone are found to have a maximum of 1.086 ksi in member 17. This Table 5.4 also presents the maximum of the combined stresses from the Dead load ± Earthquake load (EQ) ± Thermal load (90° F). Shear stresses are much less with a maximum of 2.57 ksi in member 175. Maximum of the combined stresses is found to be 34.7 ksi in member 274, which is less than the yield strength of steel.

Under the seismic excitation case LL11, the stresses calculated for selected members (Figs. 2.3-2.7) are presented in Table 5.5. The maximum axial stress is found to be 1.65 ksi in member 1. Maximum of the combined axial and bending stress is found to be 4.06 ksi in member 222, which is less than the yield strength. Shear stress is found to have a maximum of 0.14 ksi in member 276.

Table 5.6 lists the stresses at selected members (Figs. 2.3-2.7) when the seismic excitation LL22 is applied. The maximum axial stress is found to be 1.037 ksi in member 17. Maximum of the combined axial and bending stress is 3.2 ksi in member 222, which is far less than the yield stress of steel. Shear stress is found to have a maximum of 0.085 ksi in member 276.

For the seismic excitation case TT11, the stresses at selected members (Figs. 2.3-2.7) are presented in Table 5.7. The maximum axial stress is found to be 1.06 ksi in member 277. Maximum of the combined axial and bending stress is 3.04 ksi in member 304, which is less than the yield strength of steel. Shear stress is found to have a maximum of 0.2 ksi in member 175.

Table 5.8 lists the stresses at selected members (Figs. 2.3-2.7) when the seismic excitation TT22 is applied. The maximum axial stress is found to be 0.98 ksi in member

224. The maximum of the combined axial and bending stresses is 3.71 ksi in member 176 which is less than the yield stress of steel. The shear stress is found to have a maximum of 0.22 ksi in member 276.

The stresses at selected members (Figs. 2.3-2.7) due to a differential temperature of 90°F are presented in Table 5.9. The coefficient of thermal expansion for steel is taken as 6.5 x 10^{-6}/°F. Maximum axial stress is found to be 14.4 ksi in member 1. Maximum shear stress is obtained as 0.2 ksi in member 179. Combined stress from axial and bending is 24.22 ksi in member 1.

Table 5.10 lists the stresses at selected members (Figs. 2.3-2.7) due to the self-weight of the bridge. Maximum axial stress is found to be 11.54 ksi in member 102. Maximum shear stress is obtained as 2.26 ksi in member 175. Combined stresses from axial and bending stresses have a maximum of 30.6 ksi in member 221.

In previous calculations, the stresses produced were checked purely from the material yield point of view. Under earthquake loading, truss members may experience tensile force at one time interval and compressive force at some other time interval.

$$\frac{f_a}{F_y} + \frac{f_{bx}}{F_{bx}} + \frac{f_{by}}{F_{by}} \le 1.0 \qquad (5.3)$$

Therefore, it is necessary to check for the buckling of truss members. Since the bridge truss members are subjected to axial forces and bending moments, the equations (10-42) to (10-44) from AASHTO are used to check whether they satisfy the inequality condition.

AASHTO Eq. (10.42):

$$\frac{C_{mx} f_{bx}}{\left(1 - \frac{f_a}{F_{ex}}\right) F_{bx}} + \frac{C_{my} f_{by}}{\left(1 - \frac{f_a}{F_{ey}}\right) F_{by}} \le 1.0 \qquad (5.2)$$

AASHTO Eq. (10-43): At points of support
AASHTO Eq. (10-44): Euler Buckling Stress:

$$F_e = \frac{\pi^2 E}{(0.75\ L/r)^2} \qquad (5.4)$$

$$F_{ey} = \frac{\pi^2 E}{(0.75\ L/r_y)^2} \qquad (5.5)$$

In Table 5.11 and 5.12, the stresses are checked by also considering the buckling of the member for the earthquake excitation cases L1T2V3 and L2T1V3, respectively. It is seen that the inequalities given in equations 10-42 and 10-43 are satisfied, and hence there will not be any member failure due to combined axial and bending stresses.

The displacements at selected nodes (Figs. 2.3-2.7) are presented in Table 5.13 for different excitation cases (Table 5.1). Maximum displacement in the longitudinal direction is 0.36" at joint 9 under LL11 case. Maximum displacement in the transverse direction is 0.5" at joint 140 under L1T2V3 case. Maximum displacement in the vertical direction is 0.47" at joint 62 under LL11 case.

Under static dead load and temperature, the displacements at selected joints (Figs. 2.3-2.7) are listed in Table 5.14. Due to a temperature difference of 90°F, maximum displacement in the longitudinal direction is 2.4" at the joint 1. The transverse displacement is maximum at joint 10 is 1.6". Maximum vertical displacement is 1.32" at joint 62. Due to dead load, maximum longitudinal displacement is 0.68" at joint 13. Transverse displacement is with a maximum of 0.58" at joint 10. The maximum vertical displacement is 10.03" at joint 44.

Maximum and minimum base shears obtained for the bridge are listed in Table 5.15. These values are presented for different excitation cases listed in Table 5.1. Then, based on the translational stiffnesses of the piers, longitudinal and transverse seismic forces on top of the pier are calculated and presented in Table 5.16.

5.3 Capacity/Demand Ratios and Retrofit for the Main Bridge

Since the superstructure of the bridge is connected to the substructure through bearings, it is necessary to check these bearings against anchor bolt shear failure. Table 5.16 lists the available anchor bolt shear capacity (V_c) and seismic forces on each pier. The anchor bolt capacity V_c is calculated by assuming the shear strength of the bolt as 26.97 ksi.. The resultant of seismic force is calculated as the square root of the sum of squares (SRSS)of the longitudinal and transverse seismic forces. Then the seismic demand (V_b) is calculated by multiplying by 1.25 as per *FHWA Retrofitting manual.* All the piers have C/D ratio less than 1.0. Therefore, additional anchor bolts or seismic isolation bearings are required.

The expansion bearings at piers A, B and E are roller bearings. Hence complete loss-of-span may not occur. Therefore bearing displacement capacity/demand ratio is not calculated.

5.4 Retrofit for the Main Bridge

From the previous sections, it is clear that all the bearings are to be strengthened to resist the 0.15g earthquake corresponding to 50-year event. It is suggested that additional anchor bolts may be provided to retrofit the bearings at piers A, B, C, D and E. Alternatively, the bearings may be replaced with seismic isolation bearings. The recommendations are listed in Table 5.16 and in Figures 5.9 through 5.13.

6. Approach Spans

6.1 General

The northbound US41 bridge over the Ohio river consists of straight approach spans on Kentucky and Indiana sides. The approach bridges towards the Henderson, KY side and Evansville, IN side are shown in Figures 6.1a-d. The plan and elevation of the Evansville, IN and Henderson, KY approaches are shown in Figures 6.2 and 6.3, respectively. The Evansville, IN approach, consists of 8-simply supported spans with a total length of 1064′ , and the Henderson, IN approach consists of 35 simple spans covering a total length of 2038′ 6″ which provides a clear 30′ wide roadway and 2′ wide side walk on either sides. The spans in both the approaches are supported on piers through fixed bearing and expansion bearing as indicated in figures 6.2 and 6.3. All the piers and abutments are founded on friction piles which extend up to 60′ to 100′ depending on the soil resistance.

The Evansville, IN approach has 5 deck truss spans of each 150′ and 3 girder spans of each 100'. The Henderson, KY approach has 3 deck-truss spans of each 150', 2 girder spans of each 100' and 30 girder spans of each 46'. The 150′-spans are made of two deck-type parallel chord trusses spaced at 28′ c/c. The 7″ thick concrete deck is supported on a steel stringer and floor beam system. The superstructure in the 100′-spans is similar to 150′-spans except that the trusses are replaced with plate girders. In the 46′-spans, the 7″-concrete deck is directly supported by 7-nos. of steel girders (I-section).The reinforced concrete bridge piers have rectangular sections and taper along the height with a batter of $\frac{1}{2}$″ per foot length. The sub-structure in the approach spans is made with class A concrete.

6.2 Structural Modeling

The approach spans on the Evansville, IN side and Henderson, KY side are idealized as simple structural units depending on the type of bearing (attachment of superstructure mass) to the pier top. These idealized units are assumed to act independently when subjected to motion in the longitudinal direction of the bridge. These simplified systems are treated as single degree of freedom systems (SDOF) for mathematical modeling of the bridge in the longitudinal direction. The models are designated as EV1-EV6 for the Evansville, IN approach and HE1-HE33 for the Henderson, KY approach. The details of the components of these models are given in Figure 6.4 and 6.5 respectively. The mass of the SDOF systems is assumed to be contributed by the mass of the superstructure and one-third mass of the pier. The stiffness

is the longitudinal translation stiffness of the piers that is calculated using $\frac{3EI}{L^3}$. The modulus of elasticity of concrete is assumed as 3275 ksi. The average moment of inertia of the pier is used for the stiffness calculation.

An important point to be noted at this time is that there exists a lot of uncertainty in quantifying the soil-structure (pile foundation) interaction effect in the stiffness calculation. Due to the unavailability of detailed site soil investigations, representative models with maximum and minimum stiffness are adopted in the forces and displacements calculations, respectively. The maximum stiffness is obtained by assuming the pier is fixed at the bottom of pile cap. The minimum stiffness is obtained by assuming the pier is extended up to an imaginary depth equal to half-pile-length and fixed at that level. The extended length is assumed to have the same flexural properties as that of the pier. This simplified procedure for stiffness estimation has been validated to represent the most stiff and most flexible model and hence adopted for the conservative estimate of seismic forces and displacements in this study.

The weight calculations for the superstructure in the 150′, 100′ and 46′ spans is given in Tables 6.1a-c. The dimensions and section properties of the pier and the stiffness (maximum and minimum) in the longitudinal direction calculations for all the models in the approach spans are listed in Table 6.2. The mass includes one-third mass of the pier and that of the super-structure attached to the pier by fixed bearing.

6.3 Seismic Response Analysis

Since the bridge is located in Henderson county, KY, it is analyzed under seismic motion corresponding to 0.15g earthquake of the 50-year event. The response spectra of this earthquake is presented by Street et al. (1996). The study of damage to multi-span simple bridges reveals that longitudinal seismic waves have caused more damage than transverse (Zimmerman and Brittain, 1979). In this work, seismic analysis is performed to determine any loss-of-span due to excessive longitudinal displacement or shear failure of the bearings. In this work, seismic analysis of the simplified SDOF models for the approach spans is carried out using the response spectrum method.

The response spectrum method is a technique for obtaining the solution of the coupled, second-order, linear, differential equations of motion that govern the forced vibration of a bridge. This method involves an initial eigenvalue analysis to determine the natural frequencies and mode shapes of the bridge. The orthogonality of the mode shapes with respect to the mass, stiffness and damping matrices is then used to uncouple the equations of motion. The peak response associated with the single-degree-of-freedom system represented by each of the uncoupled equations of motion is obtained through the use of an elastic earthquake response spectrum. An estimate of the maximum response

of the structure is determined by combining the peak responses of the individual modes based on statistical procedures.

The results of the seismic analysis are utilized to determine the possibility of any loss-of-span due to the excessive longitudinal displacements at expansion bearings or shear failure of anchor bolts in fixed bearings. Seismic analysis is carried out using the response spectrum method.

The natural frequencies of the SDOF models are presented in Table 6.3 with corresponding masses and stiffness. The calculated natural frequencies range from 2.86 Hz to 12.5 Hz for the model with maximum stiffness and 0.88 Hz to 1.75 Hz for the model with minimum stiffness.

The response spectra for the Henderson, KY is shown in Figure 6.6. This response spectra corresponds to a damping of 5%. The site soil coefficient S is assumed as 1.5 for the calculation of the seismic response coefficient C_s based on AASHTO (Div. IA, section 3), $C_s = \frac{1.2(PSA)(S)}{g}$. The C_s is limited to 2.5A, i.e 0.375 as per AASHTO. In the calculation of forces, for all models, C_s is governed by this maximum limit of 0.375. Seismic forces and displacements are calculated and presented in Table 6.3. The calculated displacements range from 1" to 4". The seismic forces range from 94 kips to 664 kips.

6.4 Capacity/Demand Ratios

For both the approach spans, the bearing force capacity $V_b(c)$ /demand $V_b(d)$ ratios, have been calculated as per section A.4.3 of *FHWA Seismic Retrofitting Manual for Highway Bridges* (Buckle et al. 1995). The seismic force demand $V_b(d)$ is considered as the maximum of 1.25 times the seismic force and 0.2 times the weight of the superstructure. The anchor bolt ultimate shear capacity $V_b(c)$ is calculated by assuming the shear strength of bolt material as 19.0 ksi (for 33 ksi steel). The Capacity / Demand ratios are less than 1.0 for thirteen out of forty-two supports having fixed bearings. The bearings at these locations are to be retrofitted with additional anchor bolts or the bearings need to be replaced with seismic isolation bearings so as to withstand the forces due to an earthquake.

For both the approach spans, the expansion bearing displacement Capacity/Demand ratios (rbd) are calculated as per section A.4.2 of FHWA seismic Retrofitting Manual for Highway Bridges (Buckle et al. 1995). The C/D ratios are calculated according to both method-1 and method-2. The expansion bearings at pier S6 to S35 in the Henderson, KY approach span are of sliding plate type. The movement in the longitudinal direction at this type of bearing during an earthquake is limited. And

therefore, only method-2 is used for calculating the displacement Capacity/Demand ratios at these bearings. All other expansion bearings are of roller type, and both methods are used for C/D calculations. The bearing displacement Capacity/Demand ratios, r_{bd}, are greater than 1.0 for all the expansion bearings and hence loss-of-span cannot occur due to the relative displacements occurring due to the projected earthquake.

For the Evansville, IN approach, the bearing Capacity $V_b(c)$/Demand $V_b(d)$ ratios and displacement Capacity/Demand ratios are presented in Tables 6.4 and 6.5 respectively. Similarly for the Henderson, KY approach spans, the bearing Capacity $V_b(c)$/Demand $V_b(d)$ ratios and displacement Capacity/Demand ratios are presented in Tables 6.6 and 6.7 respectively.

6.5 Retrofit Recommendations

From the previous sections it is clear that thirteen out of forty-two supports having fixed bearings are to be strengthened to resist the 0.15g earthquake corresponding to 50-year event at Henderson, KY. It is suggested that additional anchor bolts may be provided to retrofit these bearings or all these bearings may be replaced with seismic isolation bearings.

For the Evansville, IN approach spans, the retrofit recommendations for the fixed bearings are presented in Table 6.4 and in Figures 6.7 through 6.12. Similarly, for the Henderson, KY approach spans, the retrofit recommendations for the fixed bearings are presented in Table 6.6 and in Figures 6.13 through 6.16.

7. Conclusions and Recommendations

7.1 General

The US41 northbound bridge over the Ohio river may be subjected to future earthquakes. Therefore, it is important to evaluate the bridge under the projected seismic motion. In this study, since the bridge is located in Henderson, Kentucky, 0.15g earthquake for the 50-year event is applied. Depending upon the importance of the bridge, it has been decided to use more rigorous methods for the evaluation of the main bridge and simplified methods for the approach spans.

7.2 Main Bridge

The seismic evaluation of the main bridge consisted of field ambient vibration testing, finite element modeling and seismic response analysis using the modal time-history method. Field testing was mainly carried out to identify the natural frequencies and their mode shapes. These frequencies and mode shapes have been compared with the results from the finite element model. Comparisons have been performed for three transverse modes, three vertical modes and one longitudinal mode.

A three dimensional finite element model was developed with frame elements and spring elements. This model has been calibrated with the field test for natural frequencies and mode shapes. Frequencies from the field test for the first modes in the transverse, vertical and longitudinal directions are 0.5344, 0.8016 and 1.9372 Hz, respectively. Frequencies from the finite element model for the first modes in the transverse, vertical and longitudinal directions are 0.5342, 0.7807 and 1.8536 Hz, respectively. Reasonable agreement between the field test and the finite element model has been obtained.

Seismic response analyses have been carried out using the modal time-history method. Displacements of selected joints and stresses for selected members have been calculated. The results are also presented for different seismic excitation cases by reversing the seismic excitation directions. Stresses for selected members are also presented for combined earthquake, dead load and thermal loads. For the selected joints, under earthquake excitation, the maximum displacement in the transverse, vertical and longitudinal direction was found to be 0.5", 0.47" and 0.36", respectively. Maximum of combined axial and bending stress in the member is found to be 34.7 ksi. These stresses are less than the yield stress of steel and hence material yielding may not occur. Bending stresses have been combined with axial stresses by considering the buckling of members. It was found that for the selected members buckling failure will not occur.

Bearing force Capacity/Demand ratios have been calculated for the bearings at all the piers. All the piers have C/D ratios less than 1.0 and hence retrofit is required in the form of additional anchor bolts. Alternatively, the existing bearings may be replaced with seismic isolation bearings. The recommendations are presented in Table 5.16 and in Figures 5.9 through 5.13.

7.3 Approach Spans

The US41 northbound bridge has approach spans on the Kentucky and Indiana sides. Most of the approach spans are single-span with expansion bearing at one support and fixed bearing at the other. Therefore, single-degree-of-freedom models were used along with response spectrum method for the seismic response analysis. Response analysis has been carried out only in the longitudinal direction of the bridge, and maximum displacement and force responses have been calculated.

At thirteen out of forty-two supports having fixed bearings in both the approach spans, force Capacity/Demand ratios were less than 1.0; therefore, retrofit in the form of additional anchor bolts or replacing the existing bearings with the seismic isolation bearings is recommended. Displacement Capacity/Demand ratios were greater than one for all supports and hence loss-of-span cannot occur in both the approach spans.

The retrofit recommendations for the Evansville, IN approach spans are presented in Tables 6.4 and in Figures 6.7 through 6.12 for the supports having fixed bearings. Similarly, for the Henderson, KY approach spans, the retrofit recommendations are presented in Tables 6.6 and in Figures 6.13 through 6.16 for the supports having fixed bearings.

REFERENCES

AASHTO, (1996), *Standard Specifications for Highway Bridges*, 16th Edition, American Association of State Highway and Transportation Officials, Washington D.C.

Abdel-ghaffer, A.M. and R. H. Scanlan (1985a), Ambient Vibration Studies of Golden Gate Bridge: I. Suspended Structure, ASCE J. of Engrg. Mech., 111(4), 463-482.

Abdel-ghaffer, A.M. and R. H. Scanlan (1985b), Ambient Vibration Studies of Golden Gate Bridge: II. ASCE J. of Engrg. Mech., 111(4).

Alampalli, S., and Fu, G., (1994), "Instrumentation for Remote and Continuous Monitoring of Structural Condition," Paper No. 940261 Presented at the Transportation Research Board's 73rd Annual Meeting, Washington D.C., January, 1994.

Bathe, K.J., (1982), *Finite Element Procedures in Engineering Analysis*, Prentice-Hall, Inc., Englewood Cliffs, New Jersey, chapter 12.

Buckland, P.G., et al., (1979), "Suspension Bridge Vibrations: Computed and Measured," *Journal of the Structural Division*, Vol. 105, No. ST5, pp. 859-874.

Buckle, I.G. and I. M. Friedland (editors), Seismic Retrofitting Manual for Highway Bridges, Report No. FHWA-RD-94-052, Federal Highway Administration, May 1995.

Chapra, S.C., and Canale, R.P., (1988), *Numerical Methods for Engineers*, 2nd Edition, McGraw-Hill, Inc., New York, New York, Chapter 13.

DADiSP 4.0 User Manual, (1995), DSP Development Corporation, Cambridge, Massachusetts.

Doll, H., (1994), "Eigenfrequencies and Normal Modes of the Norderelb Bridge Near Hamburg: Numerical and Measuring Investigations," Proceedings of *the 12th International Modal Analysis Conference*, Honolulu, Hawaii, pp. 449-455.

EERI, Loma Prieta earthquake renaissance report, Earthqukae spectra, Special supplement to Vol.6, 448pp, May 1990.

EERI, Northridge earthquake renaissance report, Earthquake spectra, Special supplement to Vol.11, 116pp, Feb.95.

Farrar, C., White, K., and Mayes, R., (1995), "Vibration Testing of the I-40 Bridge Before and After the Introduction of Damage," Presented at the North-American Workshop on Instrumentation and Vibration Analysis of Highway Bridges, Cincinnati, Ohio, July, 1995.

Harik, I.E., D. Dietz, C. Hill and M.W. Guo, Seismic Evaluation and Retrofit of Bridges, Research Report KTC-96-5, Kentucky Transportation Center, University of Kentucky, 1997.

Harik, I.E., D. L. Allen, R. L. Street, M.W. Guo, R.C. Graves, J. Harrison and M. J. Gawry (1997a), Free and Ambient Vibration of Brent-Spence Bridge, ASCE J. of Struct. Engrg., 123(9), 1262-1268.

Harik, I.E., D. L. Allen, R. L. Street, M. W. Guo, R.C. Graves, J. Harrison, and M. J. Gawry(1997b), Seismic Evaluation of Brent-Spence Bridge, ASCE J. of Struct. Engrg., 123(9), 1269-1275.

Harik, I.E., C.M. Madasamy, D. Chen, L. Zhou, K. Sutterer, R. Street, and D.L. Allen , Seismic Evaluation of the Ohio River Bridge on US51 at Wickliffe, KY, Research Report KTC-98-20, Kentucky Transportation Center, University of Kentucky, 1998.

Hudson, D.E., (1977), "Dynamic Tests of Full-Scale Structures," Journal of the Engineering Mechanics Division, Vol. 103, No. EM6, pp. 1141-1157.

Mayes, R.L., et al., (1992), "AASHTO Seismic Isolation Design Requirements for Highway Bridges," *Journal of Structural Engineering*, Vol. 118, No. 1, pp. 284-304.

National Highway Institute (NHI) Course No. 13063, (1996), "Seismic Bridge Design Applications," Notes from Sessions 1 & 2.

Nuttli, O.W., and R.B. Herrman (1978), State-of-the-art for assessing earthquake hazards in the United States: Report 12, Credible earthquakes for the central United States, U.S. Army Corps of Engineers Miscellaneous Paper S-73-1, 99pp.

Obermeier, S.F., P.J. Munson, C.A. Munson, J.R. Martin, A.D.Frankel, T.L.Youd, and E.C.Pond (1992), Liquefaction evidence for strong Holocene earthquakes in the Wabash Valley of Indiana-Illinois, Seismological Research Letters,63, 321-335.

Paultre, P., Proulx, J., and Talbot, M., (1995), "Dynamic Testing Procedures for Highway Bridges Using Traffic Loads," *Journal of Structural Engineering*, Vol. 121, No. 2, pp. 362-376.

Press, W.H., et al., (1992), *Numerical Recipes in FORTRAN: The Art of Scientific Computing*, 2nd Edition, Cambridge University Press, New York, New York, chapter 12.

Priestly, M.J.N., F. Seible and G. M. Calvi, Seismic Design and Retrofit of Bridges, John-Wiley & Sons, Inc., 1996.

Saiidi, M., Douglas, B., and Feng, S., (1994), "Prestress Force Effect on vibration Grequency of Concrete Bridges," *Journal of Structural Engineering*, Vol. 120, No. 7, pp. 2233-2241.

Shahawy, M.A., (1995), "Non Destructive Strength Evaluation of Florida Bridges," Proceedings of SPIE Nondestructive Evaluation of Aging Infrastructure Conference, Oakland, California, June, 1995.

Shelley, S.J., et al., (1995), "Dynamic Testing (Vibration Analysis) of Highway Bridges," Notes Presented at the *North-American Workshop on Instrumentation and Vibration Analysis of Highway Bridges*, Cincinnati, Ohio, July, 1995.

Stover, C.W. and Hoffman, J.L. (1993). Seismicity of the United States, 1568-1989 (Revised), U.S. Geological Survey Professional Paper 1527, 418 p.

Taylor, K.B., R.B. Herrmann, M.W. Hamburger, G.L. Pavlis, A. Johnston, C. Langer, and C. Lam (1989), The Southern Illinois Earthquake of 10 June 1987, Seismological Research Letters, 60, 101-110.

Street, R. (1980) "The Sourhtern Illinois Earthquake of Spetember 27, 1891, Bulletin of the Seismological Society of America, 70, 915-920.

Street, R., Z. Wang, I. E. Harik, D. L. Allen and J. J. Griffin (1996), Source Zones, Recurrence Rates, and Time Histories for Earthquakes Affecting Kentucky, Report No. KTC-96-4, Kentucky Transportation Center, University of Kentucky, 1996.

Ventura, C.E., Felber, A.J., and Prion, G.L., (1994), "Seismic Evaluation of a Long Span Bridge by Modal Testing," Proceedings of the *12th International Modal Analysis Conference*, Honolulu, Hawaii, pp. 1309-1315.

Wendichansky, D.A., Chen, S.S., and Mander, J.B., (1995), "In-Situ Performance of Rubber Bearing Retrofits," Presented at National Seismic Conference on Bridges and Highways, San Diego, California, December, 1995.

Wilson, E.L. and A. Habibullah, SAP90 - Structural Analysis Users Manual, Computers and Structures, Inc, May 1992.

Wilson, E.L., M.W. Yuvan, and J.M. Dickens (1982), Dynamic Analysis by Direct Superposition of Ritz Vectors, Earthquake Engineering and Structural Dynamics, 10, 813-823.

Wilson, E.L., and Tetsuji, I.J., (1983), "An Eigensolution Strategy for Large Systems," *Computers and Structures*, Vol. 16, pp. 259-265.

Zimmerman, R. M. and Brittain, R. D. (1979), Seismic response of multi-simple span highway bridges, In: proceedings of the 3rd Canadian Conference on Earthquake Engg., Montreal, pp1091-1120.

Table 3.1a US41 Northbound Bridge Testing Details - Moving Stations on Right Lane

Station	Filename	Accelerometer Block	Channel Number (xx)	Orientation
1	E1chXX.dat	Yellow	20 21 22	Horizontal Transverse Vertical
2		White	17 18 19	Horizontal Transverse Vertical
3		Red	14 15 16	Horizontal Transverse Vertical
4		Orange	11 12 13	Horizontal Transverse Vertical
5		Green	8 9 10	Horizontal Transverse Vertical
6	E2chXX.dat	Yellow	20 21 22	Horizontal Transverse Vertical
7		White	17 18 19	Horizontal Transverse Vertical
8		Red	14 15 16	Horizontal Transverse Vertical
9		Orange	11 12 13	Horizontal Transverse Vertical
10		Green	8 9 10	Horizontal Transverse Vertical
11	E3chXX.dat	Yellow	20 21 22	Horizontal Transverse Vertical
12		White	17 18 19	Horizontal Transverse Vertical
13		Red	14 15 16	Horizontal Transverse Vertical
14		Orange	11 12 13	Horizontal Transverse Vertical
15		Green	8 9 10	Horizontal Transverse Vertical
16	E4chXX.dat	Yellow	20 21 22	Horizontal Transverse Vertical
17		White	17 18 19	Horizontal Transverse Vertical
18		Red	14 15 16	Horizontal Transverse Vertical
19		Orange	11 12 13	Horizontal Transverse Vertical
20		Green	8 9 10	Horizontal Transverse Vertical
21	E5chXX.dat	Yellow	20 21 22	Horizontal Transverse Vertical
22		White	17 18 19	Horizontal Transverse Vertical
23		Red	14 15 16	Horizontal Transverse Vertical
24		Orange	11 12 13	Horizontal Transverse Vertical
25		Green	8 9 10	Horizontal Transverse Vertical

Table 3.1b US41 Northbound Bridge Testing Details - Base Station on Right Lane

Moveable Station Locations	Filename	Accelerometer Block	Channel Number (XX)	Orientation
1	F1chXX.dat	Black	0	Horizontal
2			1	Transverse
3			2	Vertical
4		Blue	3	Horizontal
5			4	Transverse
			5	Vertical
6	F2chXX.dat	Black	0	Horizontal
7			1	Transverse
8			2	Vertical
9		Blue	3	Horizontal
10			4	Transverse
			5	Vertical
11	F3chXX.dat	Black	0	Horizontal
12			1	Transverse
13			2	Vertical
14		Blue	3	Horizontal
15			4	Transverse
			5	Vertical
16	F4chXX.dat	Black	0	Horizontal
17			1	Transverse
18			2	Vertical
19		Blue	3	Horizontal
20			4	Transverse
			5	Vertical
21	F5chXX.dat	Black	0	Horizontal
22			1	Transverse
23			2	Vertical
24		Blue	3	Horizontal
25			4	Transverse
			5	Vertical

Black Accelerometer: West side of Bridge (Left lane)
Blue Accelerometer: East side of Bridge (Right lane)
All data saved in g's

Table 3.2a US41 Northbound Bridge Testing Details- Moving Station on Left Lane

Station	Filename	Accelerometer Block	Channel Number (xx)	Orientation
1	G1chXX.dat	Yellow	20 21 22	Horizontal Transverse Vertical
2		White	17 18 19	Horizontal Transverse Vertical
3		Red	14 15 16	Horizontal Transverse Vertical
4		Orange	11 12 13	Horizontal Transverse Vertical
5		Green	8 9 10	Horizontal Transverse Vertical
6	G2chXX.dat	Yellow	20 21 22	Horizontal Transverse Vertical
7		White	17 18 19	Horizontal Transverse Vertical
8		Red	14 15 16	Horizontal Transverse Vertical
9		Orange	11 12 13	Horizontal Transverse Vertical
10		Green	8 9 10	Horizontal Transverse Vertical
11	G3chXX.dat	Yellow	20 21 22	Horizontal Transverse Vertical
12		White	17 18 19	Horizontal Transverse Vertical
13		Red	14 15 16	Horizontal Transverse Vertical
14		Orange	11 12 13	Horizontal Transverse Vertical
15		Green	8 9 10	Horizontal Transverse Vertical
16	Q2chXX.dat	Yellow	20 21 22	Horizontal Transverse Vertical
17		White	17 18 19	Horizontal Transverse Vertical
18		Red	14 15 16	Horizontal Transverse Vertical
19		Orange	11 12 13	Horizontal Transverse Vertical
20		Green	8 9 10	Horizontal ansverse Vertical
21	Q3chXX.dat	Yellow	20 21 22	Horizontal Transverse Vertical
22		White	17 18 19	Horizontal Transverse Vertical
23		Red	14 15 16	Horizontal Transverse Vertical
24		Orange	11 12 13	Horizontal ansverse Vertical
25		Green	8 9 10	Horizontal Transverse Vertical

Table 3.2b US41 Northbound Bridge Testing Details - Base Station on Left Lane

Moveable Station Locations	Filename	Accelerometer Block	Channel Number (XX)	Orientation
1	H1chXX.dat	Black	0	Horizontal
2			1	Transverse
3			2	Vertical
4		Blue	3	Horizontal
5			4	Transverse
			5	Vertical
6	H2chXX.dat	Black	0	Horizontal
7			1	Transverse
8			2	Vertical
9		Blue	3	Horizontal
10			4	Transverse
			5	Vertical
11	H3chXX.dat	Black	0	Horizontal
12			1	Transverse
13			2	Vertical
14		Blue	3	Horizontal
15			4	Transverse
			5	Vertical
16	H4chXX.dat	Black	0	Horizontal
17			1	Transverse
18			2	Vertical
19		Blue	3	Horizontal
20			4	Transverse
			5	Vertical
21	H5chXX.dat	Black	0	Horizontal
22			1	Transverse
23			2	Vertical
24		Blue	3	Horizontal
25			4	Transverse
			5	Vertical

Black Accelerometer: West Side of Bridge (Left lane)
Blue Accelerometer: East side of Bridge (Right lane)

All data saved in g's
Sampling rate is 1002 Hz

Table 3.3 Frequency Identification from the Field Test Data

Field Tested frequency, f_1 (Hz)	Number of Peaks - Right Side			Number of Peaks - Left Side			Mode Type	Finite Element Frequencies, f_2 (Hz)	Relative Error 100*(f1-f2)/f1
	Transverse Direction	Vertical Direction	Longitudinal Direction	Transverse Direction	Vertical Direction	Longitudinal Direction			
0.1336	7	12	15	11	10	14			
0.167	14	7	8	11	12	9			
0.2004	4	6	10	6	4	8			
0.2338	12	10	8	8	12	8			
0.2672	7	4	5	7	7	9			
0.3006	11	13	11	11	9	11			
0.334	6	5	9	9	10	8			
0.3674	10	12	7	6	11	5			
0.4008	6	7	5	7	6	9			
0.4342	7	7	11	4	10	10			
0.4676	7	10	5	6	6	6			
0.501	8	6	9	7	13	13			
0.5344	**16**	7	10	**16**	4	6	**First Transverse**	0.534176	0.041934
0.5678	3	12	7	4	15	9			
0.6012	10	9	10	6	6	8			
0.6346	10	8	8	8	9	7			
0.668	**9**	5	3	**9**	9	7	**Second Transverse**	0.673915	0.877707
0.7014	10	7	11	7	7	11			
0.7348	11	8	7	14	9	8			
0.7682	2	2	4	1	7	6			
0.8016	**13**	**12**	16	**14**	**12**	10	**Third Transverse/ First Vertical**	0.780711	2.675638
0.835	6	4	6	3	**6**	6			
0.8684	15	7	8	9	12	11			
0.9352	8	11	8	6	4	10			
0.9686	11	5	11	9	6	8			
1.002	4	6	5	3	7	8			
1.0354	11	6	6	11	10	6			
1.0688	9	6	11	8	7	9			
1.1022	10	**10**	2	7	**11**	7	**Second Vertical**	1.06487	0.369059
1.1356	8	7	13	13	6	7			
1.169	9	10	3	6	12	11			
1.2024	10	2	15	9	5	3			
1.2358	6	7	3	5	6	7			
1.2692	5	9	9	9	10	8			
1.3026	12	8	6	7	4	10			

Table 3.3 (Cont'd) Frequency Identification from the Field Test Data

Field Tested frequency (Hz)	Number of Peaks - Right Side			Number of Peaks - Left Side			Mode Type	Finite Element Frequencies (Hz)	Relative Error 100*(f1-f2)/f1
	Transverse Direction	Vertical Direction	Longitudinal Direction	Transverse Direction	Vertical Direction	Longitudinal Direction			
1.336	4	11	8	11	10	4			
1.3694	10	**2**	8	6	**11**	11	**Third Vertical**	1.374965	2.83389
1.4028	5	13	9	5	4	8			
1.4362	5	9	10	5	7	9			
1.4696	13	0	6	9	11	6			
1.503	7	8	11	13	5	5			
1.5364	8	14	10	4	15	11			
1.5698	5	3	7	9	6	9			
1.6032	4	9	4	5	2	4			
1.6366	7	3	14	10	10	8			
1.67	8	11	5	8	4	4			
1.7034	8	7	7	11	8	13			
1.7368	10	6	6	6	8	6			
1.7702	7	8	6	10	4	4			
1.8036	10	5	12	7	7	4			
1.837	6	3	2	10	12	7			
1.8704	5	4	4	5	4	4			
1.9038	12	19	20	13	15	7			
1.9372	6	2	1	7	5	**11**	**First Longitudinal**	1.853653	2.705307
1.9706	3	8	7	5	7	11			
2.004	9	8	10	8	11	10			
2.0374	8	12	4	7	2	**1**			
2.0708	14	2	7	10	11	11			

Table 4.1 Natural Frequencies and Mass Participat42ion of the Main Bridge (Exact Eigen System)

Mode Number	Angular Frequency (rad/sec)	Circular Frequency (Hz)	Period (Sec)	Mass Participation			Cumulative Mass Participation		
				X-DIR	Y-DIR	Z-DIR	X-SUM	Y-SUM	Z-SUM
1	3.360	0.534	1.8720	0.001	3.582	0.001	0.001	3.582	0.001
2	4.230	0.674	1.4839	0.008	0.796	0.006	0.009	4.377	0.006
3	4.910	0.781	1.2809	0	14.499	0.001	0.009	18.876	0.007
4	5.160	0.821	1.2180	0.027	0.003	1.415	0.036	18.88	1.423
5	5.600	0.891	1.1220	0.001	0.106	0.001	0.037	18.986	1.423
6	6.420	1.022	0.9784	0.001	5.987	0.001	0.038	24.972	1.424
7	6.690	1.065	0.9391	0.037	0.008	0.381	0.075	24.98	1.805
8	7.070	1.126	0.8885	0.008	1.321	0.197	0.084	26.301	2.003
9	7.380	1.174	0.8519	0.001	3.86	0.007	0.084	30.162	2.009
10	8.640	1.375	0.7273	0.186	0.027	13.104	0.271	30.189	15.113
11	9.150	1.456	0.6869	0.007	0.416	0.629	0.278	30.605	15.743
12	9.670	1.539	0.6499	0	0.22	0	0.278	30.825	15.743
13	10.300	1.637	0.6108	0.022	0.042	12.903	0.299	30.867	28.645
14	10.300	1.640	0.6099	0.01	0.132	5.349	0.309	30.999	33.994
15	11.000	1.751	0.5710	2.357	0.01	0.366	2.666	31.009	34.36
16	11.600	1.854	0.5395	29.989	0.16	0.001	32.655	31.169	34.361
17	12.000	1.903	0.5254	3.523	0.479	0.182	36.177	31.648	34.543
18	12.400	1.981	0.5048	17.24	0.009	0.234	53.417	31.657	34.777
19	12.700	2.018	0.4954	0.03	0.616	0	53.447	32.273	34.777
20	13.100	2.082	0.4803	2.256	0.123	0.044	55.703	32.395	34.822

Table 4.2 Natural Frequencies and Mass Participation of the Main Bridge (Ritz-vector based)

Mode Number	Angular Frequency (rad/sec)	Circular Frequency (Hz)	Period	Mass Participation			Cumulative Mass Participation		
				X-DIR	Y-DIR	Z-DIR	X-SUM	Y-SUM	Z-SUM
1	3.360	0.5342	1.8720	0.001	3.582	0.001	0.001	3.582	0.001
2	4.230	0.6739	1.4839	0.008	0.796	0.006	0.009	4.378	0.006
3	4.910	0.7807	1.2809	0	14.498	0.001	0.009	18.876	0.007
4	5.160	0.8210	1.2180	0.027	0.003	1.412	0.036	18.879	1.419
5	5.600	0.8913	1.1220	0.001	0.106	0.001	0.036	18.985	1.42
6	6.420	1.0221	0.9784	0.001	5.985	0.001	0.038	24.97	1.42
7	6.690	1.0649	0.9391	0.037	0.008	0.379	0.075	24.978	1.799
8	7.070	1.1255	0.8885	0.008	1.322	0.199	0.083	26.3	1.998
9	7.380	1.1738	0.8519	0.001	3.858	0.007	0.084	30.158	2.005
10	8.640	1.3750	0.7273	0.186	0.026	13.109	0.27	30.184	15.114
11	9.150	1.4557	0.6869	0.007	0.417	0.63	0.277	30.601	15.744
12	9.670	1.5387	0.6499	0	0.219	0	0.277	30.82	15.744
13	10.300	1.6371	0.6108	0.022	0.041	12.929	0.299	30.861	28.673
14	10.300	1.6397	0.6099	0.01	0.133	5.329	0.308	30.994	34.002
15	11.000	1.7512	0.5710	2.355	0.01	0.367	2.663	31.005	34.369
16	11.600	1.8536	0.5395	29.984	0.157	0.001	32.647	31.162	34.37
17	12.000	1.9034	0.5254	3.509	0.479	0.183	36.156	31.64	34.553
18	12.400	1.9808	0.5048	17.277	0.008	0.233	53.433	31.648	34.786
19	12.700	2.0185	0.4954	0.03	0.619	0	53.462	32.267	34.786
20	13.100	2.0818	0.4803	2.257	0.123	0.044	55.72	32.39	34.831
21	14.000	2.2291	0.4486	0.335	0.595	0.028	56.055	32.985	34.858
22	15.000	2.3882	0.4187	0.259	0.17	0.032	56.314	33.155	34.89
23	15.600	2.4760	0.4039	0.873	0.046	0.002	57.187	33.201	34.893
24	15.900	2.5331	0.3948	0.004	0.368	0.001	57.191	33.569	34.894
25	16.200	2.5743	0.3885	0.011	0.263	0.027	57.202	33.832	34.921
26	16.600	2.6403	0.3787	0.15	0.048	0.177	57.352	33.88	35.099
27	16.700	2.6588	0.3761	0.125	0	0.17	57.477	33.88	35.269
28	16.900	2.6873	0.3721	0.065	0.115	0.006	57.542	33.996	35.275
29	17.700	2.8247	0.3540	0.586	0.003	0.052	58.127	33.999	35.327
30	18.900	3.0074	0.3325	0.007	0.575	0.005	58.134	34.573	35.332
31	19.300	3.0729	0.3254	0.119	0.141	0.492	58.252	34.714	35.824
32	20.000	3.1835	0.3141	0.165	0.078	1.259	58.418	34.792	37.083
33	20.400	3.2446	0.3082	0.012	0.199	0.543	58.43	34.991	37.626
34	20.700	3.3005	0.3030	0.556	0.709	0.041	58.986	35.699	37.667
35	21.700	3.4559	0.2894	0.017	0.364	0.271	59.003	36.064	37.938
36	23.800	3.7932	0.2636	5.855	0.003	0.027	64.859	36.067	37.965
37	24.100	3.8295	0.2611	1.653	0.432	0.001	66.511	36.499	37.965
38	25.200	4.0053	0.2497	1.072	0.038	0.813	67.583	36.537	38.779
39	27.200	4.3280	0.2311	7.805	0.139	0.021	75.389	36.676	38.8
40	28.100	4.4783	0.2233	1.292	1.153	0.023	76.681	37.83	38.823
41	29.300	4.6663	0.2143	0.147	0.075	0.382	76.827	37.904	39.205
42	32.300	5.1345	0.1948	16.156	0.02	0.006	92.983	37.924	39.212
43	35.900	5.7065	0.1752	1.774	0.87	0.307	94.756	38.794	39.519
44	37.000	5.8939	0.1697	0.187	2.184	0.18	94.943	40.978	39.699
45	37.400	5.9509	0.1680	4.526	0.042	0.187	99.469	41.021	39.886
46	45.300	7.2171	0.1386	0.521	0.104	0.044	99.99	41.125	39.929
47	51.100	8.1293	0.1230	0.008	0.46	0.33	99.998	41.584	40.259
48	54.000	8.5974	0.1163	0	30.03	0.012	99.998	71.614	40.271
49	64.200	10.2138	0.0979	0	20.366	0.005	99.999	91.98	40.276
50	139.000	22.1971	0.0451	0	0.004	47.382	99.999	91.984	4387.658

Table 5.1 Description of Seismic Excitation Cases

Seismic Excitation Cases	Description
LL11	Horizontal Component of 50-year Earthquake Applied Along Longitudinal Direction of the Bridge.
LL22	Transverse Component of 50-year Earthquake Applied Along Longitudinal Direction of the Bridge.
TT11	Horizontal Component of 50-year Earthquake Applied Along Transverse Direction of the Bridge.
TT22	Transverse Component of 50-year Earthquake Applied Along Transverse Direction of the Bridge.
L1T2V3	Horizontal, Vertical and Transverse Components of 50-year Earthquakes are Applied Along Longitudinal, Vertical and Transverse Directions of the Bridge, respectively.
L2T1V3	Horizontal, Vertical and Transverse Components of 50-year Earthquakes are Applied Along Transverse, Vertical and Longitudinal Directions of the Bridge, respectively.

Table 5.2 Cross Sectional Properties of Members for Stress Calculation

Element Number	Area, A (in^2)	Moment of Inertia, I_{13} (in^4)	Section Modulus, Z_{13} (in^3)	Distance from centroid to extreme fiber, y (in)	Moment of Inertia, I_{12} (in^4)	Section Modulus, Z_{13} (in^3)	Distance from centroid to extreme fiber (in)
1	89.50	9370	669.2	14	3620	378.9	9.5625
16	159.70	18300	1305.4	14	9500	910.6	10.4375
17	145.40	8960	639.8	14	12900	1147.9	11.20833
32	145.40	8960	639.8	14	12900	1147.9	11.20833
33	159.70	18300	1305.4	14	9500	910.6	10.4375
54	159.70	18300	1305.4	14	9500	910.6	10.4375
55	135.70	8410	600.6	14	11700	1095.3	10.6875
66	89.50	9370	669.2	14	3620	378.9	9.5625
85	108.00	729	1300.0	7	9670	1381.4	7
86	108.00	729	1300.0	7	9670	1381.4	7
101	108.00	729	1300.0	7	9670	1381.4	7
102	108.00	729	1300.0	7	9670	1381.4	7
123	108.00	729	1300.0	7	9670	1381.4	7
124	108.00	729	1300.0	7	9670	1381.4	7
141	60.31	5320	423.2	12.5625	5510	408.4	13.5
174	77.19	5110	365.2	14	5550	573.3	9.6875
175	19.80	625	73.6	8.5	1350	193.0	7
176	99.94	1250	65.9	19	8980	691.0	13
177	99.94	1250	65.9	19	8980	691.0	13
178	77.19	5110	365.2	14	5550	573.3	9.6875
179	19.80	625	73.6	8.5	1350	193.0	7
219	77.19	5110	365.2	14	5550	573.3	9.6875
220	19.80	625	73.6	8.5	1350	193.0	7
221	99.94	1250	65.9	19	8980	691.0	13
222	99.94	1250	65.9	19	8980	691.0	13
223	77.19	5110	365.2	14	5550	573.3	9.6875
224	19.80	625	73.6	8.5	1350	193.0	7
272	77.19	5110	365.2	14	5550	573.3	9.6875
273	19.80	625	73.6	8.5	1350	193.0	7
274	99.94	1250	65.9	19	8980	691.0	13
275	99.94	1250	65.9	19	8980	691.0	13
276	19.80	625	73.6	8.5	1350	193.0	7
277	70.69	4750	339.1	14	4950	517.8	9.5625
304	99.87	24500	1940.6	12.625	5430	362.3	15

Table 5.3 Stresses (ksi) in Members due to Seismic Excitation Case L1T2V3[a], Dead Load and Temperature

Member No.	Stresses due to L1T2V3 Earthquake								Maximum Stresses from (DL ± EQ ± Temperature)		
	Axial Stress	Bending Stress in		Bending Stress in		Combined Stress		Shear stress			
		Node I	Node J	Node I	Node J	Node I	Node J		Combine	Combine	Shear
1	1.689	0.759	0.175	1.375	0.433	3.141	2.272	0.023	30.632	24.475	0.491
16	0.961	0.165	0	0.193	0.669	1.258	1.629	0.003	13.018	15.088	0.226
17	1.24	0	0.241	0.606	0.633	1.846	1.896	0.008	21.668	17.432	0.288
32	0.995	0.274	0	0.453	0.563	1.712	1.516	0.008	12.261	17.063	0.314
33	0.983	0	0.216	0.336	0.132	1.319	1.33	0	15.578	14.14	0.041
54	1.157	0.188	0	0.133	0.307	1.449	1.465	0	12.763	15.016	0.044
55	0.853	0	0.296	0.341	0.139	1.157	1.181	0.004	13.042	7.909	0.054
66	1.13	0.19	0.311	0.243	0.768	1.536	2.109	0.002	20.319	25.389	0.247
85	0.683	0	0	0.006	0.014	0.688	0.696	0.01	14.467	14.56	0.39
86	0.693	0	0	0.013	0.006	0.706	0.699	0.01	14.349	14.251	0.394
101	0.568	0	0	0.005	0.012	0.573	0.579	0.009	15.58	15.663	0.352
102	0.493	0	0	0.013	0.008	0.506	0.498	0.003	15.554	15.446	0.076
123	0.468	0	0	0.005	0.01	0.473	0.477	0.002	14.788	14.88	0.063
124	0.443	0	0	0.013	0.004	0.455	0.447	0.003	14.888	14.804	0.065
141	0.927	0.657	1.078	2.546	2.128	4.131	4.025	0.005	20.245	14.147	0.565
174	0.648	0	0.269	2.215	1.031	2.742	1.948	0.024	20.153	13.001	0.558
175	1.314	0.311	0.243	0.306	0.201	1.822	1.726	0.16	17.595	19.112	2.501
176	0.63	0	1.837	3.155	1.326	3.785	3.693	0.008	33.073	5.899	0.414
177	0.474	2.809	2.581	0.355	0.304	3.633	3.332	0.026	10.472	8.682	0.482
178	0.753	0	0.416	1.729	1.34	2.429	2.449	0.004	19.361	6.579	0.488
179	1.202	0.254	0.269	0.202	0.549	1.586	2.02	0.017	17.819	19.084	1.904
219	0.845	0	0.405	1.502	1.092	2.2	2.217	0.003	19.185	7.665	0.43
220	0.946	0.318	0.271	0.56	0.189	1.824	1.36	0.02	18.212	17.5	1.764
221	0.6	0	3.006	2.649	1.65	3.028	4.446	0.004	34.992	7.406	0.08
222	0.451	3.431	2.915	0.446	0.407	4.328	3.636	0.003	8.835	12.52	0.069
223	0.846	0	1.364	1.694	1.15	2.512	3.271	0.001	18.244	17.714	0.093
224	0.84	0.632	0.956	0.189	0.45	1.507	2.136	0.014	21.303	23.006	0.422
273	0.608	0.203	0.219	0.297	0.165	1.068	0.951	0.009	15.482	15.869	0.349
274	0.423	0	2.505	2.243	1.08	2.666	3.781	0	33.629	8.343	0.076
275	0.345	2.49	4.145	0.323	0.268	3.131	4.758	0.001	11.011	11.437	0.078
276	0.554	0.474	0.576	0.165	0.219	1.154	1.272	0.262	16.038	16.852	0.642
277	0.979	0.956	0.584	1.358	0.718	3.293	2.214	0.007	23.591	4.15	0.102
304	0.808	0.07	0.265	2.26	1.731	3.114	2.804	0.008	12.184	9.093	0.012

[a] Seismic excitation cases described in Table 5.1

Table 5.4 Stresses (ksi) in Members due to Seismic Excitation Case L2T1V3[a], Dead Load and Temperature

Member No.	Stresses due to L2T1V3 Earthquake								Maximum Stresses from (DL ± EQ ± Temperature)		
	Axial Stress	Bending Stress in		Bending Stress in		Combined Stress		Shear stress			
		Node I	Node J	Node I	Node J	Node I	Node J		Combined	Combined	Shear
1	0.793	0.408	0.202	0.615	0.206	1.816	1.139	0.012	29.307	23.342	0.48
16	0.852	0.09	0	0.482	0.851	1.339	1.703	0.004	13.099	15.162	0.227
17	1.086	0	0.129	0.88	0.869	1.966	2.008	0.016	21.788	17.544	0.296
32	0.496	0.177	0	0.773	0.839	1.381	1.328	0.016	11.93	16.875	0.322
33	0.885	0	0.138	0.666	0.437	1.524	1.407	0.001	15.783	14.217	0.042
54	0.601	0.091	0	0.438	0.701	1.13	1.263	0	12.444	14.814	0.044
55	0.502	0	0.14	0.539	0.401	1.04	1.004	0.003	12.925	7.732	0.053
66	0.82	0.226	0.181	0.242	0.565	1.194	1.565	0.002	19.977	24.845	0.247
85	0.539	0	0	0.007	0.019	0.546	0.553	0.008	14.325	14.417	0.388
86	0.557	0	0	0.016	0.008	0.569	0.565	0.022	14.212	14.117	0.406
101	0.613	0	0	0.007	0.016	0.62	0.624	0.008	15.627	15.708	0.351
102	0.59	0	0	0.015	0.004	0.605	0.594	0.002	15.653	15.542	0.075
123	0.747	0	0	0.007	0.017	0.753	0.763	0.001	15.068	15.166	0.062
124	0.762	0	0	0.015	0.006	0.774	0.768	0.002	15.207	15.125	0.064
141	0.582	0.536	0.638	1.423	1.219	2.429	2.439	0.005	18.543	12.561	0.565
174	0.599	0	0.199	1.252	0.757	1.852	1.553	0.037	19.263	12.606	0.571
175	0.657	0.133	0.117	0.438	0.241	1.225	1.01	0.225	16.998	18.396	2.566
176	0.435	0	1.332	1.997	0.839	2.407	2.497	0.009	31.695	4.703	0.415
177	0.404	1.64	1.685	0.344	0.232	2.347	2.243	0.041	9.186	6.249	0.497
178	0.511	0	0.258	1.397	0.877	1.908	1.541	0.006	18.84	5.671	0.49
179	0.591	0.151	0.158	0.238	0.355	0.916	1.069	0.021	17.149	18.133	1.908
219	0.486	0	0.301	1.246	0.705	1.727	1.402	0.005	18.712	6.85	0.432
220	0.593	0.203	0.192	0.386	0.31	1.182	1.078	0.022	17.57	17.218	1.766
221	0.415	0	2.217	1.853	0.8	2.248	3.432	0.002	34.212	6.392	0.078
222	0.382	1.564	2.338	0.258	0.191	2.203	2.889	0.002	6.71	8.886	0.068
223	0.459	0	0.865	1.343	0.757	1.781	1.901	0.001	17.513	16.344	0.093
224	0.668	0.325	0.521	0.314	0.459	1.258	1.502	0.011	21.054	22.372	0.419
273	0.864	0.115	0.111	0.467	0.274	1.446	1.24	0.005	15.86	16.158	0.345
274	0.528	0	1.093	3.184	1.462	3.712	2.932	0.001	34.675	7.494	0.077
275	0.485	2.065	1.64	0.589	0.437	3.023	2.471	0.001	10.903	6.68	0.078
276	0.861	0.247	0.252	0.275	0.301	1.327	1.314	0.151	16.211	16.894	0.531
277	1.042	0.758	0.295	1.445	0.705	3.165	2.004	0.003	23.463	3.94	0.098
304	0.572	0.044	0.206	2.666	2.169	3.164	2.907	0.005	12.234	9.196	0.009

[a] Seismic excitation cases described in Table 5.1

Table 5.5 Stresses (ksi) in Members due to Seismic Excitation Case: LL11[a]

Member No.	Stresses due to LL11 Earthquake							
	Axial Stress	Bending Stress in 1-2		Bending Stress in 1-3		Combined Stress		Shear stress
		Node I	Node J	Node I	Node J	Node I	Node J	
1	1.648	0.828	0.17	0.855	0.254	2.666	2.04	0.02
16	1.115	0.219	0	0.069	0.271	1.325	1.387	0.003
17	1.315	0	0.227	0.551	0.402	1.665	1.931	0.005
32	0.888	0.322	0	0.378	0.478	1.588	1.195	0.005
33	0.709	0	0.202	0.21	0.051	0.919	0.945	0
54	0.951	0.189	0	0.04	0.155	1.126	1.106	0
55	0.924	0	0.226	0.199	0.062	1.123	1.189	0.005
66	1.205	0.173	0.314	0.146	0.528	1.518	1.849	0.002
85	0.724	0	0	0.004	0.01	0.728	0.734	0.009
86	0.704	0	0	0.008	0.004	0.712	0.707	0.007
101	0.612	0	0	0.003	0.01	0.614	0.622	0.007
102	0.642	0	0	0.009	0.004	0.65	0.647	0.002
123	0.581	0	0	0.003	0.006	0.584	0.586	0.002
124	0.577	0	0	0.004	0.003	0.581	0.579	0.003
141	0.826	0.86	1.373	0.808	0.453	2.494	2.651	0.009
174	0.64	0	0.361	1.509	0.553	2.148	1.514	0.012
175	1.118	0.245	0.215	0.193	0.11	1.541	1.443	0.123
176	0.587	0	2.429	2.301	0.653	2.888	3.669	0.008
177	0.505	2.566	3.401	0.198	0.156	3.269	4.036	0.022
178	0.962	0	0.416	1.34	0.759	2.235	2.126	0.005
179	1.006	0.25	0.281	0.111	0.36	1.367	1.618	0.018
219	0.753	0	0.422	1.068	0.654	1.821	1.732	0.003
220	0.792	0.283	0.268	0.396	0.115	1.43	1.175	0.019
221	0.473	0	2.976	1.592	0.686	2.065	4.045	0.003
222	0.413	3.492	2.733	0.207	0.175	4.057	3.151	0.002
223	0.589	0	0.972	0.895	0.508	1.466	2.067	0.001
224	0.789	0.48	0.688	0.113	0.233	1.373	1.695	0.016
273	0.956	0.169	0.148	0.124	0.061	1.248	1.129	0.007
274	0.538	0	1.761	2.446	0.709	2.984	2.893	0
275	0.442	2.733	2.915	0.213	0.165	3.331	3.451	0
276	0.897	0.322	0.431	0.06	0.08	1.279	1.409	0.136
277	1.177	1.044	0.593	1.23	0.382	3.138	2.152	0.005
304	0.839	0.076	0.277	1.201	0.875	1.826	1.921	0.009

[a] Seismic excitation cases described in Table 5.1

Table 5.6 Stresses (ksi) in Members due to Seismic Excitation Case: LL22[a]

Member No.	Stresses due to LL22 Earthquake							
	Axial Stress	Bending Stress in 1-2		Bending Stress in 1-3		Combined Stress		Shear stress
		Node I	Node J	Node I	Node J	Node I	Node J	
1	0.713	0.435	0.127	0.454	0.148	1.504	0.983	0.01
16	0.568	0.133	0	0.056	0.223	0.756	0.742	0.003
17	1.037	0	0.186	0.271	0.237	1.308	1.452	0.005
32	0.443	0.247	0	0.198	0.24	0.887	0.675	0.003
33	0.689	0	0.218	0.142	0.04	0.811	0.841	0
54	0.416	0.107	0	0.033	0.105	0.549	0.522	0
55	0.439	0	0.134	0.109	0.034	0.547	0.588	0.002
66	0.768	0.202	0.121	0.125	0.433	1.077	1.282	0.002
85	0.62	0	0	0.004	0.012	0.623	0.632	0.007
86	0.637	0	0	0.009	0.003	0.645	0.641	0.004
101	0.716	0	0	0.002	0.007	0.718	0.723	0.005
102	0.74	0	0	0.008	0.004	0.747	0.744	0.002
123	0.716	0	0	0.003	0.006	0.718	0.721	0.001
124	0.737	0	0	0.004	0.003	0.741	0.739	0.002
141	0.583	0.506	0.796	0.612	0.446	1.663	1.657	0.006
174	0.803	0	0.285	1.329	0.56	1.949	1.552	0.009
175	0.755	0.14	0.174	0.186	0.051	1.065	0.924	0.065
176	0.543	0	1.549	2.113	0.683	2.497	2.614	0.006
177	0.454	1.245	2.414	0.214	0.165	1.914	2.891	0.012
178	0.595	0	0.304	1.526	0.713	2.028	1.597	0.005
179	0.716	0.154	0.173	0.052	0.236	0.907	1.116	0.017
219	0.85	0	0.301	0.717	0.481	1.567	1.461	0.002
220	0.675	0.215	0.23	0.264	0.072	1.07	0.893	0.022
221	0.566	0	1.807	1.621	0.46	2.143	2.596	0.002
222	0.494	1.266	2.794	0.162	0.128	1.883	3.162	0.001
223	0.515	0	0.734	0.886	0.45	1.375	1.698	0
224	0.694	0.296	0.47	0.071	0.196	1.061	1.36	0.011
273	0.822	0.196	0.186	0.083	0.047	1.039	1.053	0.006
274	0.549	0	1.286	1.881	0.55	2.282	2.385	0
275	0.508	2.308	1.868	0.174	0.13	2.989	2.471	0
276	0.878	0.185	0.271	0.047	0.075	1.107	1.177	0.085
277	0.902	0.702	0.375	1.026	0.323	2.427	1.507	0.002
304	0.552	0.059	0.182	0.817	0.58	1.29	1.308	0.005

[a] Seismic excitation cases described in Table 5.1

Table 5.7 Stresses (ksi) in Members due to Seismic Excitation Case: TT11[a]

Member No.	Stresses due to TT11 Earthquake							
	Axial Stress	Bending Stress in 1-2		Bending Stress in 1-3		Combined Stress		Shear stress
		Node I	Node J	Node I	Node J	Node I	Node J	
1	0.324	0.276	0.22	0.575	0.21	1.114	0.754	0.01
16	0.933	0.105	0	0.476	0.848	1.504	1.62	0.004
17	1.028	0	0.116	0.746	0.814	1.774	1.821	0.016
32	0.615	0.136	0	0.716	0.709	1.464	1.298	0.017
33	0.72	0	0.134	0.675	0.44	1.395	1.212	0.001
54	0.562	0.145	0	0.441	0.7	1.115	1.262	0
55	0.49	0	0.183	0.541	0.404	0.983	1.077	0.003
66	0.285	0.191	0.112	0.258	0.618	0.734	0.961	0.002
85	0.655	0	0	0.008	0.018	0.66	0.673	0.006
86	0.746	0	0	0.015	0.007	0.761	0.752	0.022
101	0.765	0	0	0.005	0.014	0.769	0.779	0.008
102	0.721	0	0	0.016	0.005	0.735	0.725	0.002
123	0.539	0	0	0.006	0.016	0.546	0.556	0.001
124	0.588	0	0	0.014	0.005	0.602	0.592	0.002
141	0.59	0.456	0.567	1.481	1.339	2.393	2.442	0.008
174	0.721	0	0.183	1.139	0.495	1.86	1.399	0.036
175	0.687	0.152	0.141	0.451	0.252	1.21	1.059	0.201
176	0.571	0	0.94	2.041	0.769	2.612	2.042	0.008
177	0.521	1.204	1.609	0.275	0.204	1.942	2.093	0.036
178	0.63	0	0.263	1.286	0.771	1.858	1.664	0.007
179	0.698	0.174	0.188	0.249	0.324	1.121	1.182	0.029
219	0.615	0	0.331	1.327	0.651	1.942	1.525	0.004
220	0.761	0.237	0.218	0.341	0.346	1.339	1.313	0.026
221	0.602	0	1.549	2.171	0.897	2.773	2.791	0.002
222	0.546	1.326	1.837	0.265	0.206	1.886	2.307	0.001
223	0.477	0	0.936	1.183	0.576	1.646	1.961	0.001
224	0.835	0.356	0.555	0.349	0.448	1.541	1.685	0.011
273	0.868	0.189	0.204	0.396	0.267	1.381	1.338	0.006
274	0.442	0	1.171	2.012	0.906	2.368	2.306	0.001
275	0.394	1.137	1.913	0.456	0.327	1.987	2.564	0.001
276	0.818	0.243	0.227	0.268	0.277	1.328	1.19	0.155
277	1.059	0.216	0.301	1.049	0.848	2.212	2.208	0.002
304	0.581	0.042	0.178	2.412	2.103	3.036	2.744	0.005

[a] Seismic excitation cases described in Table 5.1

Table 5.8 Stresses (ksi) in Members due to Seismic Excitation Case: TT22[a]

Member No.	Stresses due to TT22 Earthquake							
	Axial Stress	Bending Stress in 1-2		Bending Stress in 1-3		Combined Stress		Shear stress
		Node I	Node J	Node I	Node J	Node I	Node J	
1	0.281	0.269	0.166	0.76	0.219	1.234	0.642	0.012
16	0.572	0.126	0	0.16	0.445	0.858	0.975	0.003
17	0.629	0	0.108	0.369	0.364	0.998	1.101	0.007
32	0.563	0.149	0	0.394	0.458	1.069	1.022	0.007
33	0.467	0	0.149	0.282	0.143	0.737	0.747	0
54	0.434	0.102	0	0.143	0.277	0.665	0.711	0
55	0.575	0	0.149	0.252	0.127	0.827	0.851	0.003
66	0.226	0.173	0.114	0.191	0.618	0.548	0.939	0.001
85	0.734	0	0	0.005	0.013	0.737	0.746	0.005
86	0.724	0	0	0.012	0.005	0.736	0.729	0.008
101	0.715	0	0	0.005	0.011	0.72	0.726	0.008
102	0.719	0	0	0.012	0.005	0.731	0.724	0.002
123	0.539	0	0	0.005	0.01	0.544	0.549	0.001
124	0.538	0	0	0.013	0.004	0.548	0.541	0.002
141	0.528	0.409	0.591	2.272	1.839	3.139	2.958	0.008
174	0.595	0	0.17	1.797	1.094	2.326	1.781	0.017
175	0.805	0.151	0.139	0.339	0.187	1.272	1.13	0.093
176	0.55	0	0.665	3.242	1.427	3.712	2.642	0.005
177	0.448	0.909	1.189	0.417	0.342	1.775	1.915	0.022
178	0.712	0	0.209	2.076	1.123	2.562	2.02	0.004
179	0.801	0.136	0.129	0.185	0.323	1.11	1.241	0.016
219	0.634	0	0.249	1.546	0.886	2.1	1.77	0.003
220	0.953	0.154	0.16	0.301	0.131	1.397	1.218	0.02
221	0.47	0	1.098	2.243	1.227	2.709	2.79	0.002
222	0.438	0.82	1.852	0.342	0.308	1.511	2.491	0.002
223	0.572	0	0.901	1.207	0.794	1.639	2.156	0.001
224	0.979	0.326	0.518	0.132	0.269	1.411	1.765	0.013
273	0.857	0.152	0.152	0.395	0.159	1.378	1.168	0.006
274	0.328	0	0.844	2.316	1.143	2.56	2.232	0
275	0.324	0.847	1.579	0.349	0.302	1.52	2.072	0.001
276	0.816	0.184	0.17	0.159	0.207	1.155	1.164	0.222
277	0.834	0.14	0.262	1.53	0.83	2.504	1.853	0.004
304	0.636	0.051	0.131	2.352	1.722	3.021	2.311	0.003

[a] Seismic excitation cases described in Table 5.1

Table 5.9 Stresses (ksi) Due to a Temperature of 90° F

Member No.	Stresses due Temperature							
	Axial Stress	Bending Stress in 1-2		Bending Stress in 1-3		Combined Stress		Shear stress
		Node I	Node J	Node I	Node J	Node I	Node J	
1	14.444	-3.197	-0.386	-6.58	1.819	24.222	15.878	0.096
16	7.679	0.036	0	-0.009	0.627	7.706	8.306	0.022
17	14.297	0	-0.958	0.495	0.138	14.792	15.117	0.005
32	9.978	-0.464	0	0.113	-0.125	10.329	10.103	0.016
33	8.767	0	-0.249	0.07	-0.031	8.837	9.048	0
54	8.215	-0.312	0	0.119	-0.562	8.409	8.777	0.001
55	5.209	0	-0.085	0.681	-0.211	5.89	5.505	0.001
66	12.717	-0.535	-1.601	1.71	-5.957	13.893	20.276	0.146
85	4.091	0	0	-0.01	-0.01	4.101	4.101	0.033
86	3.751	0	0	0.056	-0.025	3.807	3.775	0.016
101	3.536	0	0	-0.003	-0.005	3.539	3.541	0.064
102	3.398	0	0	0.033	-0.006	3.431	3.405	0.023
123	3.711	0	0	-0.008	0.02	3.718	3.73	0
124	3.723	0	0	0.017	-0.01	3.739	3.733	0.024
141	1.916	-1.445	-0.894	-8.878	3.693	12.239	4.716	0.041
174	2.975	0	-0.039	4.839	-2.988	7.814	6.002	0.017
175	5.02	1.01	-0.988	-1.136	-0.243	5.146	6.252	0.083
176	-3.476	0	-1.904	3.047	-1.146	-0.429	-0.426	0.032
177	-2.71	-4.155	-2.284	-0.287	0.246	1.732	-0.672	0.009
178	2.226	0	-0.383	-2.002	1.938	4.228	3.781	0.051
179	5.058	-0.096	0.08	-0.26	1.6	5.414	6.738	0.203
219	2.859	0	0.158	-1.013	0.621	3.872	3.638	0.016
220	4.069	0.544	-0.535	0.119	-0.026	4.732	4.63	0.107
221	-3.129	0	0.213	-1.716	0.987	-1.413	-1.929	0.012
222	-2.466	1.317	0.853	0.193	-0.259	-0.956	-1.873	0.02
223	2.593	0	2.88	-0.976	0.583	3.569	6.056	0.003
224	4.069	-1.479	2.28	-0.026	0.203	5.573	6.552	0.143
273	3.304	0.59	-0.57	0.012	0.011	3.906	3.863	0.006
274	-3.211	0	0.431	2.028	-0.474	-1.183	-3.168	0.022
275	-2.66	1.009	0.648	-0.167	0.085	-1.818	-1.927	0.022
276	3.291	-0.913	1.368	0.011	-0.002	4.192	4.657	0.072
277	1.193	4.524	0.389	1.499	-0.425	7.216	1.229	0.001
304	1.156	0.737	0.486	-7.177	2.204	7.595	3.845	0.002

Table 5.10 Self-Weight Induced Stresses (ksi)

Member No.	Stresses due to Self-Weight							
	Axial Stress	Bending Stress in 1-2		Bending Stress in 1-3		Combined Stress		Shear stress
		Node I	Node J	Node I	Node J	Node I	Node J	
1	2.545	0.922	3.34	-1.646	0.441	3.269	6.325	0.372
16	-5.781	1.987	0	-0.261	0.628	-4.054	-5.153	0.201
17	-5.801	0	5.311	-0.772	0.072	-5.03	-0.419	0.275
32	-5.469	5.359	0	-0.109	0.026	-0.22	-5.444	0.29
33	-5.694	0	2.041	0.272	-0.11	-5.422	-3.762	0.041
54	-4.845	1.957	0	-0.017	-0.071	-2.905	-4.774	0.043
55	-6.29	0	5.179	0.296	-0.112	-5.995	-1.223	0.049
66	1.922	2.63	2.26	0.338	-1.177	4.89	3.004	0.099
85	9.646	0	0	-0.032	0.075	9.678	9.763	0.347
86	9.8	0	0	0.036	-0.02	9.836	9.777	0.368
101	11.424	0	0	-0.044	0.076	11.468	11.543	0.279
102	11.541	0	0	0.076	-0.045	11.617	11.543	0.05
123	10.561	0	0	-0.035	0.069	10.597	10.673	0.061
124	10.635	0	0	0.059	-0.031	10.694	10.624	0.038
141	-8.908	-1.312	-1.4	6.345	-2.009	-3.875	-5.406	0.519
174	-9.56	0	0.911	19.157	-5.335	9.597	-5.051	0.517
175	9.335	0.855	1.997	0.437	-0.24	10.627	11.134	2.258
176	-8.928	0	0.204	37.787	-10.799	28.859	1.78	0.374
177	-7.33	0.723	0.276	-2.946	2.319	-5.107	-4.678	0.447
178	-7.234	0	-0.877	19.938	-6.62	12.704	0.349	0.433
179	9.324	1.728	1.294	-0.233	-0.25	10.819	10.326	1.684
219	-7.465	0	0.889	20.578	-6.458	13.113	-1.81	0.411
220	10.032	1.368	1.747	0.256	-0.312	11.656	11.51	1.637
221	-10.261	0	0.8	40.812	-11.979	30.551	1.031	0.064
222	-8.522	-1.733	-1.139	-3.239	2.593	-3.551	-7.011	0.046
223	-8.58	0	-10.478	20.744	-6.405	12.163	8.387	0.089
224	10.144	4.392	-4.087	-0.313	-0.13	14.223	14.318	0.265
273	9.48	1.045	1.82	-0.017	-0.287	10.508	11.055	0.334
274	-9.701	0	0.507	39.481	-11.488	29.78	1.394	0.054
275	-8.043	1.138	0.745	-3.119	2.49	-6.062	-4.752	0.055
276	9.51	1.47	1.46	-0.287	-0.003	10.692	10.923	0.308
277	-8.079	0.464	-0.742	20.698	-6.546	13.082	-0.707	0.094
304	-2.838	0.898	0.616	3.415	-0.957	1.475	-2.444	0.002

Table 5.11 Stress Requirement Based on AASHTO Equations for L1T2V3

Earthquake

Member Number	Axial Stress f_a (ksi)	Bending Stress (ksi)		Euler Buckling Stress (ksi), AASHTO Eq.(10-44)		Stress Requirement ≤ 1.0	
		f_{bx}	f_{by}	F_{ex}	F_{ey}	AASHTO Eq. (10-42)	AASHTO Eq.(10-43)
1	1.689	0.759	1.375	285.45	110.28	0.09	0.21
16	0.961	0.165	0.669	312.43	162.19	0.04	0.10
17	1.24	0.241	0.633	154.84	222.93	0.04	0.12
32	0.995	0.274	0.563	154.84	222.93	0.04	0.10
33	0.983	0.216	0.336	312.43	162.19	0.02	0.09
54	1.157	0.188	0.307	312.43	162.19	0.02	0.09
55	0.853	0.296	0.341	168.98	235.08	0.03	0.08
66	1.13	0.311	0.768	285.45	110.28	0.05	0.12
85	0.683	0	0.014	16.42	217.86	0.00	0.04
86	0.693	0	0.013	15.26	202.49	0.00	0.04
101	0.568	0	0.012	15.26	202.49	0.00	0.03
102	0.493	0	0.013	16.42	217.86	0.00	0.03
123	0.468	0	0.01	16.42	217.86	0.00	0.03
124	0.443	0	0.013	16.42	217.86	0.00	0.03
141	0.927	1.078	2.546	288.54	298.85	0.15	0.24
174	0.648	0.269	2.215	194.77	211.54	0.11	0.16
175	1.314	0.311	0.306	76.80	165.90	0.03	0.11
176	0.63	1.837	3.155	39.78	285.75	0.21	0.29
177	0.474	2.809	0.355	159.11	1143.01	0.13	0.19
178	0.753	0.416	1.729	187.14	203.25	0.09	0.15
179	1.202	0.269	0.549	71.38	154.19	0.04	0.11
219	0.845	0.405	1.502	187.14	203.25	0.08	0.15
220	0.946	0.318	0.56	71.38	154.19	0.04	0.10
221	0.6	3.006	2.649	39.78	285.75	0.24	0.32
222	0.451	3.431	0.446	159.11	1143.01	0.17	0.22
223	0.846	1.364	1.694	187.14	203.25	0.13	0.20
224	0.84	0.956	0.45	76.80	165.90	0.06	0.12
273	0.608	0.219	0.297	76.80	165.90	0.02	0.06
274	0.423	2.505	2.243	39.78	285.75	0.20	0.26
275	0.345	4.145	0.323	159.11	1143.01	0.19	0.24
276	0.554	0.576	0.219	163.50	170.38	0.03	0.07
277	0.979	0.956	1.358	92.87	200.60	0.10	0.17
304	0.808	0.265	2.26	802.45	177.85	0.11	0.17

Table 5.12 Stress Requirement Based on AASHTO Equations for L2T1V3

Earthquake

Member Number	Axial Stress f_a (ksi)	Bending Stress (ksi)		Euler Buckling Stress (ksi), AASHTO Eq.(10-44)		Stress Requirement ≤ 1.0	
		f_{bx}	f_{by}	F_{ex}	F_{ey}	AASHTO Eq. (10-42)	AASHTO Eq.(10-43)
1	0.793	0.408	0.615	285.45	110.28	0.04	0.10
16	0.852	0.09	0.851	312.43	162.19	0.04	0.10
17	1.086	0.129	0.88	154.84	222.93	0.04	0.11
32	0.496	0.177	0.839	154.84	222.93	0.04	0.08
33	0.885	0.138	0.666	312.43	162.19	0.03	0.09
54	0.601	0.091	0.701	312.43	162.19	0.03	0.08
55	0.502	0.14	0.539	168.98	235.08	0.03	0.06
66	0.82	0.226	0.565	285.45	110.28	0.03	0.09
85	0.539	0	0.019	16.42	217.86	0.00	0.03
86	0.557	0	0.016	15.26	202.49	0.00	0.03
101	0.613	0	0.016	15.26	202.49	0.00	0.04
102	0.59	0	0.015	16.42	217.86	0.00	0.04
123	0.747	0	0.017	16.42	217.86	0.00	0.04
124	0.762	0	0.015	16.42	217.86	0.00	0.05
141	0.582	0.638	1.423	288.54	298.85	0.09	0.14
174	0.599	0.199	1.252	194.77	211.54	0.06	0.11
175	0.657	0.133	0.438	76.80	165.90	0.02	0.07
176	0.435	1.332	1.997	39.78	285.75	0.14	0.19
177	0.404	1.685	0.344	159.11	1143.01	0.09	0.13
178	0.511	0.258	1.397	187.14	203.25	0.07	0.11
179	0.591	0.158	0.355	71.38	154.19	0.02	0.06
219	0.486	0.301	1.246	187.14	203.25	0.07	0.11
220	0.593	0.203	0.386	71.38	154.19	0.03	0.06
221	0.415	2.217	1.853	39.78	285.75	0.17	0.23
222	0.382	2.338	0.258	159.11	1143.01	0.11	0.15
223	0.459	0.865	1.343	187.14	203.25	0.09	0.14
224	0.668	0.521	0.459	76.80	165.90	0.04	0.09
273	0.864	0.115	0.467	76.80	165.90	0.02	0.08
274	0.528	1.093	3.184	39.78	285.75	0.18	0.24
275	0.485	2.065	0.589	159.11	1143.01	0.11	0.16
276	0.861	0.252	0.301	163.50	170.38	0.02	0.08
277	1.042	0.758	1.445	92.87	200.60	0.09	0.17
304	0.572	0.206	2.666	802.45	177.85	0.12	0.18

Table 5.13 Displacements (in) due to Seismic Excitation of the 50-year Earthquake

Node	L1T2V3[a]			L2T1V3[a]			LL11[a]			LL22[a]			TT11[a]			TT22[a]		
	Ux	Uy	Uz	Ux	Uy	Uz	Ux	Uy	Uz	Ux	Uy	Uz	Ux	Uy	Uz	Ux	Uy	Uz
1	0.239	0.007	0.059	0.127	0.017	0.037	0.234	0.001	0.057	0.124	0.001	0.032	0.036	0.017	0.052	0.031	0.006	0.045
8	0.335	0.345	0.327	0.158	0.205	0.302	0.349	0.101	0.375	0.152	0.085	0.285	0.058	0.201	0.307	0.046	0.334	0.301
9	0.339	0.323	0.305	0.161	0.174	0.285	0.356	0.094	0.31	0.151	0.076	0.273	0.063	0.166	0.294	0.048	0.323	0.305
10	0.335	0.317	0.298	0.165	0.222	0.272	0.354	0.114	0.263	0.15	0.116	0.28	0.067	0.184	0.279	0.047	0.298	0.305
11	0.329	0.294	0.301	0.167	0.225	0.254	0.348	0.13	0.227	0.15	0.135	0.286	0.07	0.193	0.268	0.047	0.258	0.291
13	0.315	0.255	0.279	0.162	0.229	0.218	0.331	0.136	0.206	0.149	0.126	0.263	0.068	0.2	0.243	0.044	0.215	0.261
17	0.265	0.015	0.147	0.162	0.043	0.093	0.268	0 002	0.141	0.151	0.002	0.114	0.033	0.044	0.141	0.029	0.016	0.133
24	0.262	0.39	0.47	0.212	0.175	0.368	0.268	0.095	0.417	0.218	0.064	0.421	0.034	0.183	0.491	0.025	0.394	0.416
25	0.278	0.409	0.431	0.215	0.2	0.372	0.279	0.097	0.424	0.218	0.077	0.432	0.03	0.193	0.501	0.026	0.437	0.438
26	0.292	0.419	0.376	0.213	0.199	0.36	0.286	0.141	0.438	0.213	0.106	0.439	0.026	0.167	0.5	0.026	0.444	0.441
33	0.266	0.016	0.171	0.185	0.043	0.101	0.262	0.003	0.1	0.197	0.002	0.112	0.025	0.043	0.113	0.029	0.016	0.117
37	0.282	0.28	0.368	0.222	0.128	0.209	0.28	0.049	0.23	0.222	0.052	0.18	0.062	0.121	0.165	0.038	0.283	0.244
39	0.284	0.333	0.414	0.233	0.144	0.241	0.287	0.054	0.252	0.233	0.06	0.21	0.069	0.143	0.188	0.043	0.328	0.276
43	0.279	0.432	0.293	0.231	0.268	0.327	0.291	0.118	0.257	0.229	0.093	0.348	0.046	0.264	0.373	0.039	0.428	0.252
44	0.276	0.413	0.269	0.223	0.297	0.366	0.288	0.118	0.283	0.225	0.101	0.376	0.039	0.279	0.391	0.036	0.396	0.234
45	0.271	0 393	0.282	0.214	0.25	0.365	0.283	0.085	0.289	0.222	0.095	0.374	0.04	0.247	0.377	0.037	0.389	0.202
49	0.258	0.391	0.415	0.195	0.148	0.256	0.266	0.095	0.26	0.2	0.086	0.255	0.036	0.155	0.245	0.04	0.307	0.21
51	0.239	0.34	0.373	0.193	0.133	0.226	0.255	0.09	0.226	0.193	0.084	0.216	0.039	0.138	0.212	0.037	0.265	0.189
55	0.22	0.016	0.126	0.203	0.043	0.121	0.247	0.002	0.139	0.192	0.001	0.112	0.056	0.044	0.124	0.036	0.016	0.101
60	0.25	0.312	0.342	0.196	0.161	0.385	0.265	0.061	0.413	0.199	0.057	0.356	0.068	0.161	0.386	0.035	0.316	0.372
61	0.251	0.356	0.325	0.195	0.205	0.404	0.266	0.07	0.443	0.192	0.066	0.382	0.055	0.199	0.389	0.032	0.353	0.386
62	0.248	0.351	0.317	0.184	0.193	0.427	0.261	0.071	0.469	0.179	0.065	0.395	0.041	0.193	0.39	0.034	0.349	0.375
67	0.211	0.008	0.082	0.097	0.021	0.062	0.195	0.002	0.079	0.122	0.002	0.052	0.057	0.021	0.055	0.049	0.008	0.054
101	0.307	0.431	0.304	0.168	0.242	0.249	0.309	0.162	0.227	0.163	0.177	0.284	0.044	0.177	0.265	0.039	0.43	0.288
102	0.308	0.413	0.28	0.172	0.25	0.219	0.308	0.147	0.207	0.169	0.166	0.264	0.041	0.187	0.244	0.042	0.446	0.262
127	0.302	0.469	0.409	0.213	0.244	0.239	0.309	0.192	0.253	0.215	0.193	0.209	0.066	0.294	0.187	0.052	0.4	0.275
129	0.292	0.48	0.407	0.214	0.255	0.231	0.304	0.101	0.248	0.214	0.098	0.214	0.044	0.224	0.22	0.044	0.477	0.268
139	0.248	0.495	0.412	0.203	0.28	0.256	0.243	0.071	0.255	0.211	0.062	0.245	0.054	0.284	0.241	0.064	0.474	0.21
140	0.261	0.501	0.375	0.201	0.258	0.227	0.25	0.057	0.228	0.212	0.053	0.217	0.062	0.248	0.213	0.074	0.489	0.19

[a] Seismic excitation cases described in Table 5.1

Ux = Longitudinal displacement; Uy = Transverse displacement; Uz=Vertical displacement

Table 5.14 Displacements (in) due to Self-weight and Temperature

Joint Number	Temperature			Self-weight		
	Ux	Uy	Uz	Ux	Uy	Uz
1	2.363	0.127	0.091	-0.078	-0.004	-0.510
8	1.827	-1.416	0.310	0.448	0.526	-6.962
9	1.730	-1.531	0.618	0.541	0.565	-6.834
10	1.643	-1.583	0.752	0.601	0.582	-6.522
11	1.562	-1.551	1.042	0.659	0.577	-6.052
13	1.786	-1.392	0.983	0.681	0.520	-5.229
17	1.251	0.129	-0.056	0.346	-0.023	-2.215
24	0.777	1.402	0.178	0.022	-0.436	-3.600
25	0.719	1.023	0.373	0.042	-0.304	-3.590
26	0.651	0.749	0.334	0.060	-0.207	-3.560
33	-0.102	0.126	-0.036	-0.259	-0.021	-2.304
37	-0.533	-0.017	0.693	-0.602	0.054	-5.732
39	-0.245	-0.041	0.779	-0.595	0.066	-6.776
43	-0.478	-0.070	0.695	-0.308	0.068	-9.764
44	-0.573	-0.060	0.645	-0.207	0.065	-10.027
45	-0.668	-0.047	0.769	-0.105	0.060	-9.894
49	-0.933	0.052	1.035	0.225	0.033	-7.249
51	-0.668	0.077	0.905	0.260	0.021	-6.143
55	-1.139	0.126	-0.139	-0.028	-0.021	-2.261
60	-1.974	0.166	-0.893	-0.367	-0.009	-2.101
61	-2.084	0.170	-1.058	-0.389	-0.006	-2.180
62	-2.104	0.171	-1.324	-0.338	-0.002	-2.319
67	-2.158	0.128	0.095	-0.056	-0.003	-0.288
101	2.131	-1.089	0.684	0.017	0.387	-5.926
102	2.037	-0.771	0.551	-0.108	0.290	-5.244
127	-0.803	-0.402	0.388	0.376	0.163	-6.634
129	-0.210	-0.274	0.216	0.378	0.119	-7.671
139	-0.306	-0.010	0.653	-0.843	0.036	-7.118
140	-0.403	0.011	0.472	-0.983	0.042	-6.158

Ux = Longitudinal displacement; Uy = Transverse displacement; Uz=Vertical displacement

Table 5.15 Maximum and Minimum Base Shear Force (kips) from Modal Time-History (Sec) for the 50-Year Earthquake

Seismic Excitation Case	Longitudinal Direction				Transverse Direction				Vertical Direction			
	Maximum		Minimum		Maximum		Minimum		Maximum		Minimum	
	Force	Time	Force	Time	Force	Time	Force	Time	Force	Time	Force	Time
LL11	4806	0.96	-2711	1.28	199.5	1.485	-168.5	1.94	9286	0.96	-8817	0.935
TT11	164.5	1.24	-146.4	2.485	6396	1.445	-5113	1.50	9326	0.96	-8762	0.935
LL22	1405	0.57	-1702	0.84	99.15	1.58	-101.8	0.935	9299	0.96	-8749	0.935
TT22	113	1.25	-133.8	2.50	2316	1.05	-1964	0.59	9337	0.96	-8791	0.935
L1T2V3	4777	0.96	-2761	1.28	2278	1.045	-1954	0.595	5436	0.78	-4955	0.755
L2T1V3	1394	0.57	-1652	0.845	6301	1.445	-5081	1.50	5342	0.78	-4747	0.755

Table 5.16 Bearing Force Capacity/Demand Ratios (r_{bf}) of the Main bridge without site soil coefficients for the 50-Year Earthquake

Pier	Anchor Bolt Capacity, V_c			Seismic Force (kip)			Seismic Demand V_b=1.25x H_R	C/D ratio $r_{bf}=V_c/V_b$	Minimum Additional Capacity of Bolts Required[b] per Pier to make $r_{bf} \geq 1$
	Number of 2" dia. bolts per bearing	Available shear area of bolts per bearing (in^2)	Available force capacity of two bearings on each pier[a] (kips)	Longitudinal H_L (kips)	Transverse H_T (kips)	Resultant H_R (kips)	(kips)		(kips)
A	4	12.566	452.4	646	2001.628	2103.219	2629.024	0.172	2180
B	4	12.566	452.4	1089	897.3588	1410.749	1763.437	0.257	1315
C	4	12.566	452.4	1585	875.6124	1811.09	2263.863	0.200	1815
D	4	12.566	452.4	816	897.2053	1213.077	1516.347	0.298	1065
E	4	12.566	452.4	670	1724	1850	2312	0.196	1860

[a]Shear strength of anchor bolts is assumed as 18 ksi

[b]Alternate retrofit would be to replace the existing fixed bearings with seismic isolation bearings

Table 6.1a Calculation of Superstructure Weights for 150′ Truss Spans

Component		Particulars		Weight (lb)
Truss	Bottom chord	Channels - 2x(42.7x120+58x30) Plate - 17.5x0.5x90x12x0.2833	2x1.1x(16405+ 23034+15610+ 3456)*	128,711
	Top chord	Channels -2x42.7x(4x15x2)+2x58x30 Plate - 20x0.5x150x12x0.2833 Flat- 2x5x(3x15x2)x12x0.2833 Web plate- 2x15x3/8x30x12x0.2833		
	Diagonals	2x(116+77+77+49+49)x21.21		
	Verticals	36x6x16		
Laterals		9.8x41x10		3,731
Floor beams		151x34x1.1		56,474
Stringers		43x150x5		32,250
Side walk stringers		Channels-33.9x150x2; Angle-22x150x2		16,770
Deck (concrete)		30x150x7/12x150		393,750
Curb, Side walk(concrete)		(7/12x2.5x150+1.75+0.5x150)x150		52,500

* For 2 Trusses and 10% extra for joints, splices etc. **Total ≈ 684 kips**

Table 6.1b Calculation of Superstructure Weights for 100′ Girder Spans

Component	Particulars		Weight (lb)
Girder	Web- 2x(96x7/16+4x7.5+16x0.5)x100x12x.2833 Flange-2x16x0.5x(76+2x65+2x45)x12x0.2833	1.1*x(70494 +23125 +36680 +3372)	70,494
Floor beam	(44x7/16+4x5.31)x28x12x6x0.2833		23,125
Stringers	51x100x5+(33.9x100+22x100)x2		36,680
Laterals	9.8x10x34.41		3372
Deck(concrete)	100x30x7/12x150		262,500

* 10% extra for joints, splices etc. **Total ≈ 410 kips**

Table 6.1c Calculation of Superstructure Weights for 46' Girder Span

Component	Particulars	Weight (lb)
Stringers	Main - 115x7x46 Side walk -33.9x2x46 + 22x2x46	42,173
Cross beams	(16.25x4.75x4+33.9x4.5x2)x2	1,227
Deck (concrete)	30x46x7/12x150	120,750
Curb and Side walk(concrete)	7/12x2.5x46+1.75x0.5x46)x150	16,100
Total		**180 kips**

Table 6.2 Calculation of Pier Stiffness and Pier Mass of SDOF Systems

Model[4]	Top		Bottom		Height	L'_{max}	Area			Moment of Inertia			Stiffness		Mass
	width	depth	width	depth			top	bot.	avg.	top	bot.	avg.	max[2]	min[3]	
HE1	35	5	37.54	7.55	36	76	175	283	229	365	1346	855	22663	2409	12.34
HE2	35	5	36.56	6.56	24.25	64.25	175	240	207	365	860	612	53072	2854	7.52
HE3	34	4	36.08	6.08	30	70	136	219	178	181	676	429	19618	1544	7.97
HE4	34	4	35.88	5.88	27.5	67.5	136	211	173	181	608	395	23452	1586	7.13
HE5	31	3	33.29	5.29	32.5	35.88	93	176	135	70	411	240	8649	779	6.54
HE6	31	3	33.13	5.13	30.5	70.5	93	170	131	70	373	221	9638	780	6.00
HE7	31	3	33.08	5.08	30	70	93	168	131	70	361	216	9868	777	5.86
HE8	31	3	33.08	5.08	30	70	93	168	131	70	361	216	9868	777	5.86
HE9	31	3	32.92	4.92	28	68	93	162	127	70	327	198	11162	779	5.34
HE10	31	3	32.83	4.83	27	67	93	159	126	70	308	189	11869	777	5.08
HE11	31	3	32.75	4.75	26	66	93	156	124	70	292	181	12737	779	4.83
HE12	31	3	32.67	4.67	25	65	93	153	123	70	277	174	13726	781	4.59
HE13	31	3	32.54	4.54	23.5	63.5	93	148	120	70	254	162	15405	781	4.23
HE14	31	3	32.42	4.42	22	62	93	143	118	70	233	152	17588	786	3.89
HE15	31	3	32.33	4.33	21	61	93	140	116	70	219	144	19250	785	3.66
HE16	31	3	32.38	4.38	21	61	93	142	117	70	227	148	19785	807	3.69
HE17	31	3	32.38	4.38	21	61	93	142	117	70	227	148	19785	807	3.69
HE18	31	3	32.58	4.58	24	64	93	149	121	70	261	165	14779	779	4.35
HE19	31	3	32.79	4.79	26.5	66.5	93	157	125	70	300	185	12289	778	4.95
HE20	31	3	32.79	4.79	26.5	66.5	93	157	125	70	300	185	12289	778	4.95
HE21	31	3	32.79	4.79	26.5	66.5	93	157	125	70	300	185	12289	778	4.95
HE22	31	3	32.79	4.79	26.5	66.5	93	157	125	70	300	185	12289	778	4.95
HE23	31	3	32.79	4.79	26.5	66.5	93	157	125	70	300	185	12289	778	4.95
HE24	31	3	32.79	4.79	26.5	66.5	93	157	125	70	300	185	12289	778	4.95
HE25	31	3	32.79	4.79	26.5	66.5	93	157	125	70	300	185	12289	778	4.95
HE26	31	3	32.67	4.67	25	65	93	153	123	70	277	174	13726	781	4.59
HE27	31	3	32.67	4.67	25	65	93	153	123	70	277	174	13726	781	4.59
HE28	31	3	32.67	4.67	25	65	93	153	123	70	277	174	13726	781	4.59
HE29	31	3	32.67	4.67	25	65	93	153	123	70	277	174	13726	781	4.59
HE30	31	3	32.67	4.67	25	65	93	153	123	70	277	174	13726	781	4.59
HE31	31	3	32.38	4.38	21	61	93	142	117	70	227	148	19785	807	3.69
HE32	31	3	32.00	4	17	57	93	128	111	70	171	120	30242	802	2.81
HE33	31	3	31.75	3.75	14	54	93	119	106	70	140	105	47133	821	2.22
EV1	35	5	37.58	7.58	36.5	86.5	175	285	230	365	1364	864	21967	1650	12.55
EV2	35	5	37.50	7.5	35.5	85.5	175	281	228	365	1318	841	23247	1664	12.11
EV3	35	5	37.13	7.13	31	61	175	265	220	365	1122	743	30829	4046	10.19
EV4	35	5	37.21	7.21	32	62	175	268	222	365	1162	763	28795	3959	10.61
EV5	34	4	37.50	7.5	47	82	136	281	209	181	1318	750	8927	1681	14.66
EV6	34	4	37.25	7.25	44	74	136	270	203	181	1183	682	9898	2081	13.36

All quantities are in Ft and kip units

[1]The height of Pier + Depth of pile cap + Half the depth of pile

[2]Assumed the pier is fixed at bottom of pile cap (used for force calculation)

[3]Assumed the pier extends up to half depth of pile where it is fixed (used for displacement calculation)

[4]Models are shown in Figures 6.4 and 6.5

Table 6.3 Seismic Force and Displacement Response

Model	Mass			Seismic Force							Seismic Displacement						
	Pier	Super-struc-ture	Total	Stiff ness (max)	Natural Freque ncy (Hz)	Period (sec)	PSA[1]	C^2_S	C^3_S	Force P[4]	Stiffness (min)	Natural Freque ncy (Hz)	Period (sec)	PSA[1]	C^2_S	C^3_S	Displ-cement[5] (in)
HE1	12.3	42.8	55.2	22663	3.23	0.31	350	0.65	0.375	662	2409	1.05	0.95	175	0.32	0.320	2.8
HE2	7.5	21.4	28.9	53072	6.67	0.15	550	1.01	0.375	347	2854	1.59	0.63	230	0.42	0.375	1.5
HE3	8.0	12.8	20.8	19618	5.00	0.20	450	0.83	0.375	249	1544	1.37	0.73	210	0.39	0.375	1.9
HE4	7.1	18.4	25.6	23452	4.76	0.21	430	0.79	0.375	307	1586	1.25	0.80	200	0.37	0.370	2.3
HE5	6.5	5.6	12.2	8649	4.17	0.24	400	0.74	0.375	146	779	1.27	0.79	205	0.38	0.375	2.2
HE6	6.0	5.6	11.6	9638	4.55	0.22	420	0.77	0.375	140	780	1.30	0.77	210	0.39	0.375	2.1
HE7	5.9	5.6	11.5	9868	4.76	0.21	430	0.79	0.375	138	777	1.32	0.76	210	0.39	0.375	2.1
HE8	5.9	5.6	11.5	9868	4.76	0.21	430	0.79	0.375	138	777	1.32	0.76	210	0.39	0.375	2.1
HE9	5.3	5.6	11.0	11162	5.00	0.20	450	0.83	0.375	132	779	1.33	0.75	215	0.40	0.375	2.0
HE10	5.1	5.6	10.7	11869	5.26	0.19	470	0.87	0.375	129	777	1.35	0.74	215	0.40	0.375	2.0
HE11	4.8	5.6	10.5	12737	5.56	0.18	480	0.89	0.375	126	779	1.37	0.73	210	0.39	0.375	1.9
HE12	4.6	5.6	10.2	13726	5.88	0.17	500	0.92	0.375	123	781	1.39	0.72	210	0.39	0.375	1.9
HE13	4.2	5.6	9.9	16405	6.25	0.16	500	0.92	0.375	118	781	1.41	0.71	220	0.41	0.375	1.8
HE14	3.9	5.6	9.5	17588	6.67	0.15	550	1.01	0.375	114	786	1.45	0.69	225	0.42	0.375	1.7
HE15	3.7	5.6	9.3	19250	7.14	0.14	600	1.11	0.375	111	785	1.47	0.68	230	0.42	0.375	1.7
HE16	3.7	5.6	9.3	19785	7.14	0.14	600	1.11	0.375	112	807	1.47	0.68	230	0.42	0.375	1.7
HE17	3.7	5.6	9.3	19785	7.14	0.14	600	1.11	0.375	112	807	1.47	0.68	230	0.42	0.375	1.7
HE18	4.4	5.6	10.0	14779	6.25	0.16	500	0.92	0.375	120	779	1.41	0.71	220	0.41	0.375	1.8
HE19	5.0	5.6	10.6	12289	5.56	0.18	480	0.89	0.375	127	778	1.37	0.73	210	0.39	0.375	2.0
HE20	5.0	5.6	10.6	12289	5.56	0.18	480	0.89	0.375	127	778	1.37	0.73	210	0.39	0.375	2.0
HE21	5.0	5.6	10.6	12289	5.56	0.18	480	0.89	0.375	127	778	1.37	0.73	210	0.39	0.375	2.0
HE22	5.0	5.6	10.6	12289	5.56	0.18	480	0.89	0.375	127	778	1.37	0.73	210	0.39	0.375	2.0
HE23	5.0	5.6	10.6	12289	5.56	0.18	480	0.89	0.375	127	778	1.37	0.73	210	0.39	0.375	2.0
HE24	5.0	5.6	10.6	12289	5.56	0.18	480	0.89	0.375	127	778	1.37	0.73	210	0.39	0.375	2.0
HE25	5.0	5.6	10.6	12289	5.56	0.18	480	0.89	0.375	127	778	1.37	0.73	210	0.39	0.375	2.0
HE26	4.6	5.6	10.2	13726	5.88	0.17	500	0.92	0.375	123	781	1.39	0.72	210	0.39	0.375	1.9
HE27	4.6	5.6	10.2	13726	5.88	0.17	500	0.92	0.375	123	781	1.39	0.72	210	0.39	0.375	1.9
HE28	4.6	5.6	10.2	13726	5.88	0.17	500	0.92	0.375	123	781	1.39	0.72	210	0.39	0.375	1.9
HE29	4.6	5.6	10.2	13726	5.88	0.17	500	0.92	0.375	123	781	1.39	0.72	210	0.39	0.375	1.9
HE30	4.6	5.6	10.2	13726	5.88	0.17	500	0.92	0.375	123	781	1.39	0.72	210	0.39	0.375	1.9
HE31	3.7	5.6	9.3	19785	7.14	0.14	600	1.11	0.375	112	807	1.47	0.68	230	0.42	0.375	1.7
HE32	2.8	5.6	8.4	30242	10.00	0.10	660	1.22	0.375	101	802	1.56	0.64	230	0.42	0.376	1.5
HE33	2.2	5.6	7.9	47133	12.50	0.08	780	1.44	0.375	94	821	1.64	0.61	240	0.44	0.375	1.4
EV1	12.6	42.8	55.4	21967	3.13	0.32	350	0.65	0.375	664	1650	0.87	1.15	170	0.31	0.310	4.0
EV2	12.1	42.8	54.9	23247	3.23	0.31	350	0.65	0.375	659	1664	0.88	1.14	170	0.31	0.310	3.9
EV3	10.6	21.4	32.0	28795	4.76	0.21	450	0.83	0.375	384	3959	1.75	0.57	240	0.44	0.376	1.2
EV4	14.7	12.8	27.5	8927	2.86	0.35	340	0.63	0.375	330	1681	1.25	0.80	200	0.37	0.370	2.3
EV5	13.4	12.8	26.2	9898	3.13	0.32	340	0.63	0.375	314	2081	1.43	0.70	220	0.41	0.375	1.0
EV6	14.8	12.8	27.6	19315	4.17	0.24	400	0.74	0.375	332	3015	1.67	0.60	240	0.44	0.375	1.3

All units are in kips and Ft. unless stated otherwise

[1]Acceleration determined from figure. A4 ,Ref.1

[2]As per AASHTO formula, $C_s=\frac{1.2(PSA)(S)}{g}$, with S=1.5

[3]C_S limited to 2.5A, i.e 2.5x0.15 =0.375

[4]P= C_s.Mass.g

[5] Displacement= C_s.Mass.g/stiffness

Table 6-4 Bearing Force Capacity/Demand Ratios (r_{bf}) for Fixed Pier Bearings on the Evansville, IN Approach on the US41 Northbound Bridge

Fixed Bearing at Pier (Each Pier has Two Bearings)	Span	Seismic Force (kips)	Minimum Bearing Force Demand[1] (kips)	Force Demand[2] 1.25xSeismic Force, $V_b(d)$ (kips)	Available Number of Anchor Bolts/ bolt diameter	Ultimate Shear Capacity[3] of the Bolts $V_b(c)$ (kips)	$r_{bf} = \frac{V_b(c)}{V_b(d)}$	Minimum Additional Capacity of bolts required[4] to make $r_{bf} \geq 1$ (kips)
N1	E-N1	332	137	415	4/1.5" dia	134	0.32	285
N1	N1-N2	332	137	415	,,	134	0.32	285
N3	N2-N3	329.5	137	412	,,	134	0.33	280
N3	N3-N4	329.5	137	412	,,	134	0.33	280
N5	N4-N5	384	137	480	,,	134	0.28	350
N6	N5-N6	330	82	413	,,	134	0.32	280
N7	N6-N7	314	82	393	,,	134	0.34	260
N8	N7-N8	332	82	415	,,	134	0.32	285

[1, 2] As per FHWA Seismic Retrofitting Manual for Highway Bridges.
[3] Assumed capacity of Bolt in Shear = 19.0 ksi (33ksi steel)
[4] Alternate retrofit would be to replace the fixed bearings with seismic isolation bearings

Table 6-5 Displacement C/D Ratios (r_{bd}) for Expansion Bearings in Evansville, IN Approach Bridge on the US 41 Northbound

Expansion Bearing at Pier	Method 2[2]				Method 1[2]				Retrofit Required?
	Displacement Demand Δ_{eq}(d), in	Available Seat Width Δ_s(c), in	[1]Contraction due to Temperature Δ_t(d), in	$r_{bd} = \frac{\Delta_s(c) - \Delta_t(d)}{\Delta_{eq}(d)}$	Height of Pier H, ft	Span Length L, ft	[2]Minimum seat width N(d), in	$r_{bd} = \frac{\Delta s(c)}{N(d)}$	
N2(N2-N1)	4	23	1.17	5.46	34	150	8.01	2.87	For all the expansion bearings **NO** retrofit required.
N2(N2-N3)	3.9	23	1.17	5.60	34	150	8.01	2.87	
N4(N4-N3)	3.9	23	1.17	5.60	33.5	150	10.94	2.10	
N4(N4-N5)	1.2	23	1.17	18.19	31.5	150	10.57	2.18	
N5	3.5	23	0.78	6.35	40	100	10.85	2.12	
N6	4.1	17	0.78	3.96	45.5	100	10.48	1.62	
N7	3.1	17	0.78	5.23	30	100	10.56	1.61	

[1]For Temperature T=90°F and Thermal Expansion Coeff. $\alpha = 6.5 \times 10^{-6}$/°F

[2]As per FHWA Seismic Retrofitting Manual for Highway Bridges, May 1995, Section A. 4.2.

[3]No Possibility for Loss of Span due to the Sliding Plate with Bolt type Expansion Bearing

Table 6-6 Bearing Force C/D Ratios (r_{bf}) for the Approach Bridge on the Henderson, KY of the US 41 Northbound Bridge

Fixed Bearing at Pier (Each Pier has Two Bearings)	Span	Seismic Force (kips)	Minimum Bearing Force Demand[1] (kips)	Force Demand[2] 1.25xSeismic Force $V_h(d)$ (kips)	Available Anchor Bolts in the Bearing/ diameter of bolts	Ultimate Shear Capacity[3] of the Bolts $V_h(c)$ (kips)	$r_{bf} = \frac{V_h(c)}{V_h(d)}$	Mimimum Additional Capacity of bolts required to make $r_{bf} \geq 1$ (kips)
S1	S1-A	331	137	414	4/1.5" dia	134	0.32	280
S1	S1-S2	331	137	414	,,	134	0.32	280
S3	S3-S2	347	137	434	,,	134	0.31	300
S4	S4-S3	249	82	311	,,	134	0.43	180
S5	S6-S4	307	82	384	,,	134	0.35	250
S6	S6-S7	146	36	183	14/1" dia	209	1.15	Not Applicable
S7	S7-S8	140	36	175	,,	209	1.19	
S8	S8-S9	138	36	173	,,	209	1.21	
S9	S9-S10	138	36	173	,,	209	1.21	
S10	S10-S11	132	36	165	,,	209	1.27	
S11	S11-S12	129	36	161	,,	209	1.30	
S12	S12-S13	126	36	158	,,	209	1.33	
S13	S13-S14	123	36	154	,,	209	1.36	
S14	S14-S15	118	36	148	,,	209	1.42	
S15	S15-S16	114	36	143	,,	209	1.47	
S16	S16-S17	111	36	139	,,	209	1.51	
S17	S17-S18	112	36	140	,,	209	1.49	
S18	S18-S19	112	36	140	,,	209	1.49	
S19	S19-S20	120	36	150	,,	209	1.39	
S20	S20-S21	127	36	159	,,	209	1.32	
S21	S21-S22	127	36	159	,,	209	1.32	
S22	S22-S23	127	36	159	,,	209	1.32	
S23	S23-S24	127	36	159	,,	209	1.32	
S24	S24-S25	127	36	159	,,	209	1.32	
S25	S25-S26	127	36	159	,,	209	1.32	
S26	S26-S27	127	36	159	,,	209	1.32	
S27	S27-S28	123	36	154	,,	209	1.36	
S28	S28-S29	123	36	154	,,	209	1.36	
S29	S29-S30	123	36	154		209	1.36	
S31	S31-S32	123	36	154	,,	209	1.36	
S32	S32-S33	112	36	140	,,	209	1.49	
S33	S33-S34	101	36	126	,,	209	1.66	
S34	S34-S35	94	36	118	,,	209	1.78	

Notes: All units are in kips and inches

[1,2] As per FHWA Seismic Retrofitting Manual for Highway Bridges.

[3] Assumed capacity of Bolt in Shear = 19.0 ksi (33ksi steel)

[1] Alternate retrofit would be to replace the fixed bearings with seismic isolation bearings

Table 6-7 Displacement C/D Ratios (r_{bd}) for Expansion Bearings in Henderson, KY Approach Bridge on the US 41 Northbound

Expansion Bearing at Pier	Method2[2]				Method1[2]				Retrofit Required?
	Displace-ment Demand Δ_{cd}(d) (in)	Available Seat Width Δ_s(c) (in)	[1]Contraction due to Tempera-ture Δ_t(d) (in)	$r_{bd} = \frac{\Delta_s(c) - \Delta_t(d)}{\Delta_{cd}(d)}$	Height of Pier H (ft)	Span Length L (ft)	[2]Minimum Seat Width N(d) (in.)	$r_{bd} = \frac{\Delta s(c)}{N(d)}$	
S2 (S2-S1)	2.8	23	1.17	7.80	33	150	10.89	2.11	For all the expansion bearings **NO** retrofit required
S2 (S2-S3)	1.5	23	1.17	14.55	27.125	150	9.96	2.31	
S3	3.4	23	0.78	6.54	27.125	100	10.42	2.21	
S4	4.2	17	0.78	3.86	28.75	100	10.22	1.66	
S6	4.5	11	0.36	2.36	30	46	10.62	[3]Not Applicable	
S7	4.3	11	0.36	2.47	31.5	46	10.46		
S8	4.2	11	0.36	2.53	30.25	46	10.41		
S9	4.2	11	0.36	2.53	30	46	10.41		
S10	4.1	11	0.36	2.60	29	46	10.25		
S11	3.9	11	0.36	2.73	27.5	46	10.17		
S12	3.9	11	0.36	2.73	26.5	46	10.09		
S13	3.8	11	0.36	2.80	25.5	46	10.01		
S14	3.7	11	0.36	2.88	24.25	46	9.89		
S15	3.5	11	0.36	3.04	22.75	46	9.77		
S16	3.4	11	0.36	3.13	21.5	46	9.69		
S17	3.4	11	0.36	3.13	21	46	9.69		
S18	3.4	11	0.36	3.13	21	46	9.69		
S19	3.5	11	0.36	3.04	22.5	46	9.93		
S20	3.8	11	0.36	2.80	25.25	46	10.13		
S21	4	11	0.36	2.66	26.5	46	10.13		
S22	4	11	0.36	2.66	26.5	46	10.13		
S23	4	11	0.36	2.66	26.5	46	10.13		
S24	4	11	0.36	2.66	26.5	46	10.13		
S25	4	11	0.36	2.66	26.5	46	10.13		
S26	4	11	0.36	2.66	26.5	46	10.13		
S27	3.9	11	0.36	2.73	26.75	46	10.01		
S28	3.8	11	0.36	2.80	25	46	10.01		
S29	3.8	11	0.36	2.80	25	46	10.01		
S30	3.8	11	0.36	2.80	25	46	10.01		
S31	3.8	11	0.36	2.80	25	46	10.01		
S32	3.6	11	0.36	2.96	23	46	9.69		
S33	3.2	11	0.36	3.33	19	46	9.38		
S34	2.9	11	0.36	3.67	15.5	46	9.13		
S35	1.58	11	0.36	6.73	7	46	8.02		

[1]For Temperature T=90°F and Thermal Expansion Coeff. $\alpha = 6.5 \times 10^{-6}$/°F

[2] As per FHWA Seismic Retrofitting Manual for Highway Bridges, May 1995, Section A. 4.2.

[3]No Possibility for Loss of Span due to the Sliding Plate with Bolt type Expansion Bearing

Figure 2.1a US41 Bridges over the Ohio River at Henderson, KY - Entrance View

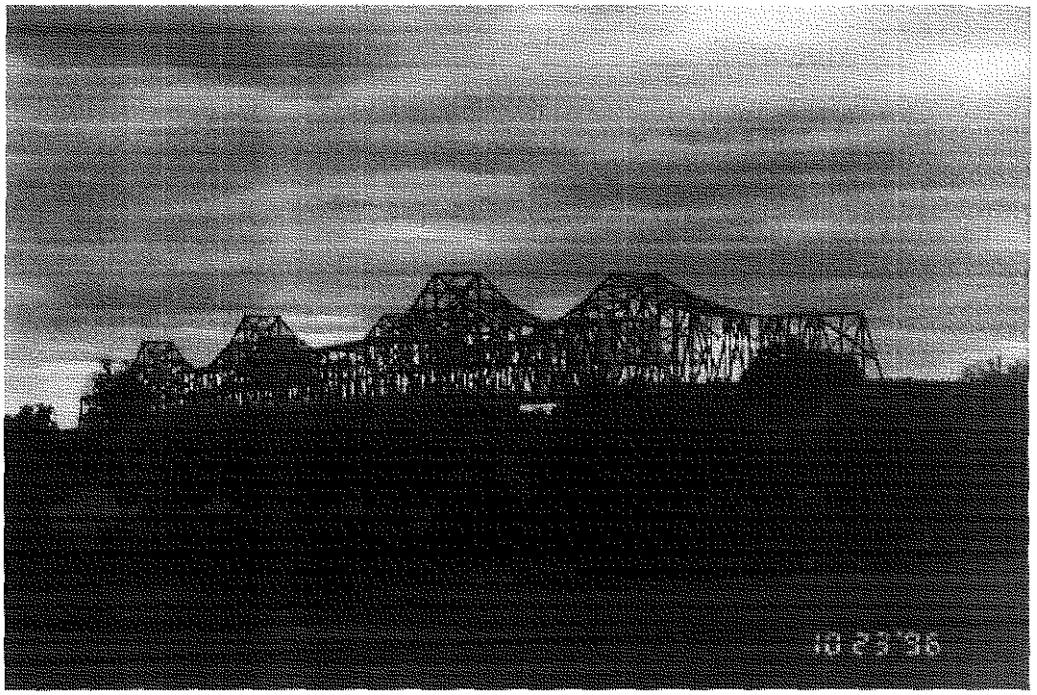

Figure 2.1b Side Views of the US41 Bridges over the Ohio river

Figure 2.1c End portal of the US41 Bridges

Figure 2.1d Typical Hinge Location on US41 Bridges

Figure 2.1e Inside View Showing Portals, Cross Bracings, etc

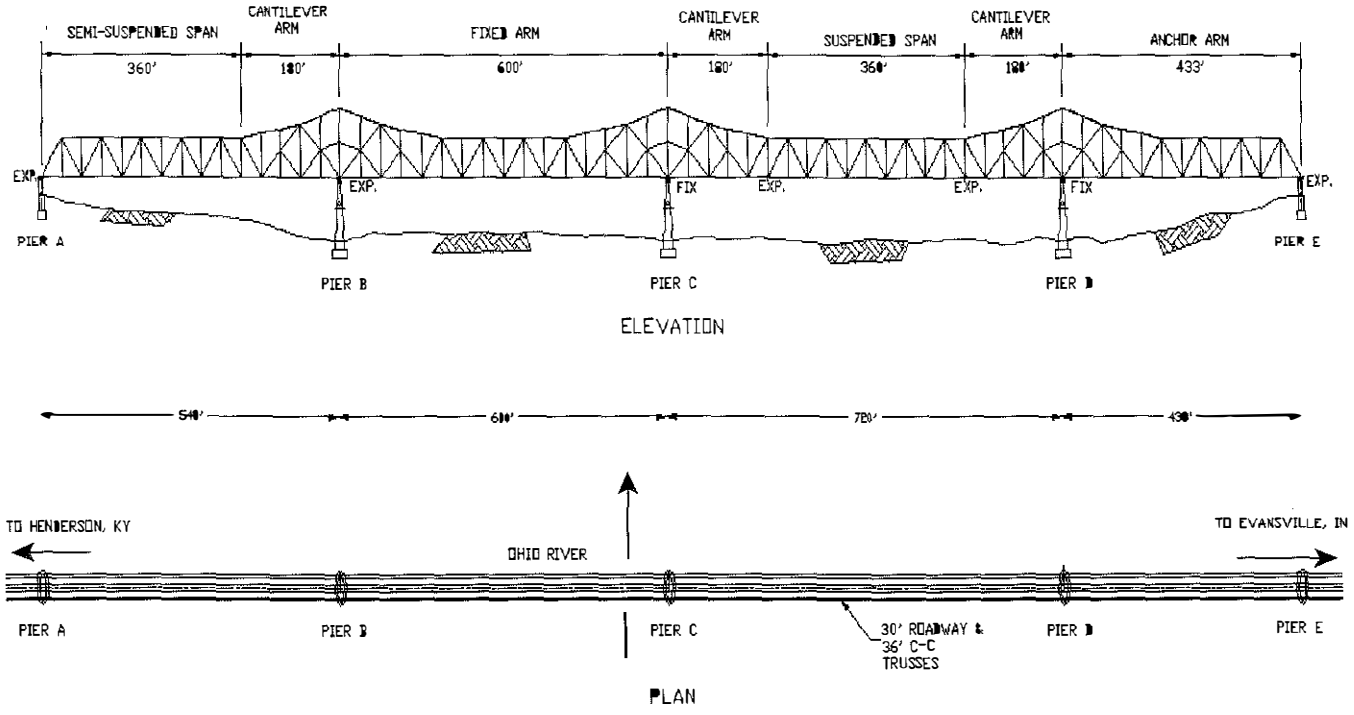

Figure 2.2 Plan and elevation of the main bridge

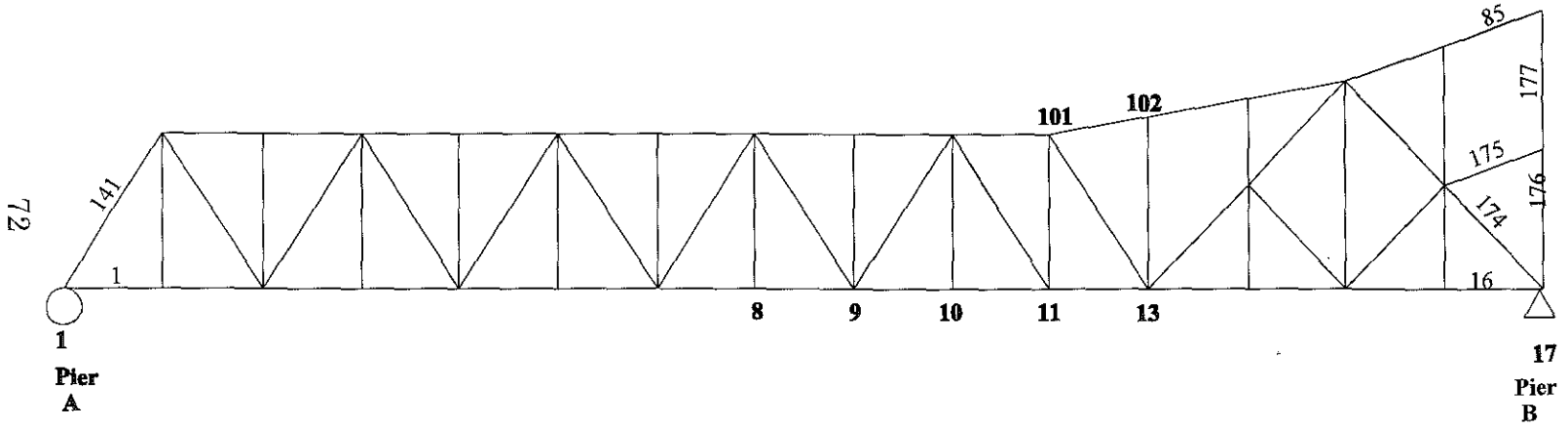

Note: Bold numbers are Joint numbers and the light ones are member numbers.

Figure 2.3 Elevation view of the first span A-B

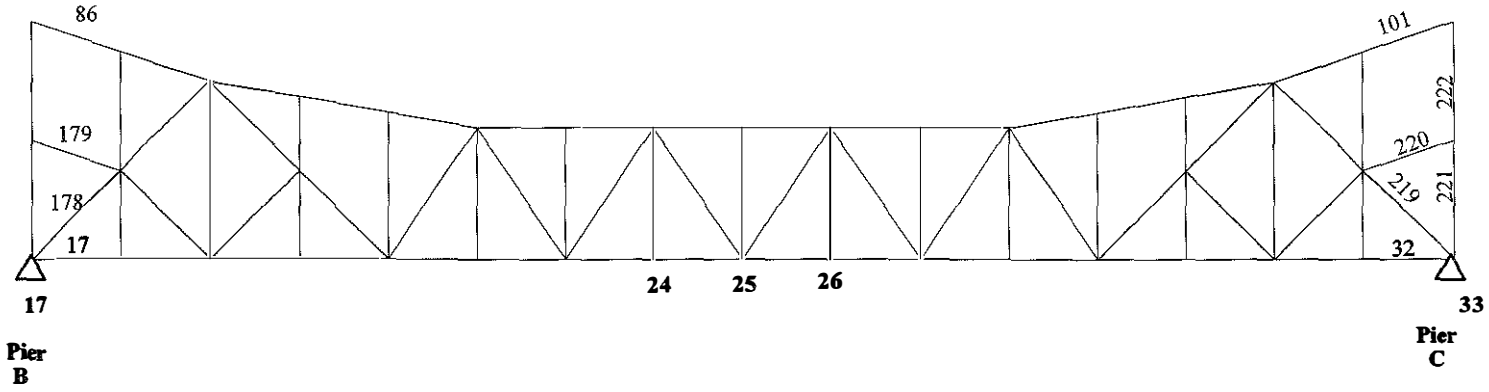

Note: Bold numbers are Joint numbers and the light ones are member numbers

Figure 2.4 Elevation view of the second span B-C

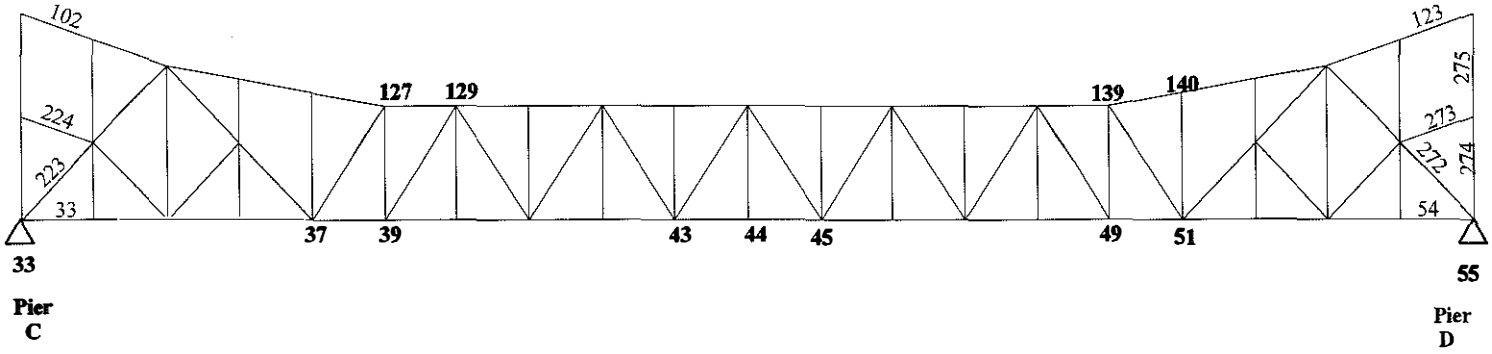

Note: Bold numbers are Joint numbers and the light ones are member numbers

Figure 2.5 Elevation of the third span C-D

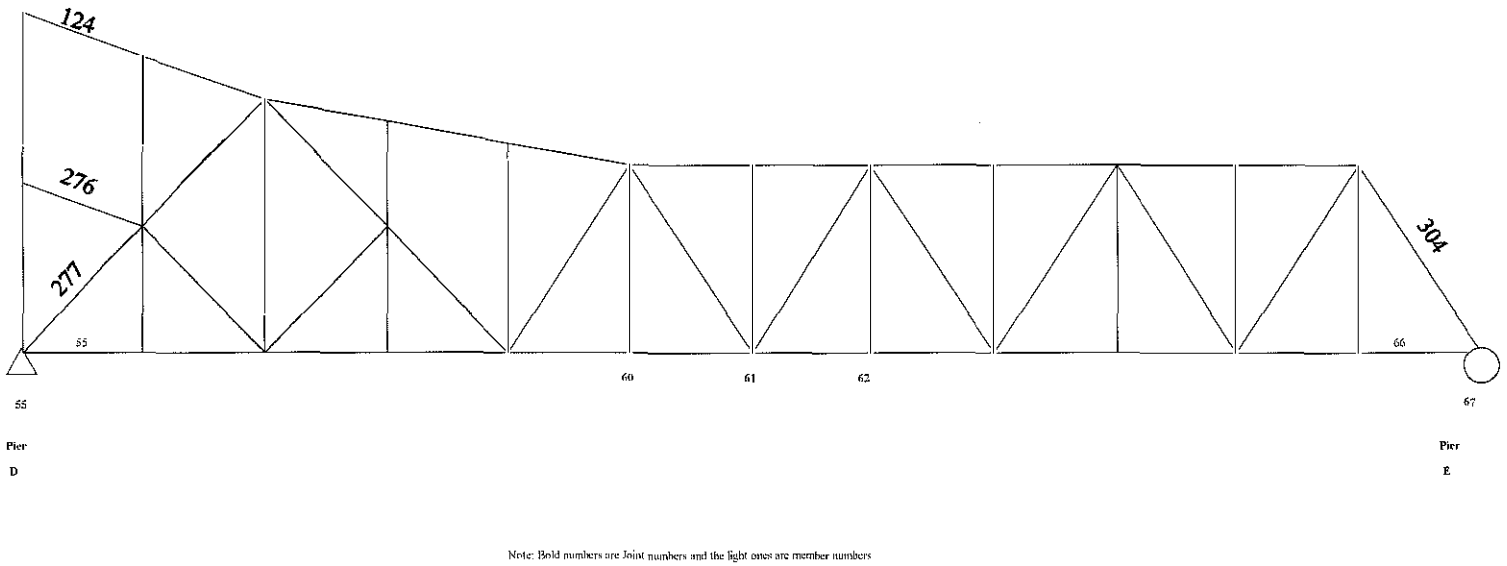

Figure 2.6 Elevation view of the fourth span D-E

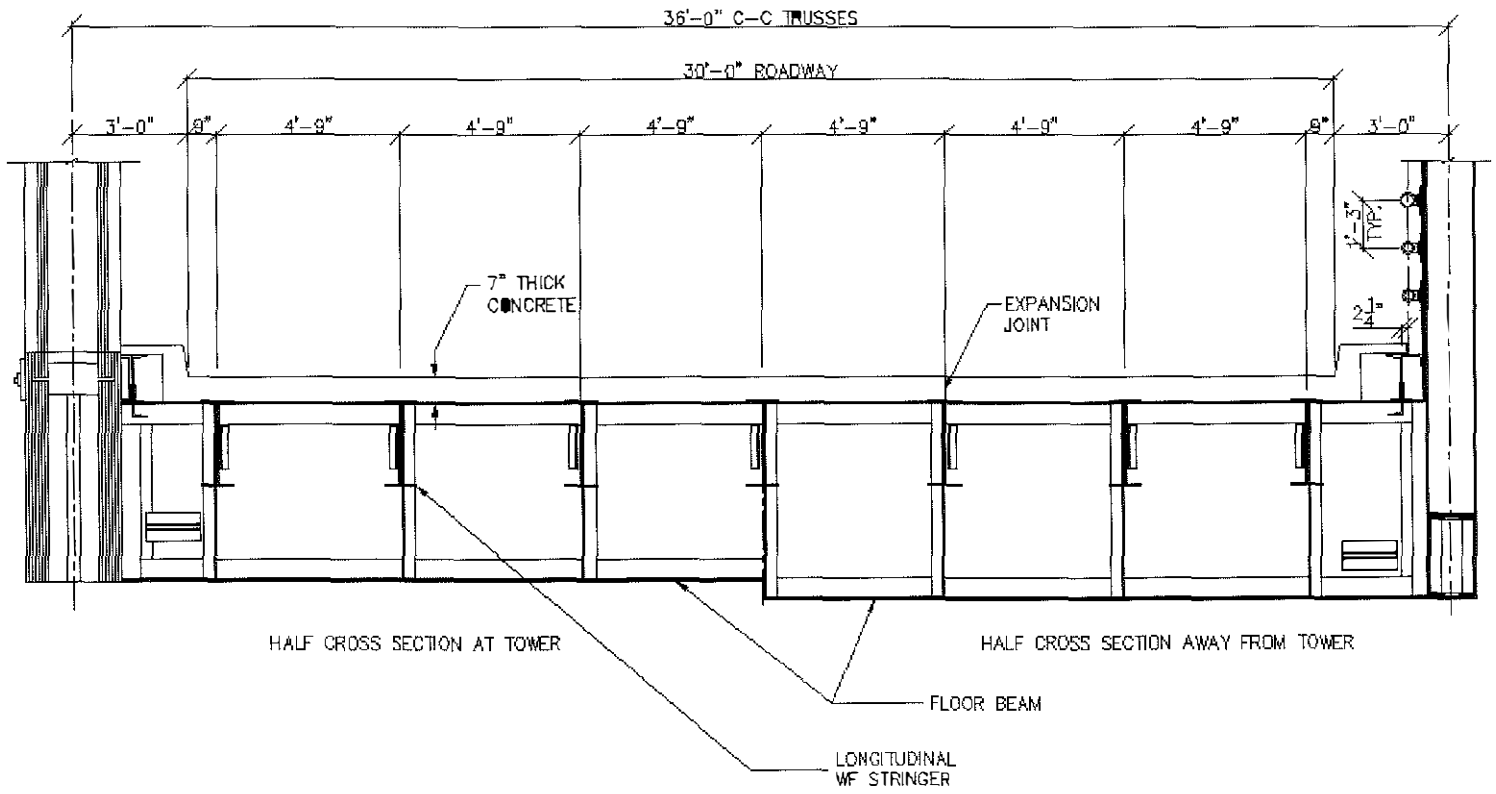

Figure 2.7 Cross section view of the main bridge deck

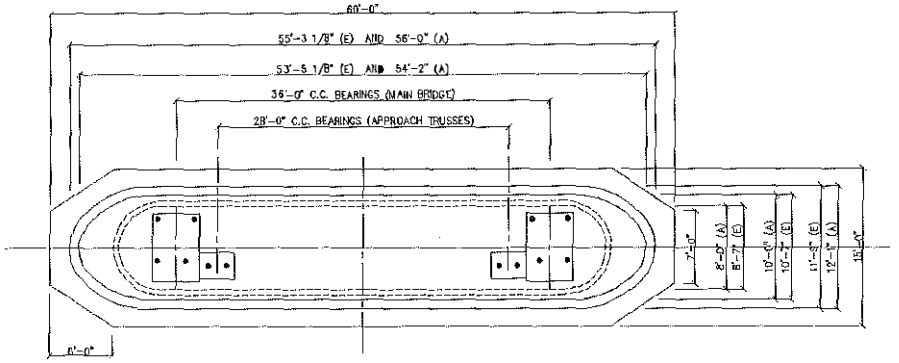

Figure 2.8a Plan view of pier A and E

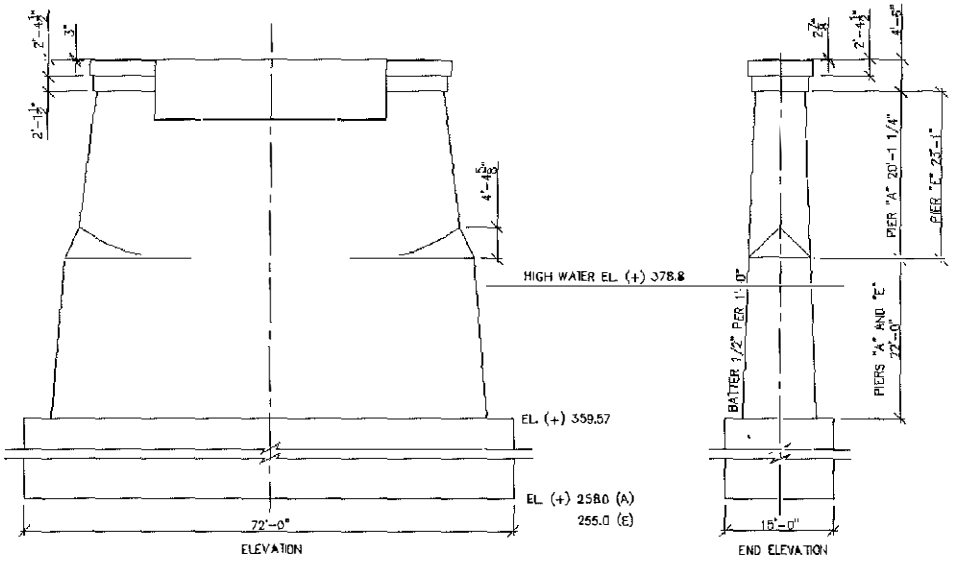

Figure 2.8b Elevation view of pier A and E

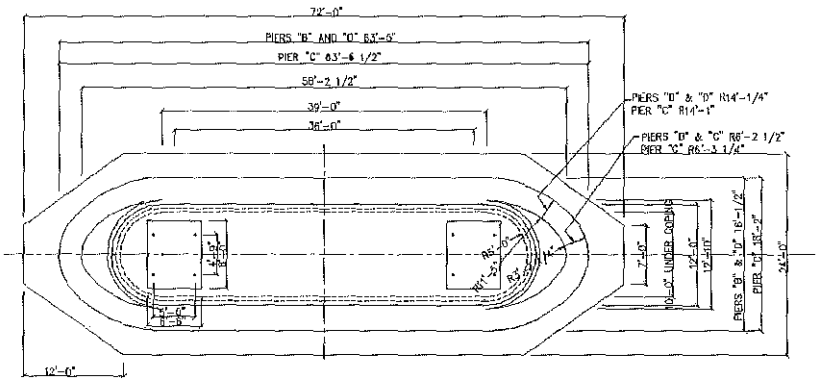

2.9a Plan view of piers B, C and D

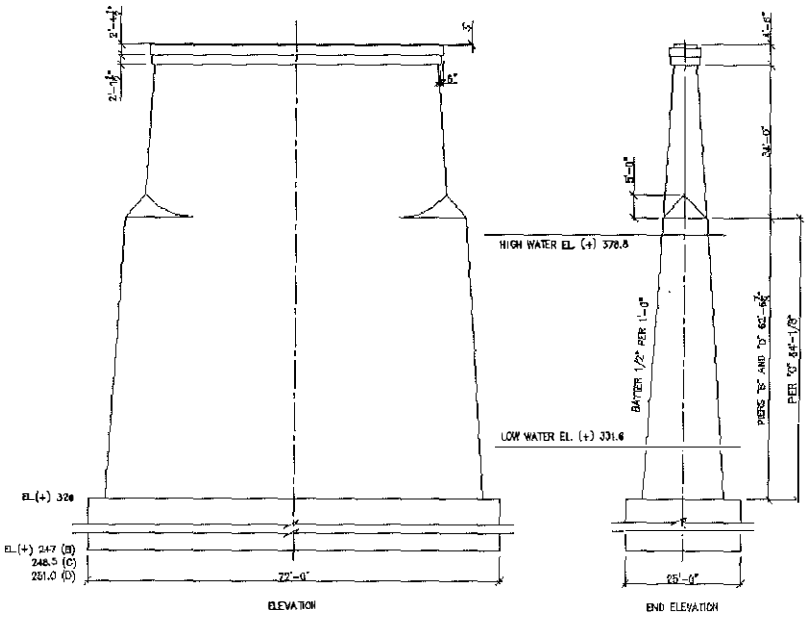

2.9b Elevation view of piers B, C, and D

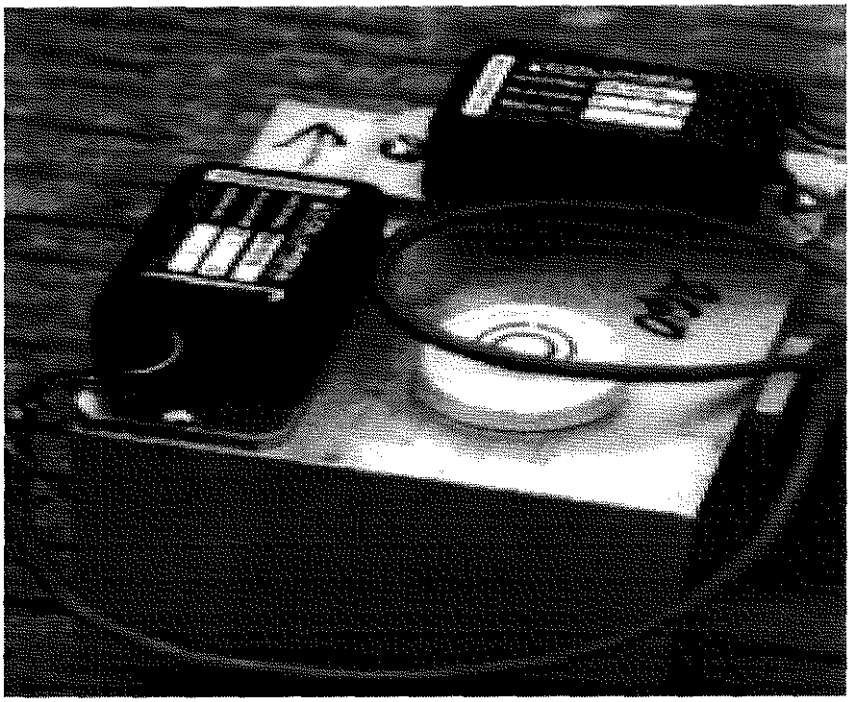

Figure 3.1a Triaxial Accelerometer Block

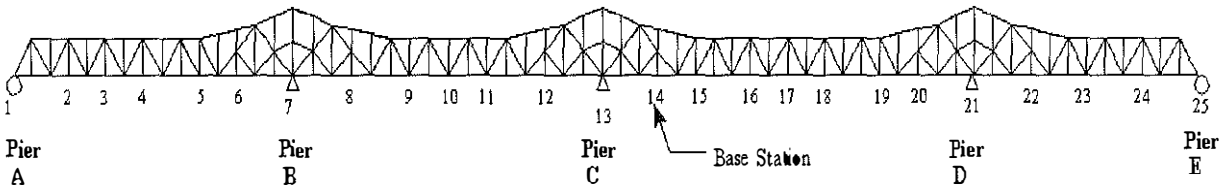

Figure 3.1b Accelerometer positions on the main bridge

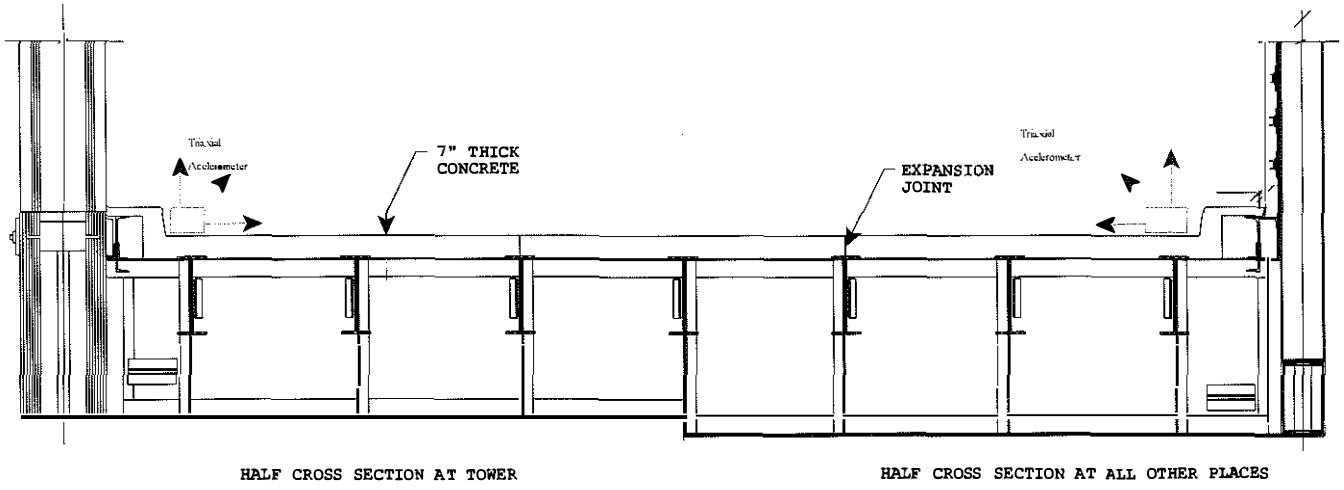

Figure 3.1c Accelerometer positions on the deck

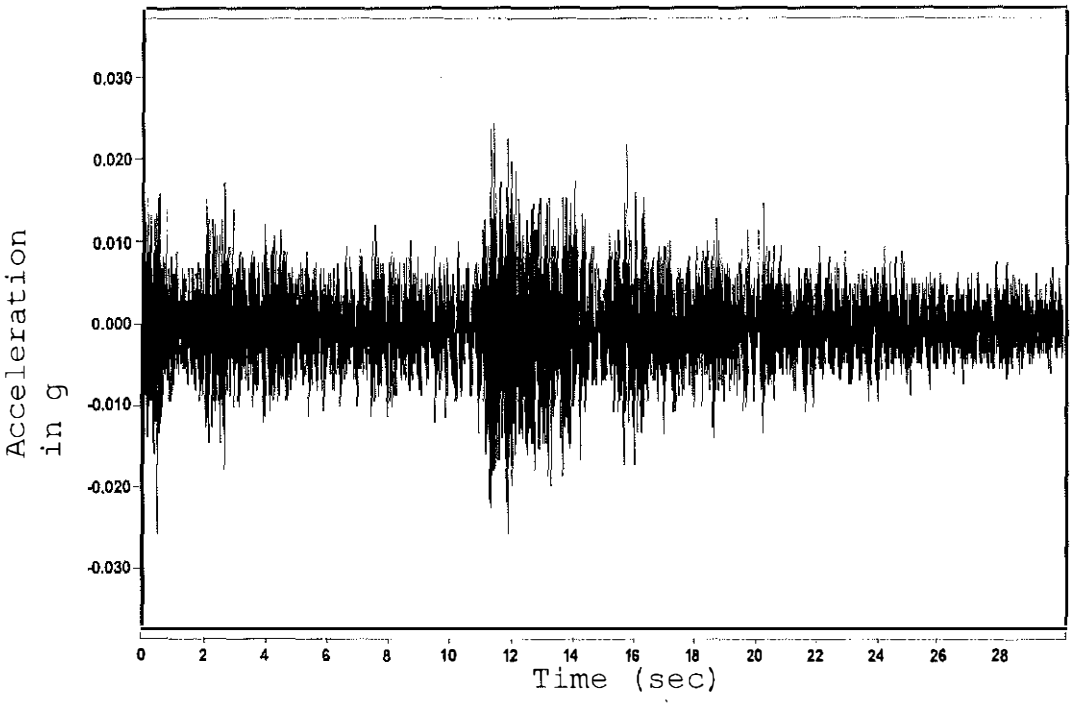

Figure 3.2a Transverse Acceleration-Time History From Field Testing at Moving Station 6

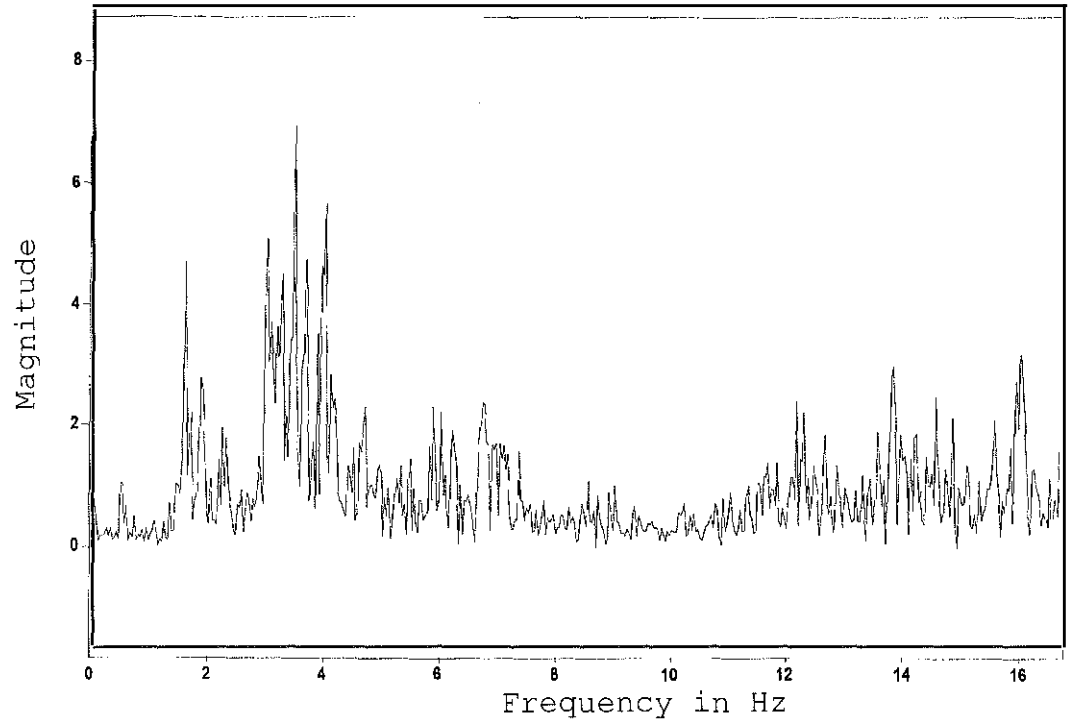

Figure 3.2b FFT of Transverse Acceleration-Time History at Moving Station 6

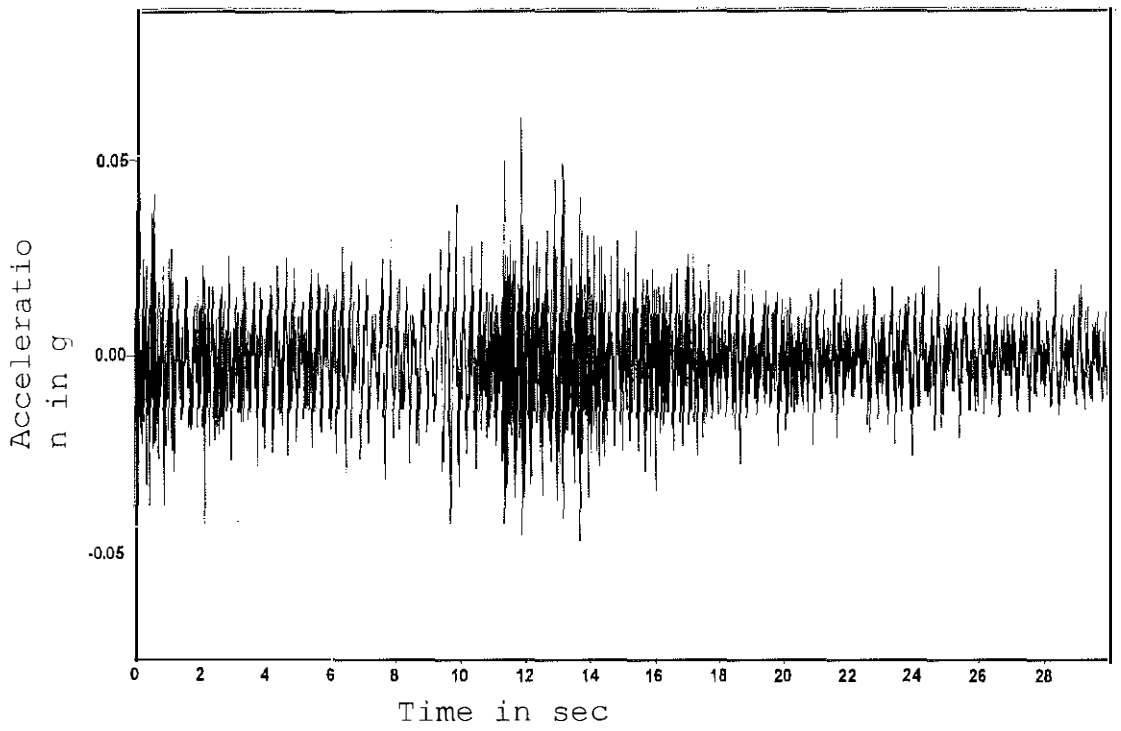

Figure 3.2c Vertical Acceleration-Time History from Field Testing at Moving Station 6

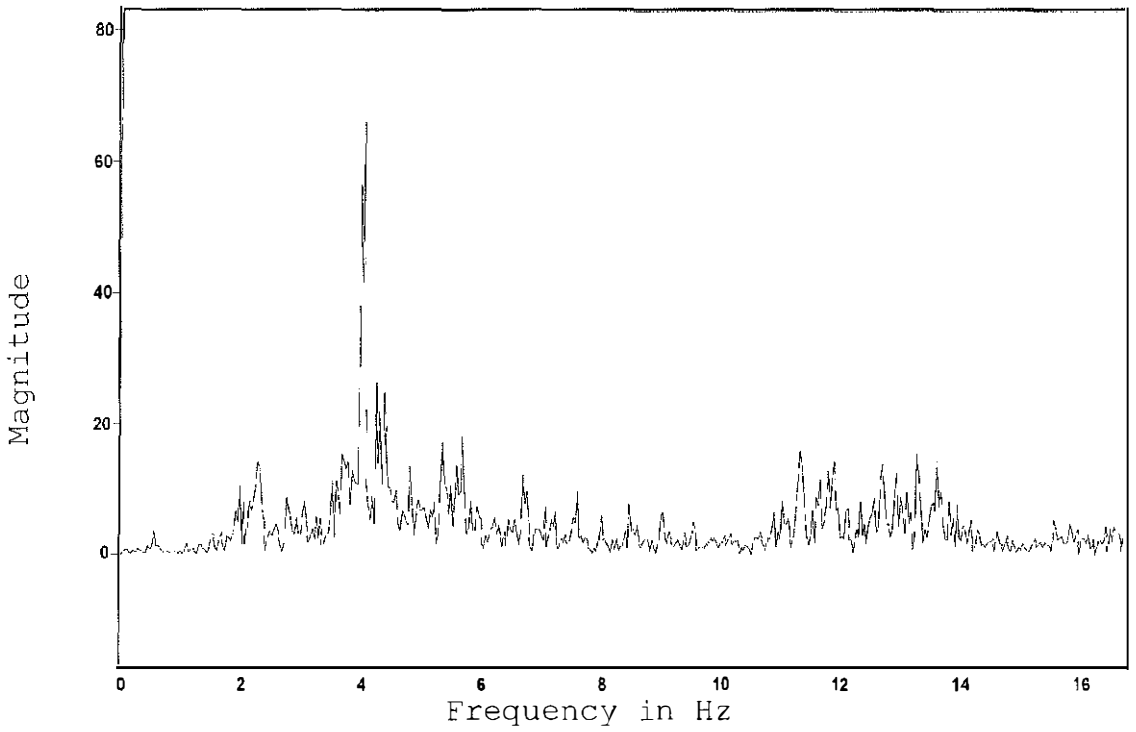

Figure 3.2d FFT of Vertical Acceleration-Time at Moving Station 6

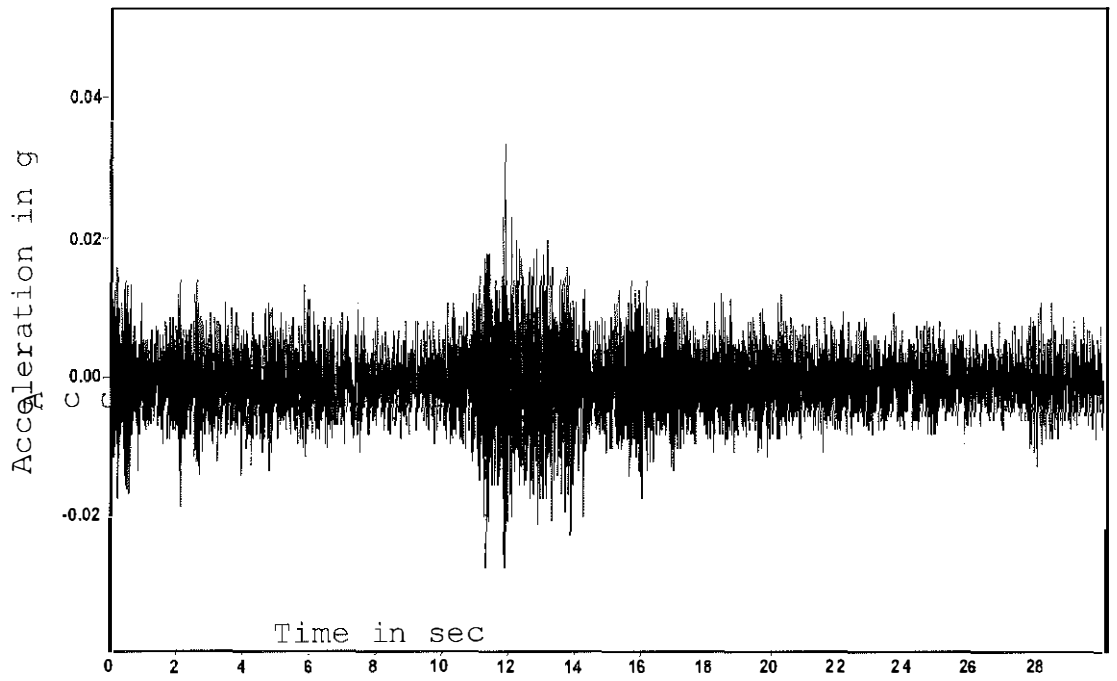

Figure 3.2e Longitudinal Acceleration-Time History from Field Testing at Moving Station 6

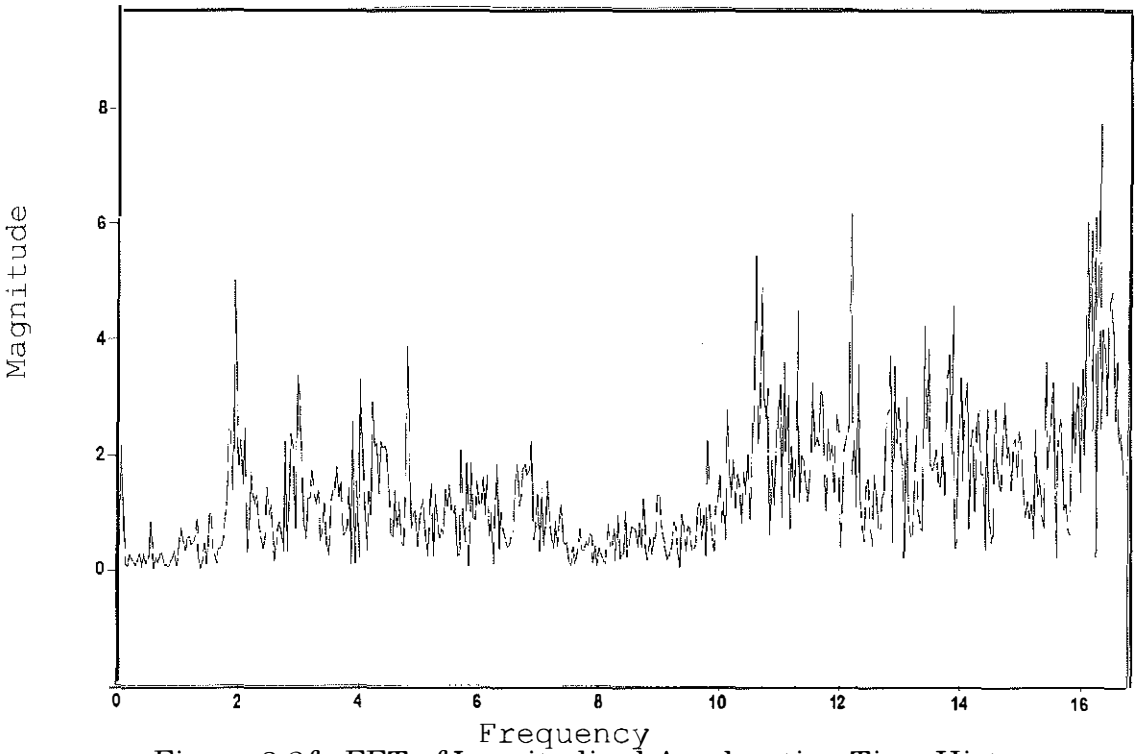

Figure 3.2f FFT of Longitudinal Acceleration-Time History at Moving Station 6

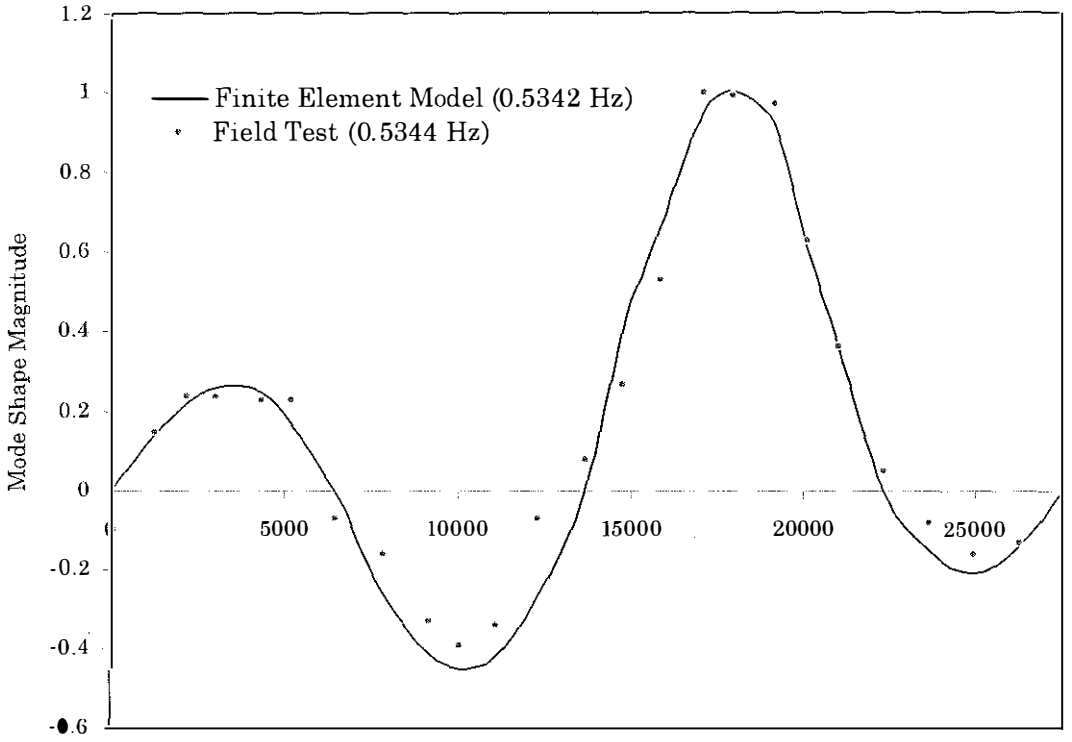

Figure 3.3a First Transverse Mode

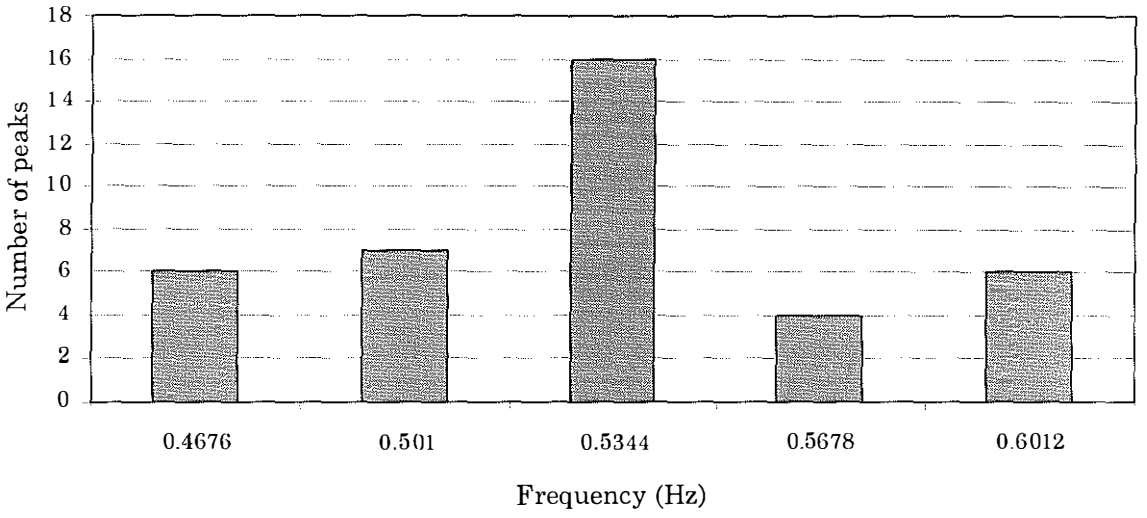

Figure 3.3b Peak Comparison for the First Transverse Mode

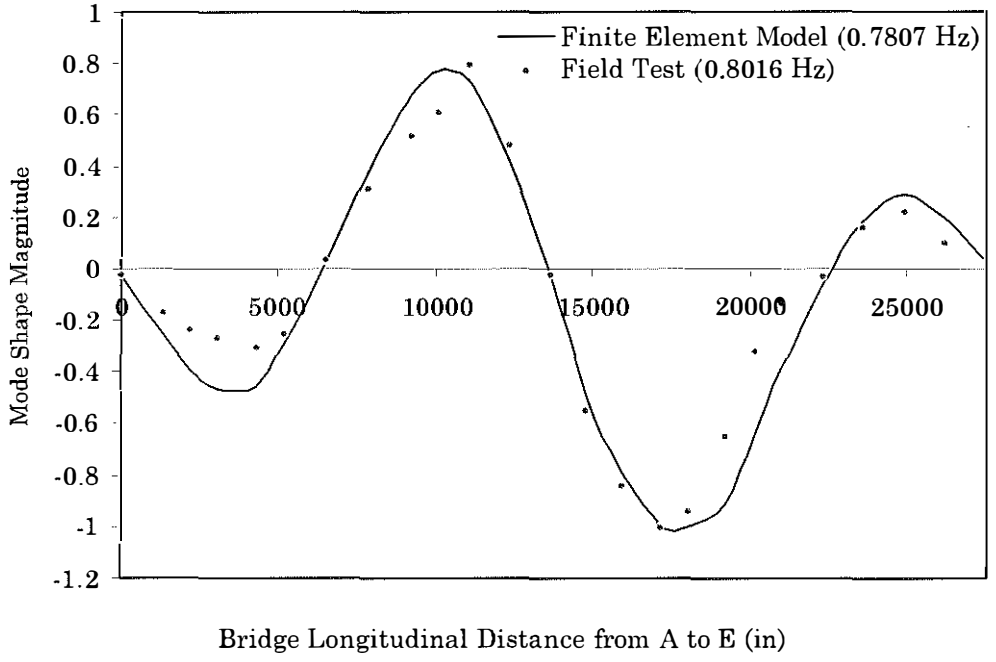

Figure 3.4a First Vertical Mode

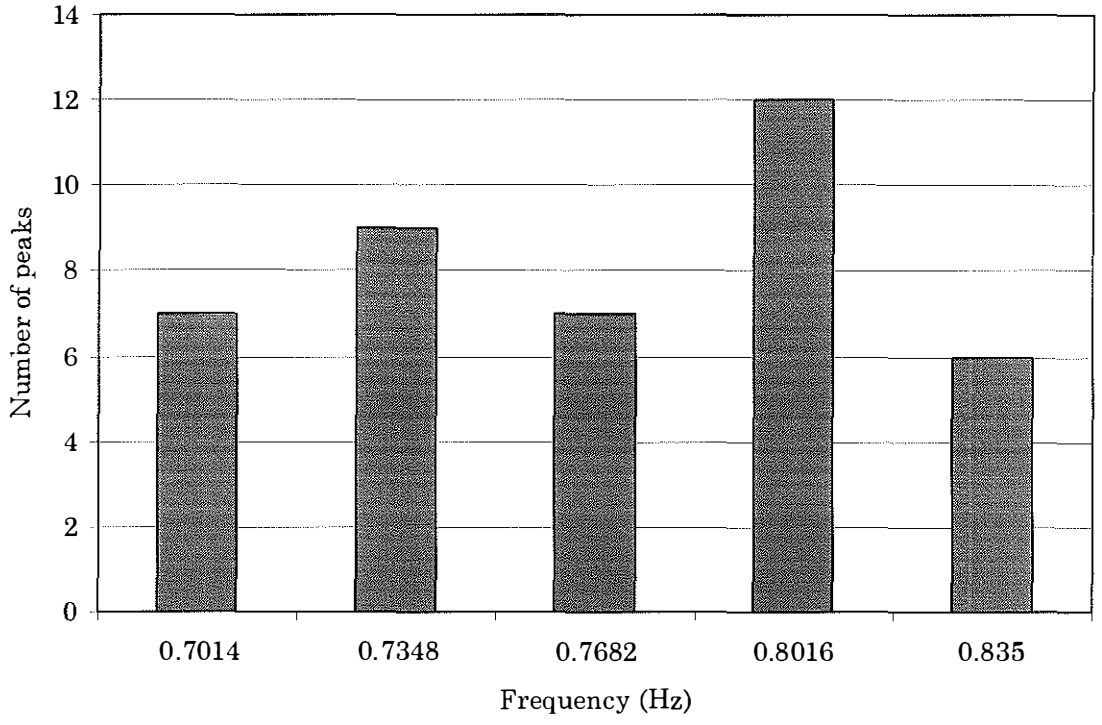

Figure 3.4b Peak Comparison for the First Vertical Mode

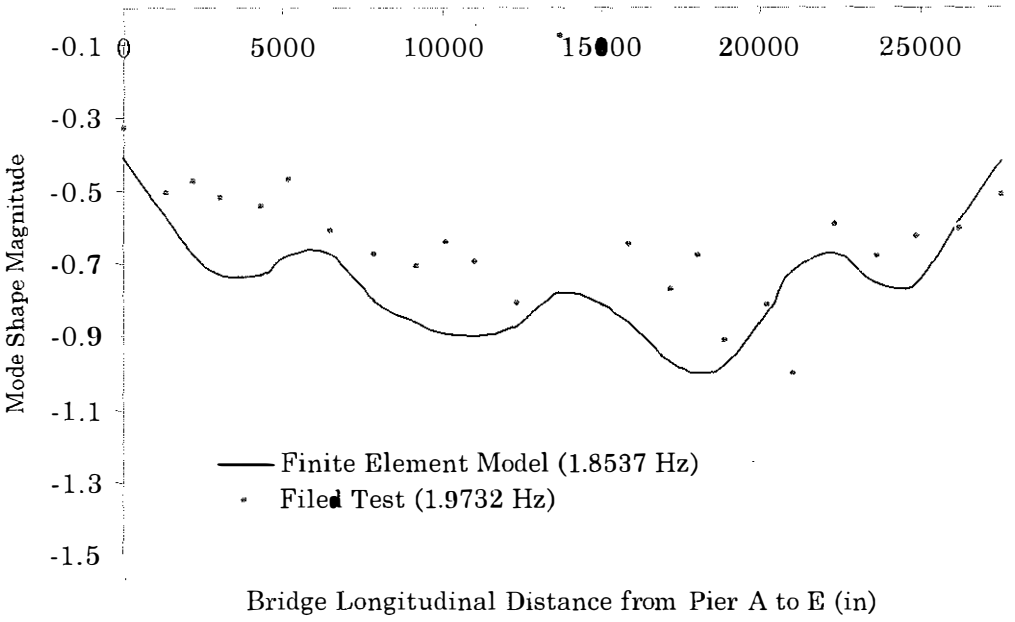

Figure 3.5a First Longitudinal Mode

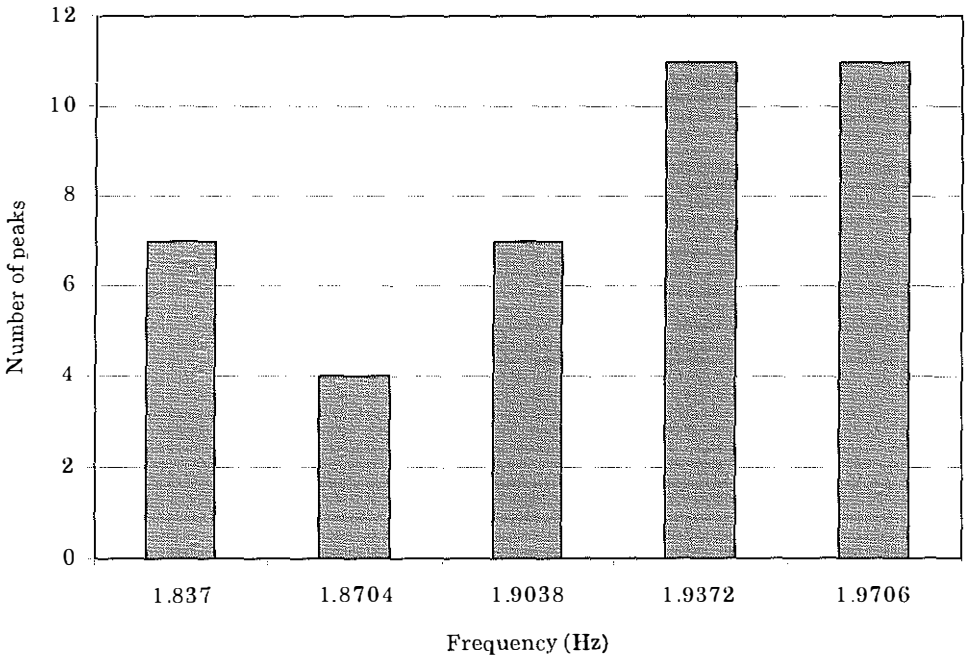

Figure 3.5b Peak Comparison for the First Longitudinal Mode

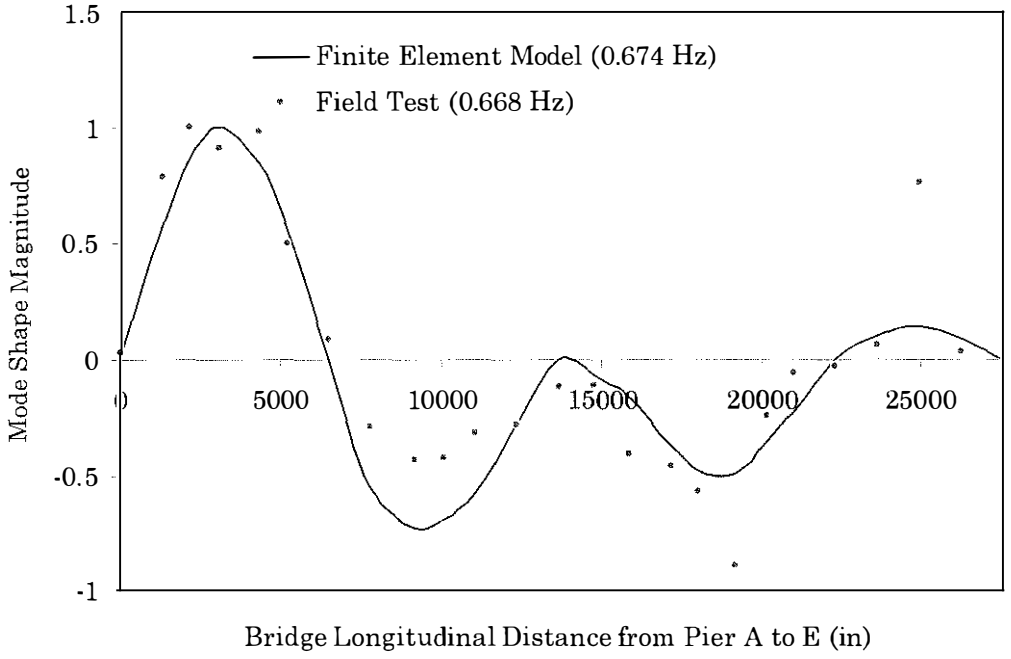

Figure 3.6a Second Transverse Mode

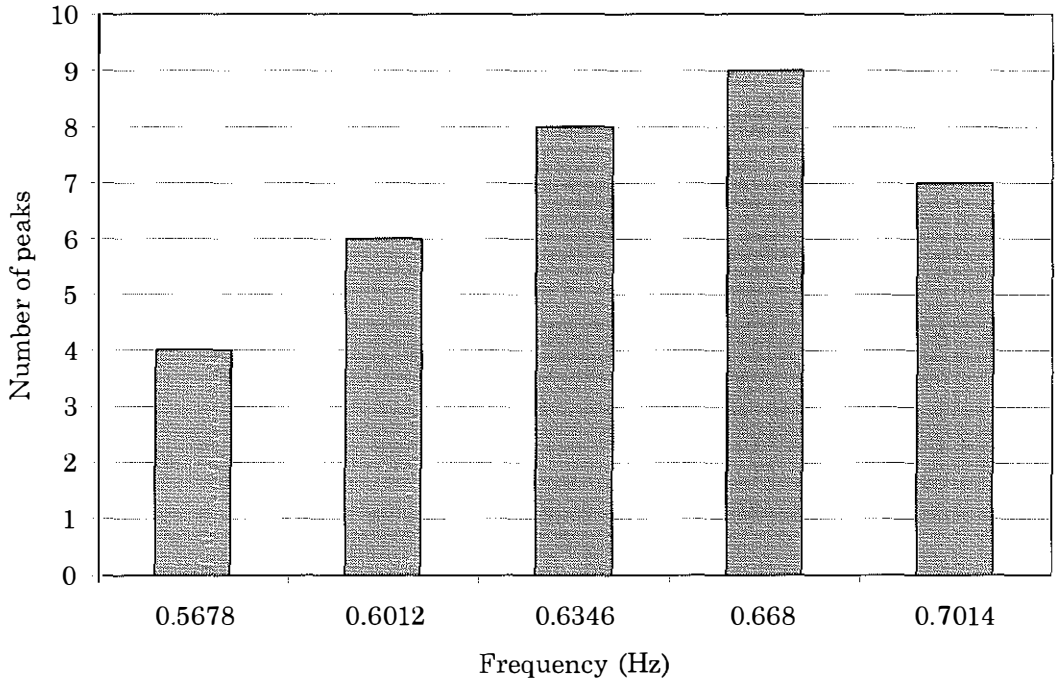

Figure 3.6b Peak Comparison for the Second Transverse Mode

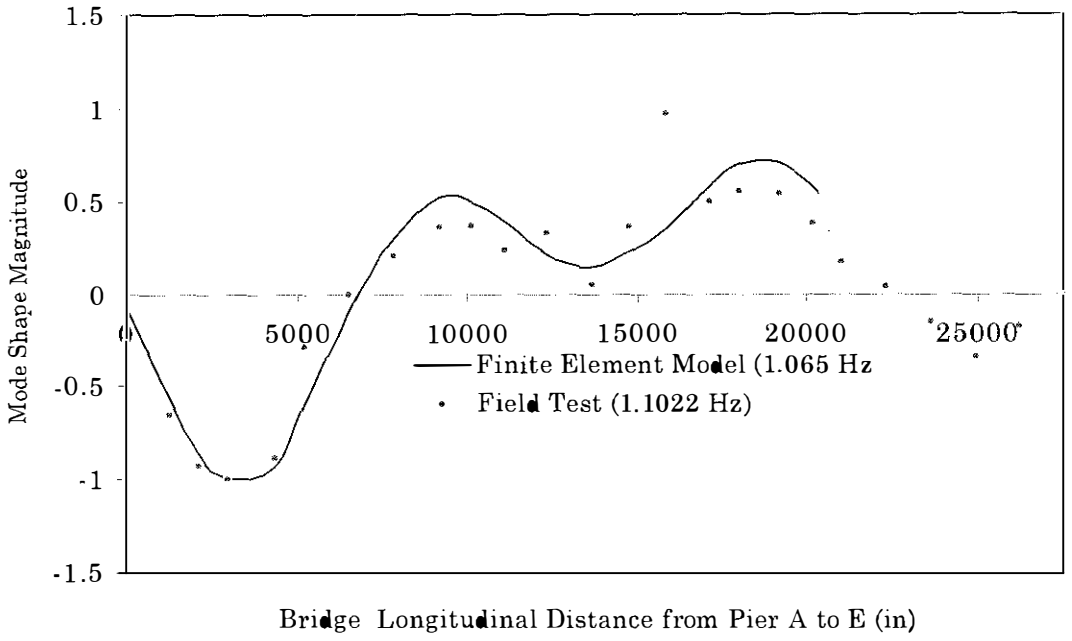

Figure 3.7a Second Vertical Mode

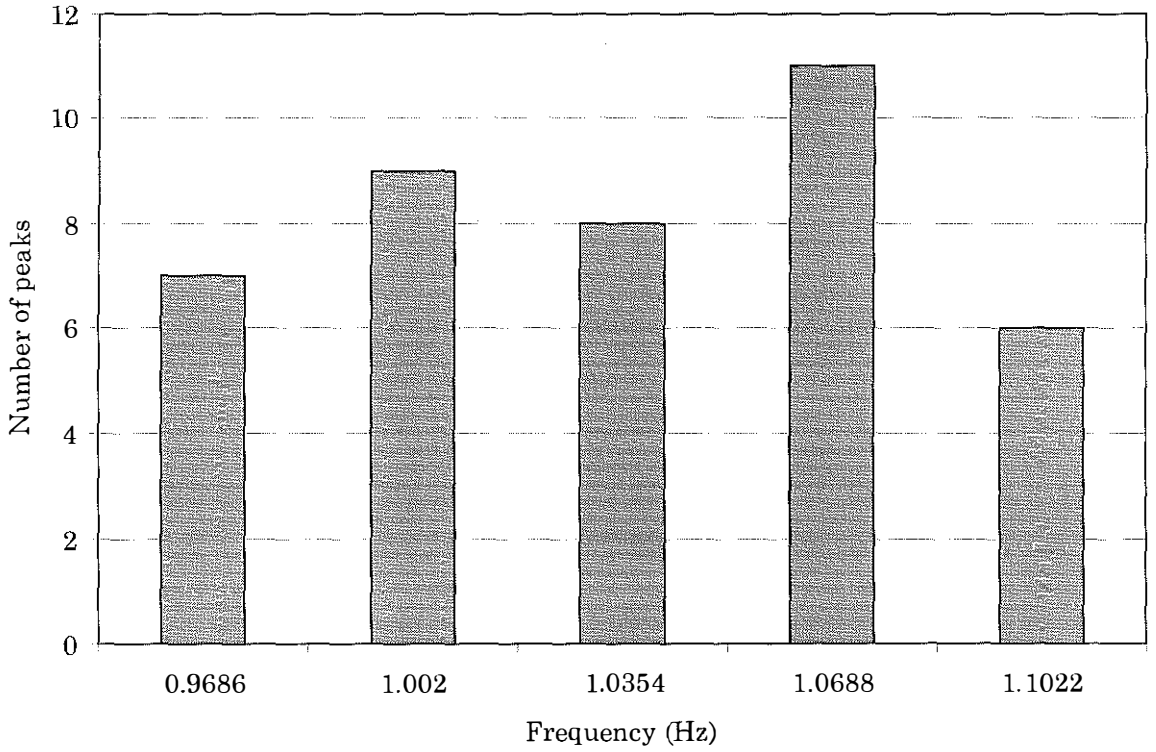

Figure 3.7b Peak Comparison for the Second Vertical Mode

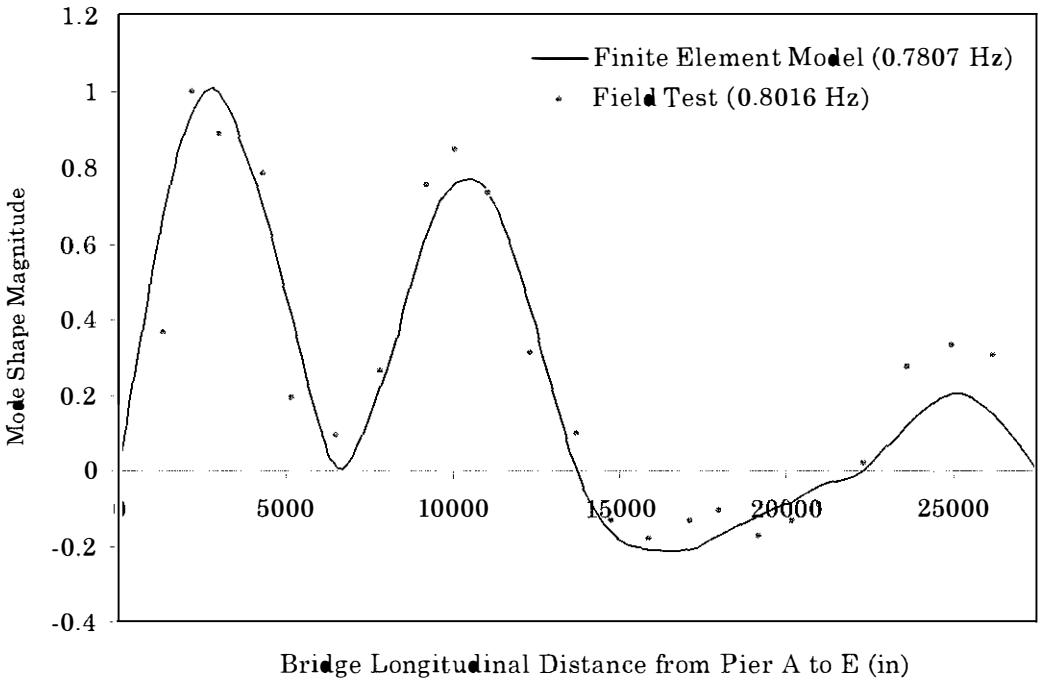

Figure 3.8a Third Transverse Mode

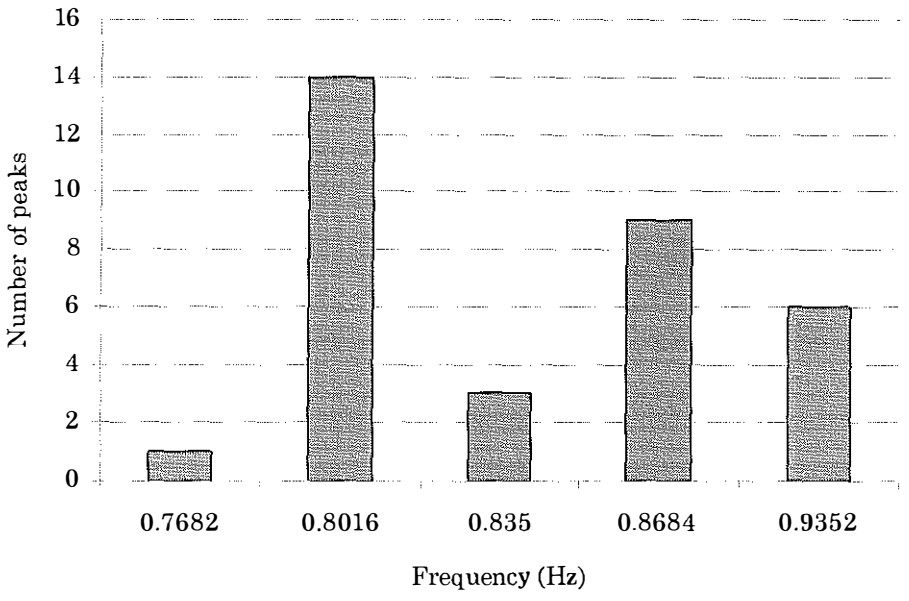

Figure 3.8b Peak Comparison for the Third Transverse Mode

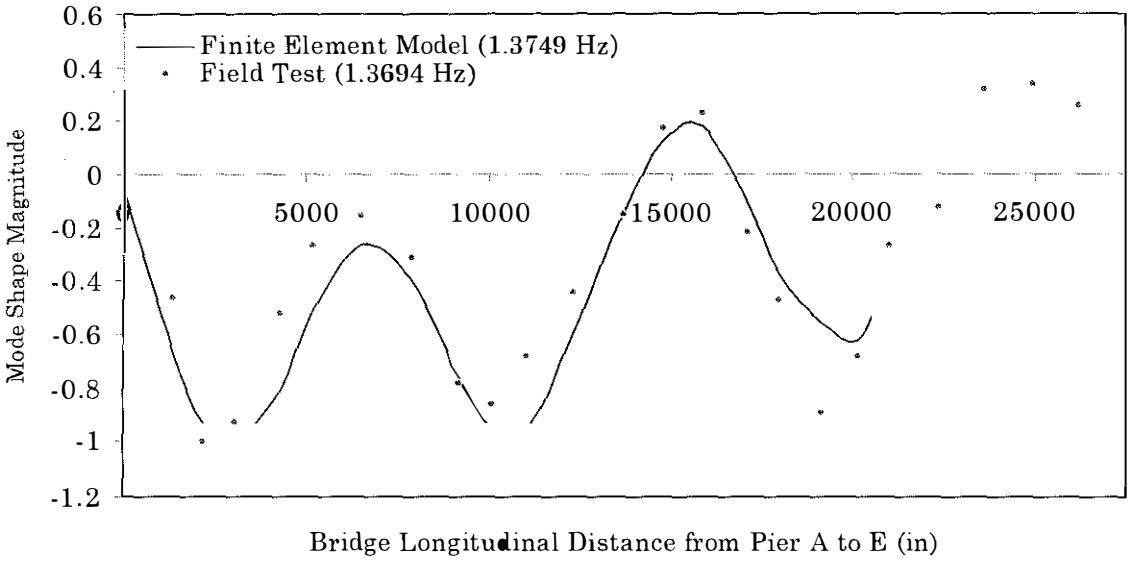

Figure 3.9a Third Vertical Mode

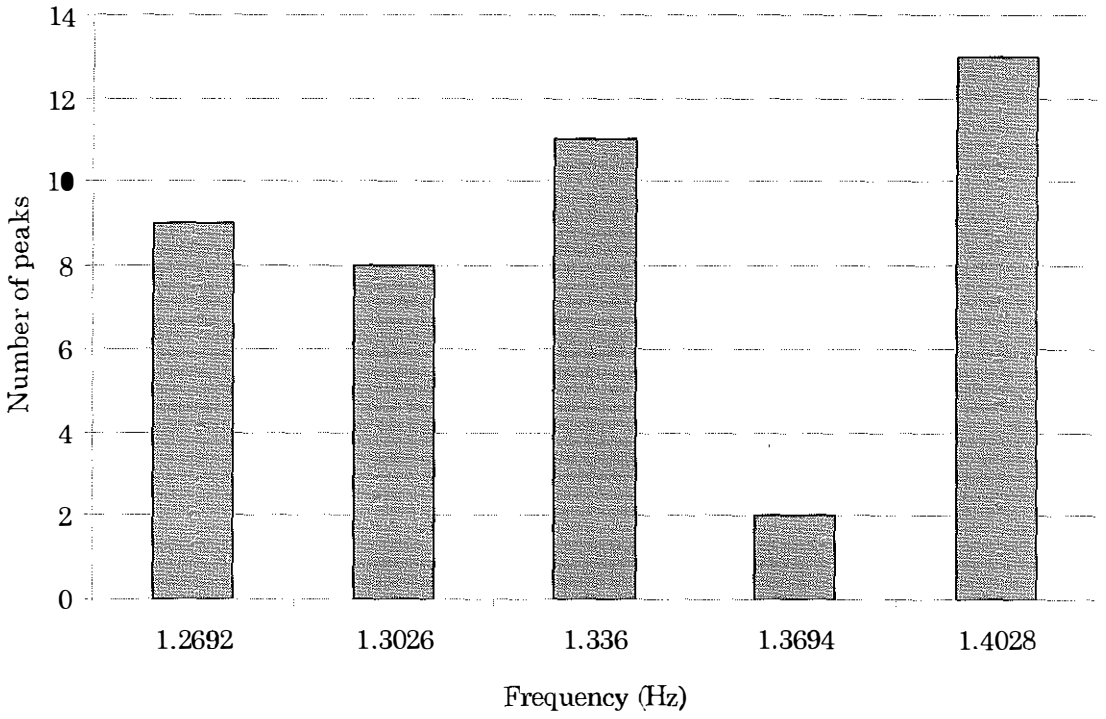

Figure 3.9b Peak Comparison for the Third Vertical Mode

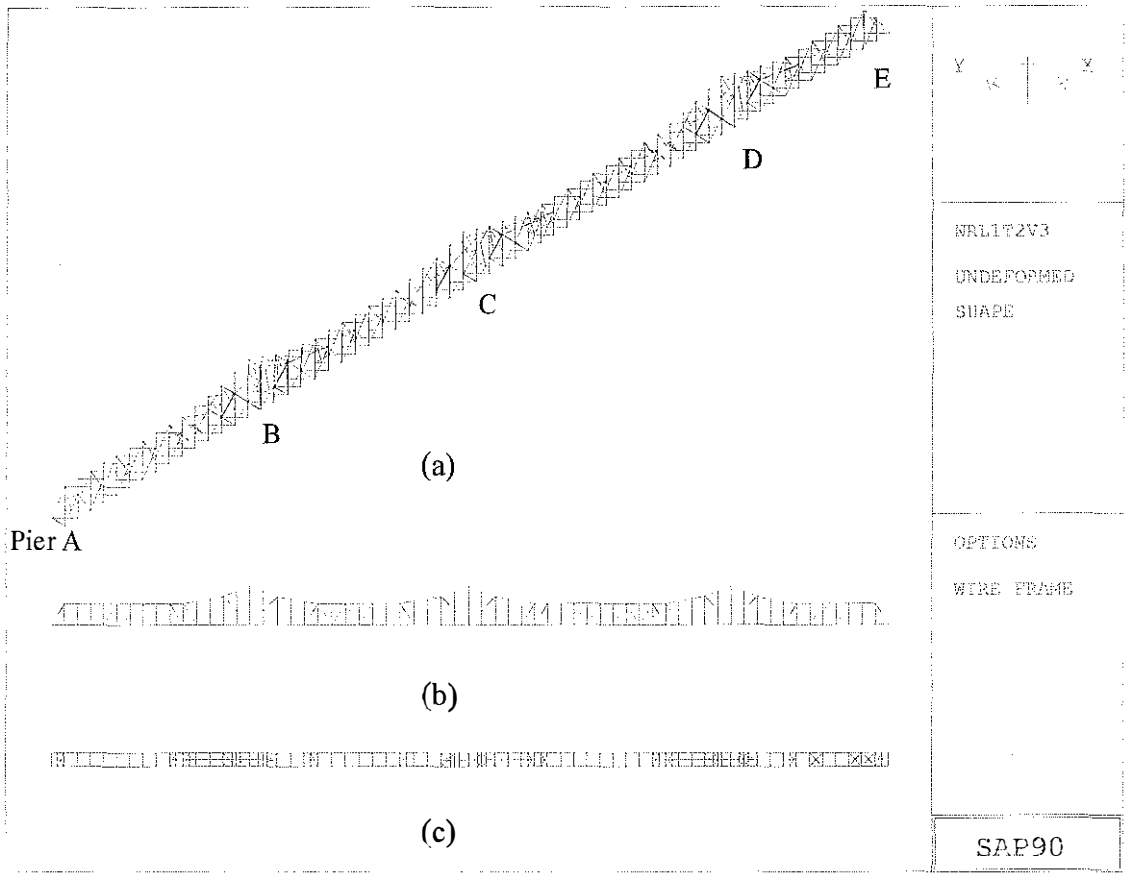

Figure 4.1 3D Finite Element Model of the US41 Northbound Bridge (a) Isometric View, (b) Elevation View, and (c) Plan View

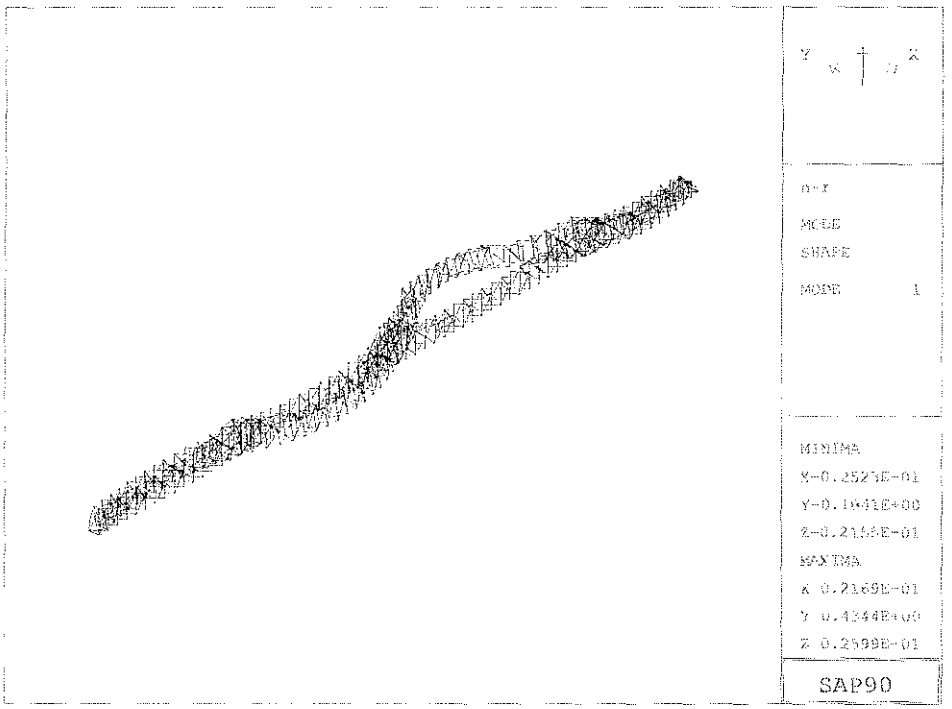

(a)

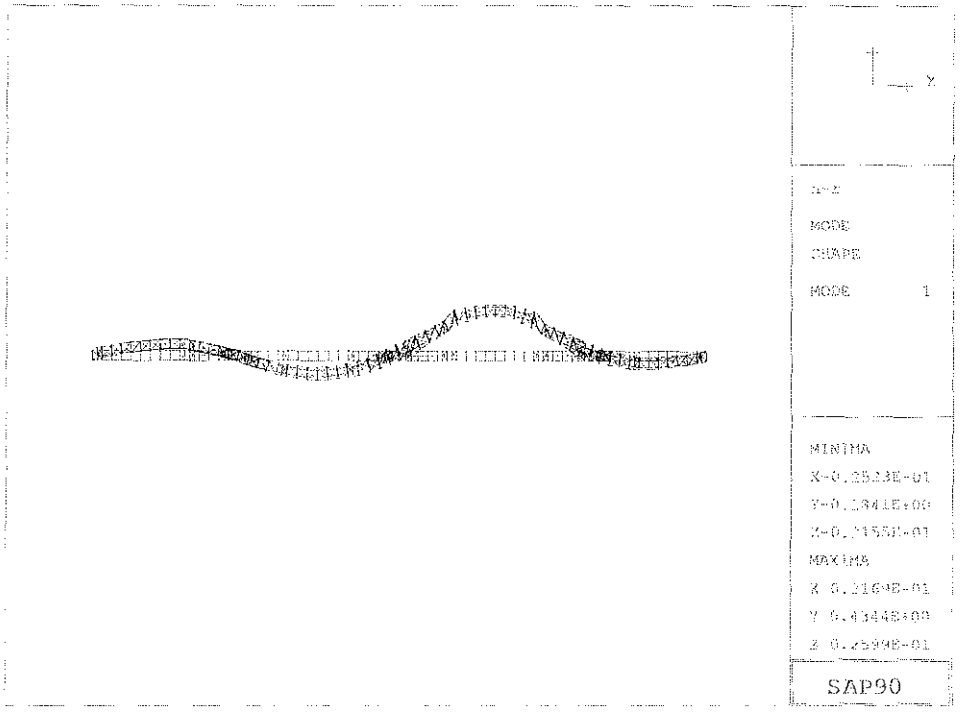

(b)

Figure 4.2 Mode Shape of the First Natural Frequency (0.534 Hz)
(a) Isometric View (b) Plan View

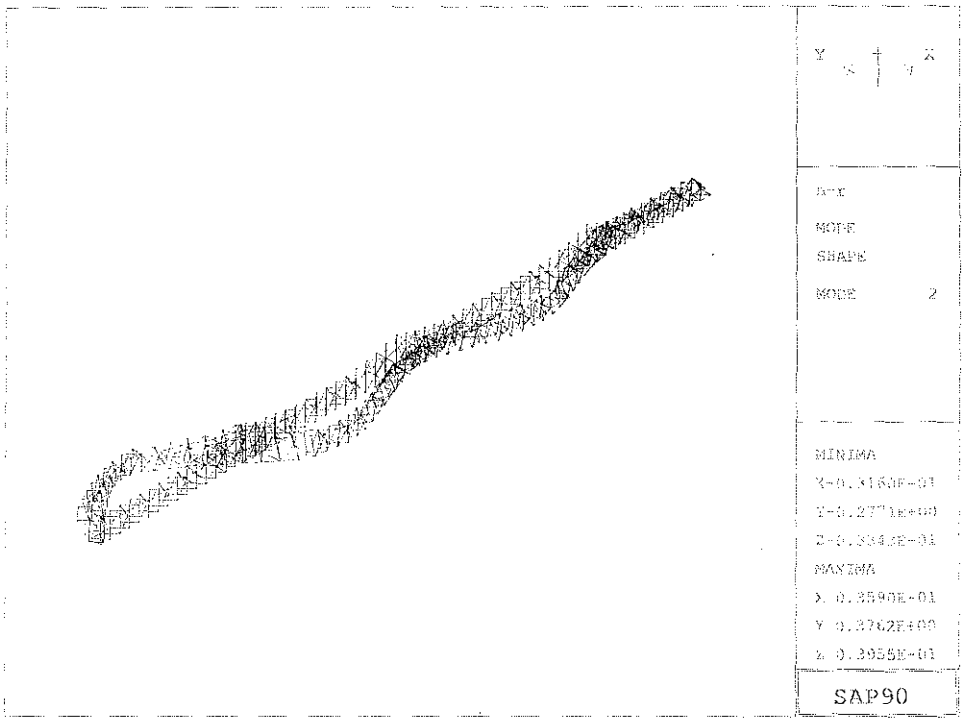

(a)

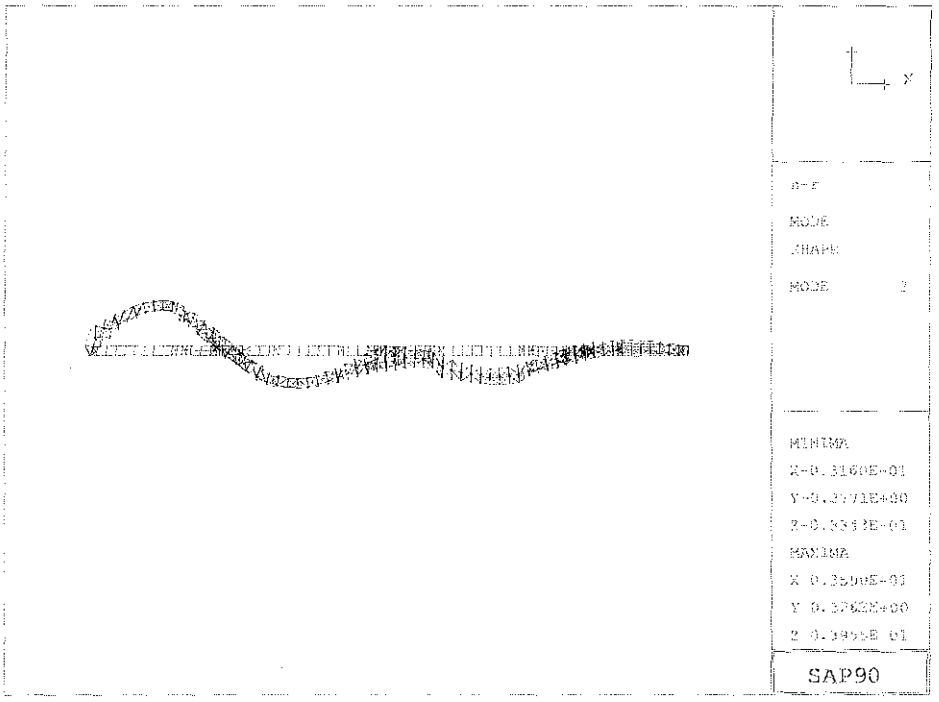

(b)

Figure 4.3 Mode Shape of the Second Natural Frequency (0.674 Hz)
(a) Isometric View and (b) Plan View

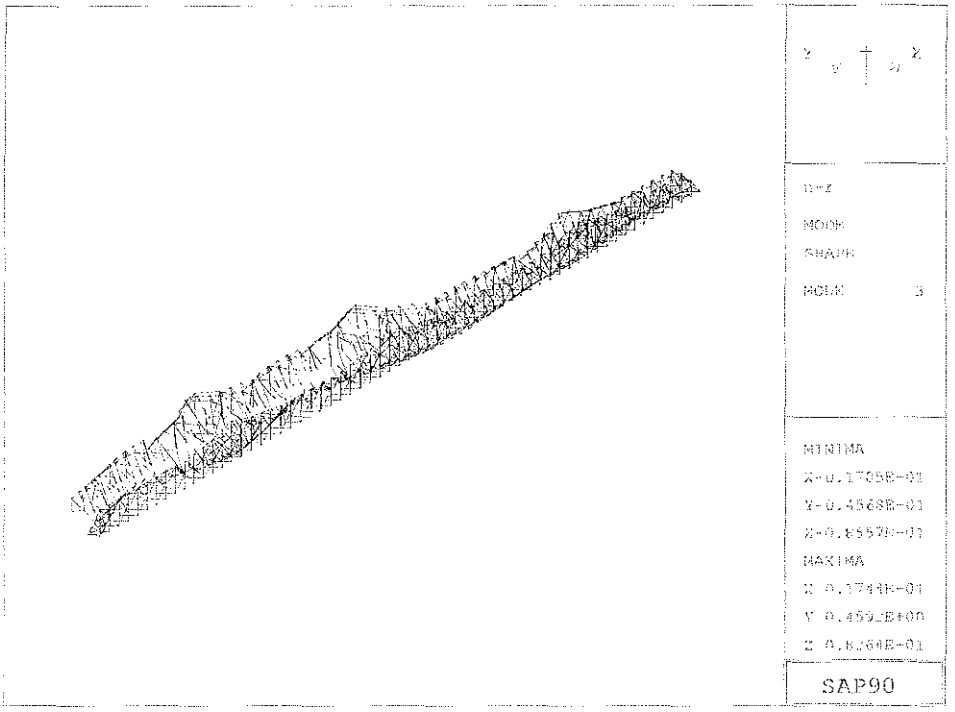

(a)

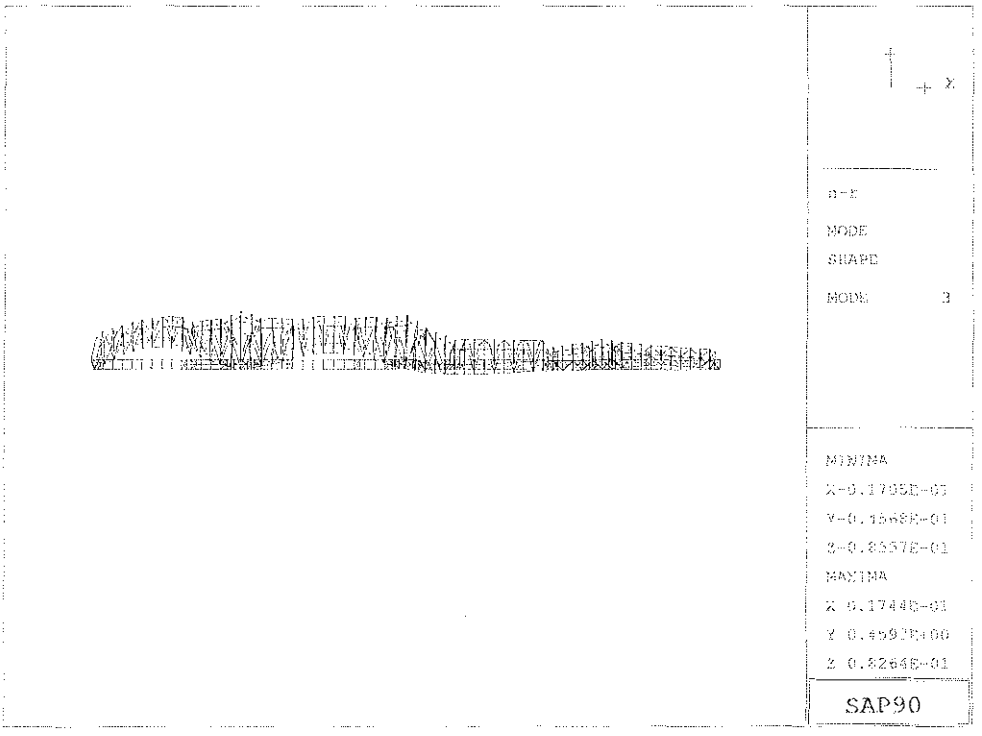

(b)

Figure 4.4 Mode Shape of the Third Natural Frequency (0.781 Hz)
(a) Isometric View and (b) Plan View

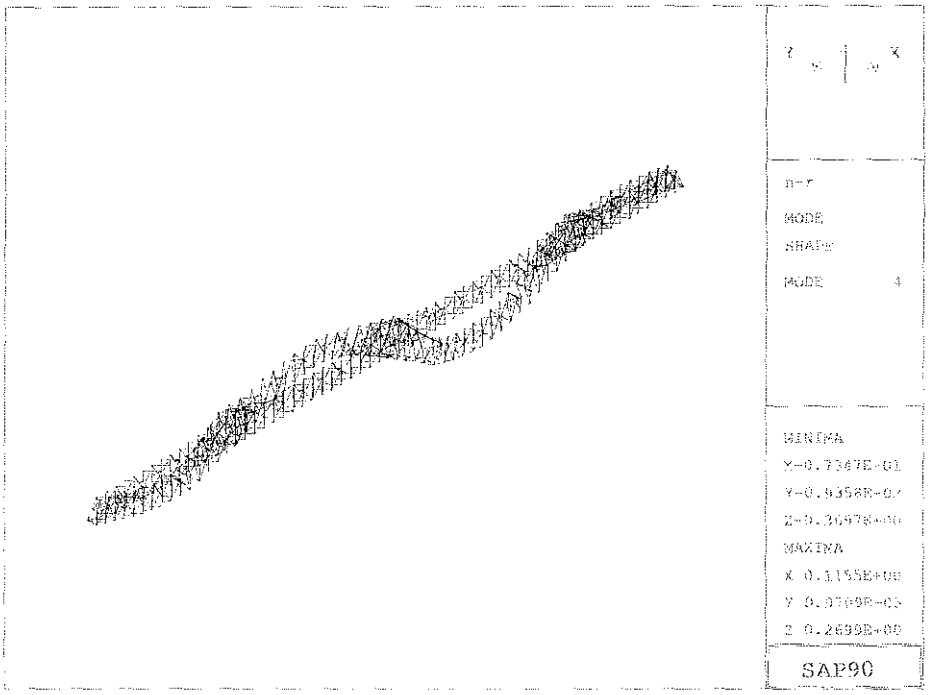

(a)

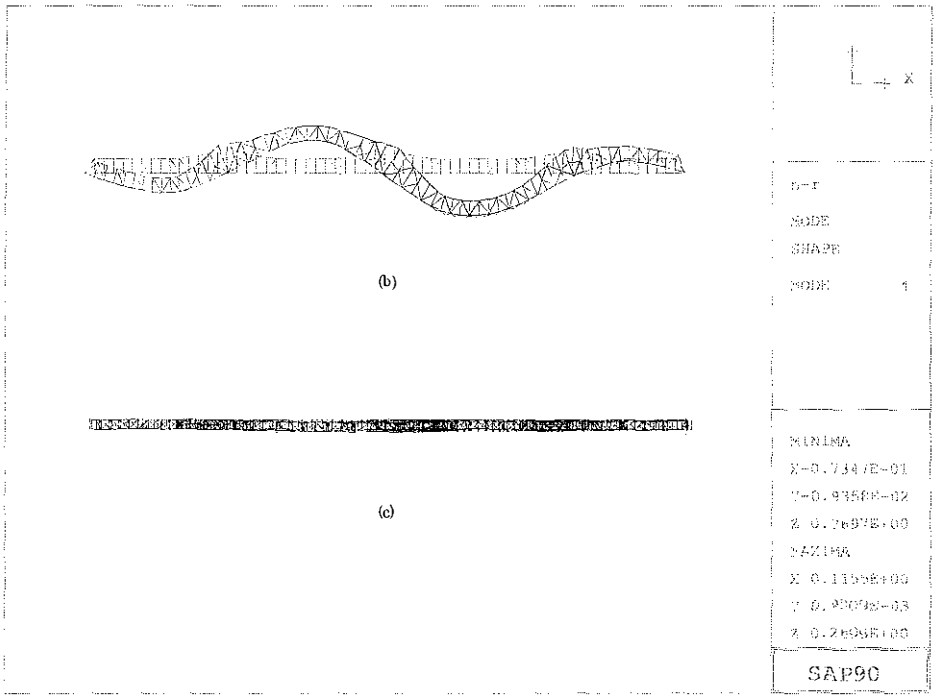

Figure 4.5 Mode Shape of the Fourth Natural Frequency (0.821 Hz) (a) Isometric View, (b) Elevation View and (c) Plan View

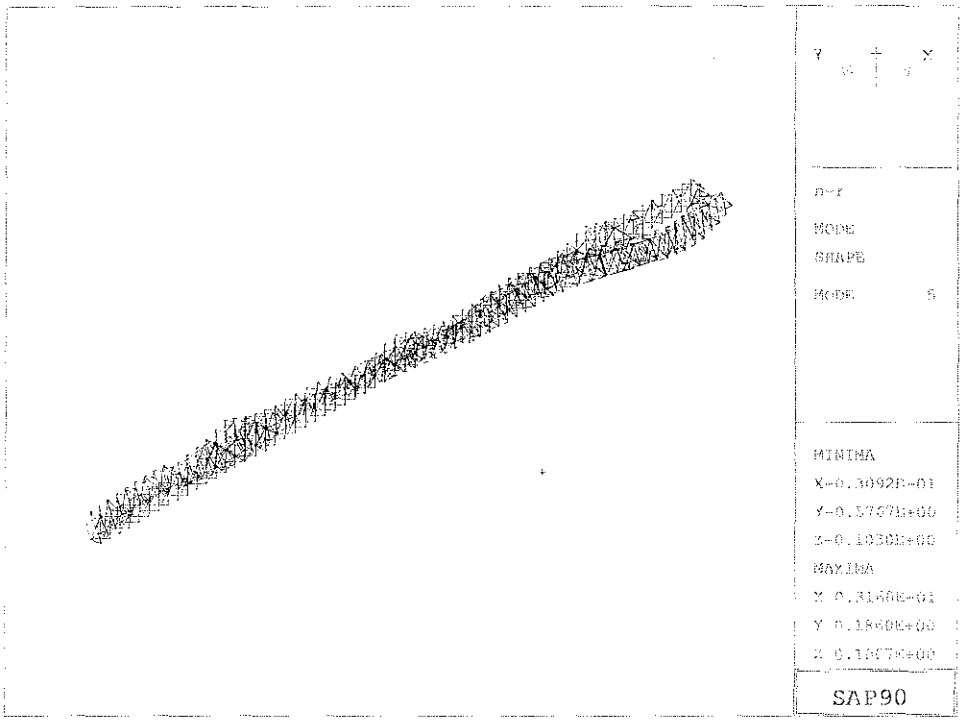

(a)

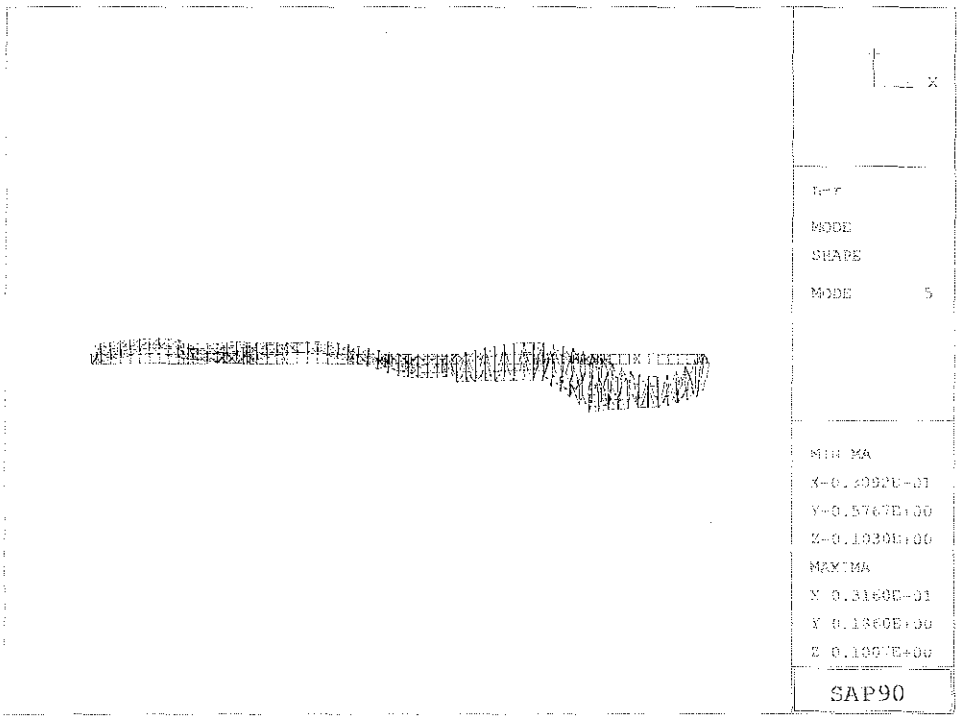

(b)

Figure 4.6 Mode Shape of the Fifth Natural Frequency (0.891 Hz)
(a) Isometric View and (b) Plan View

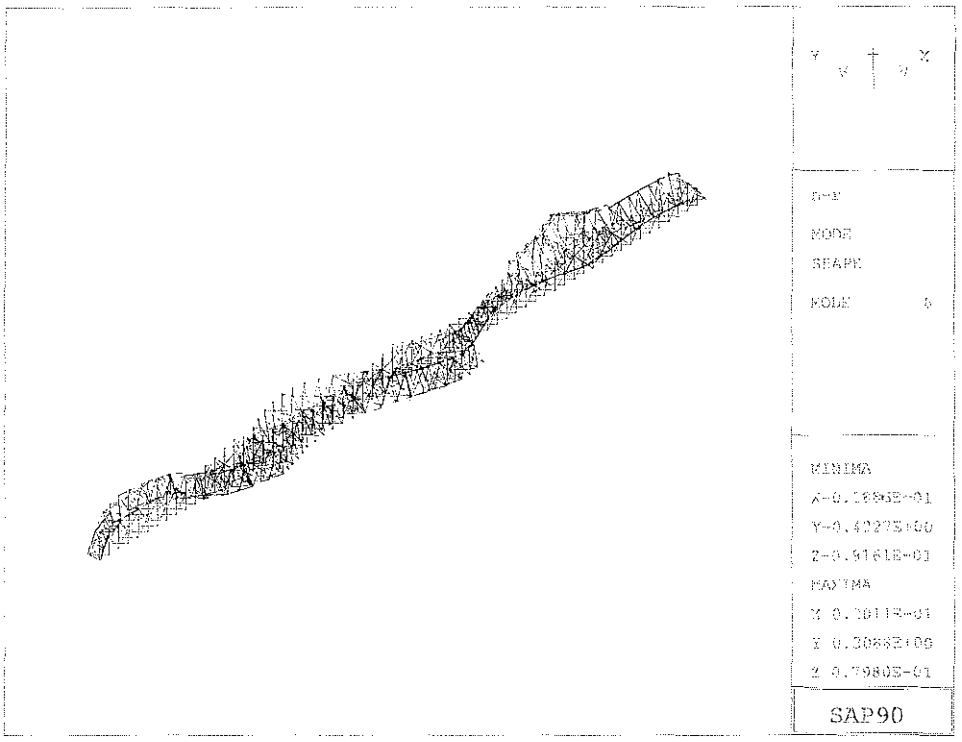

(a)

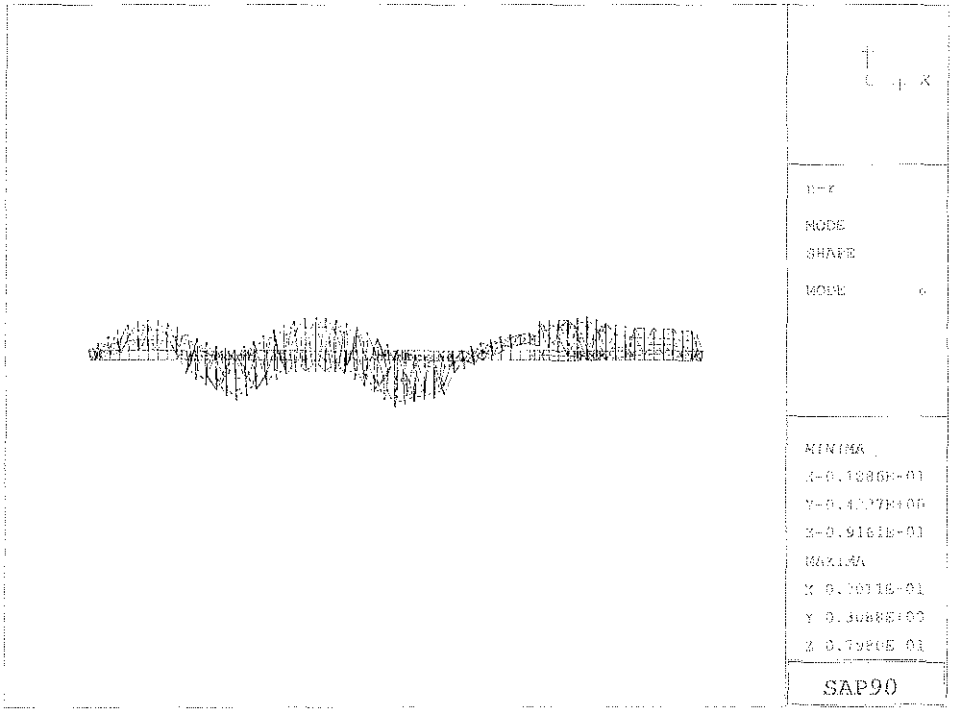

(b)

Figure 4.7 Mode Shape of the Sixth Natural Frequency (1.022 Hz)
(a) Isometric View and (b) Plan View

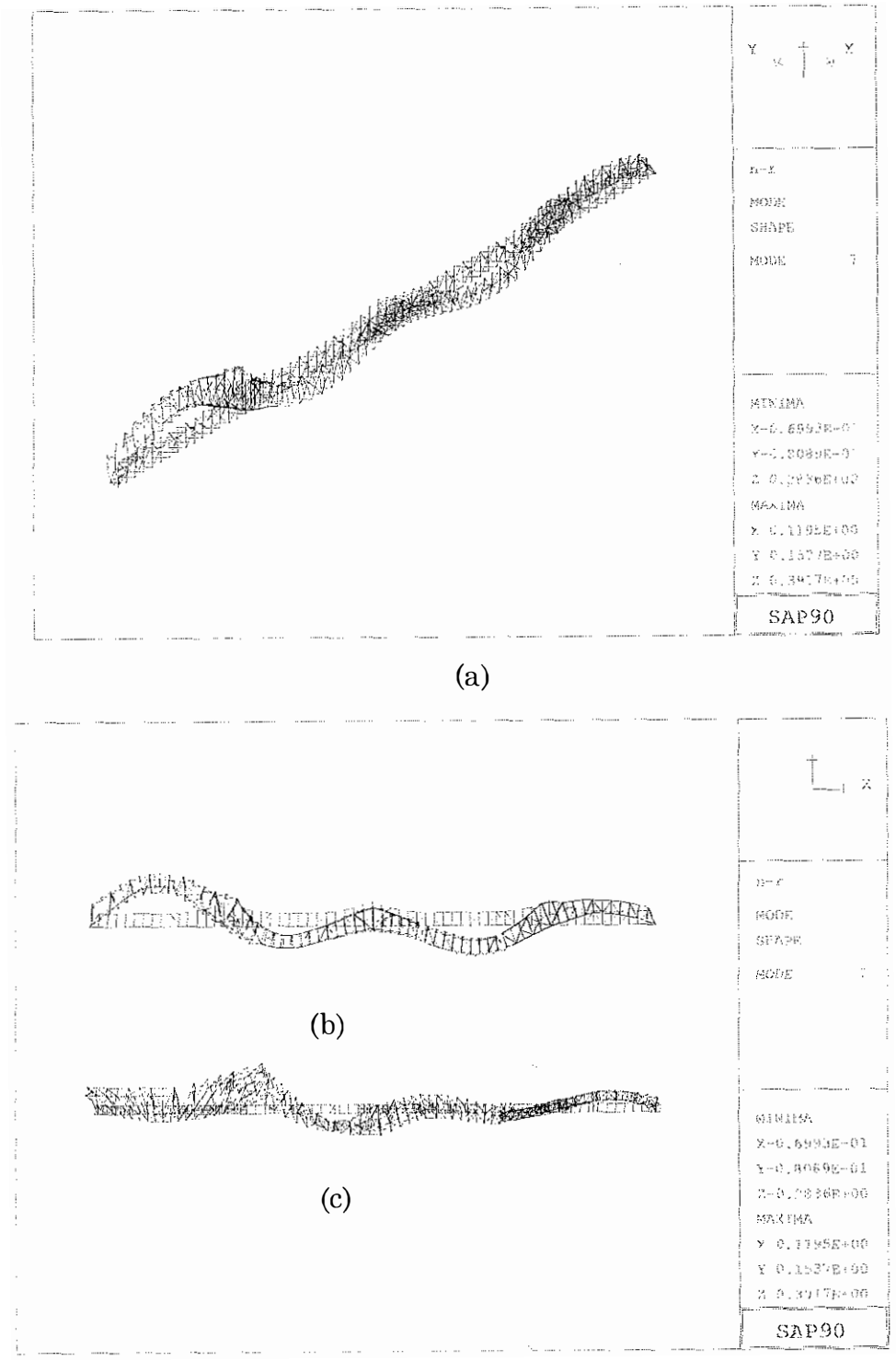

Figure 4.8 Mode Shape of the Seventh Natural Frequency (1.065 Hz)
(a) Isometric View, (b) Elevation View and (c) Plan View

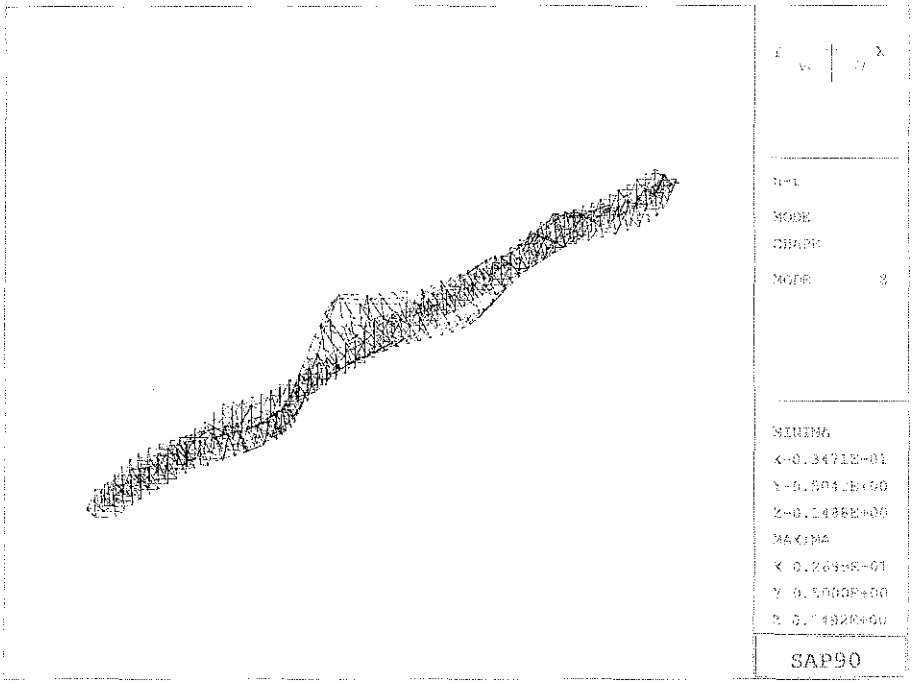

(a)

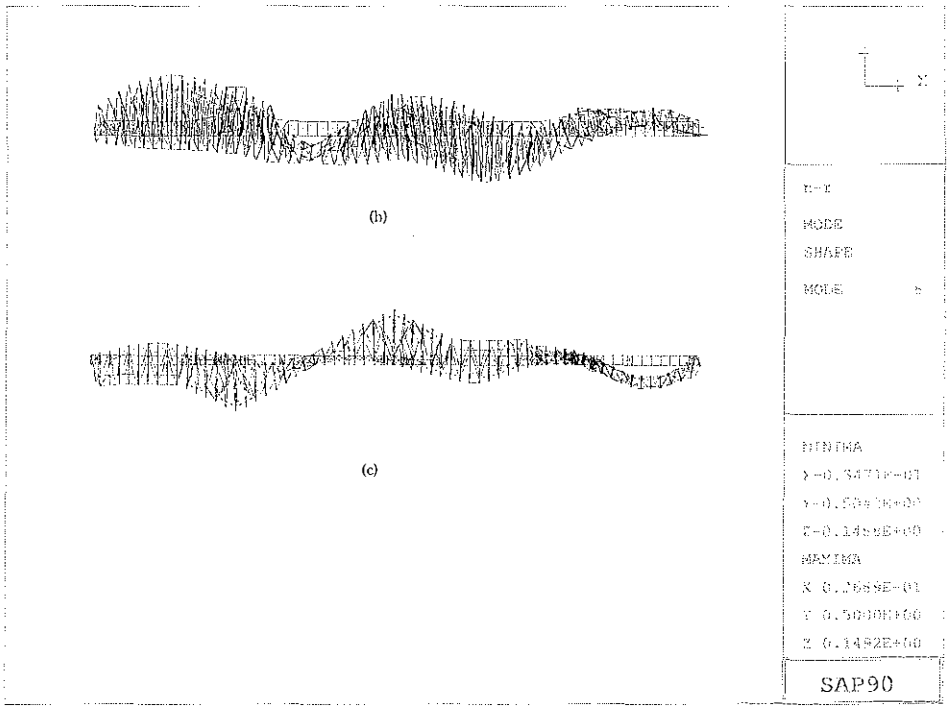

Figure 4.9 Mode Shape of the Eighth Natural Frequency (1.126 Hz)
(a) Isometric View, (b) Elevation View and (c) Plan View

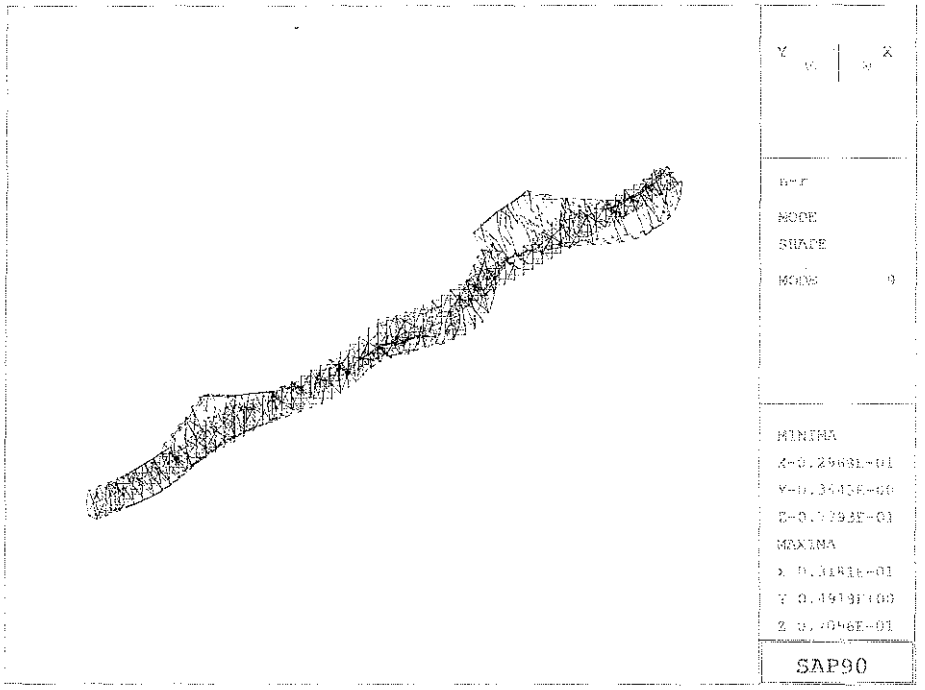

(a)

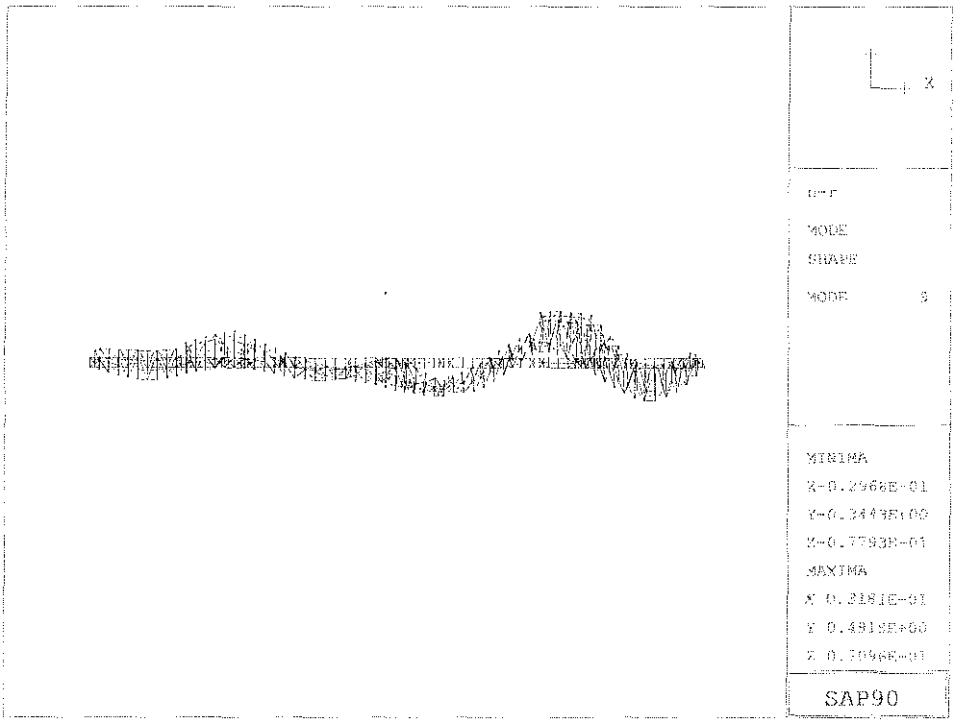

(b)

Figure 4.10 Mode Shape of the Ninth Natural Frequency (1.174 Hz)
(a) Isometric View and (b) Plan View

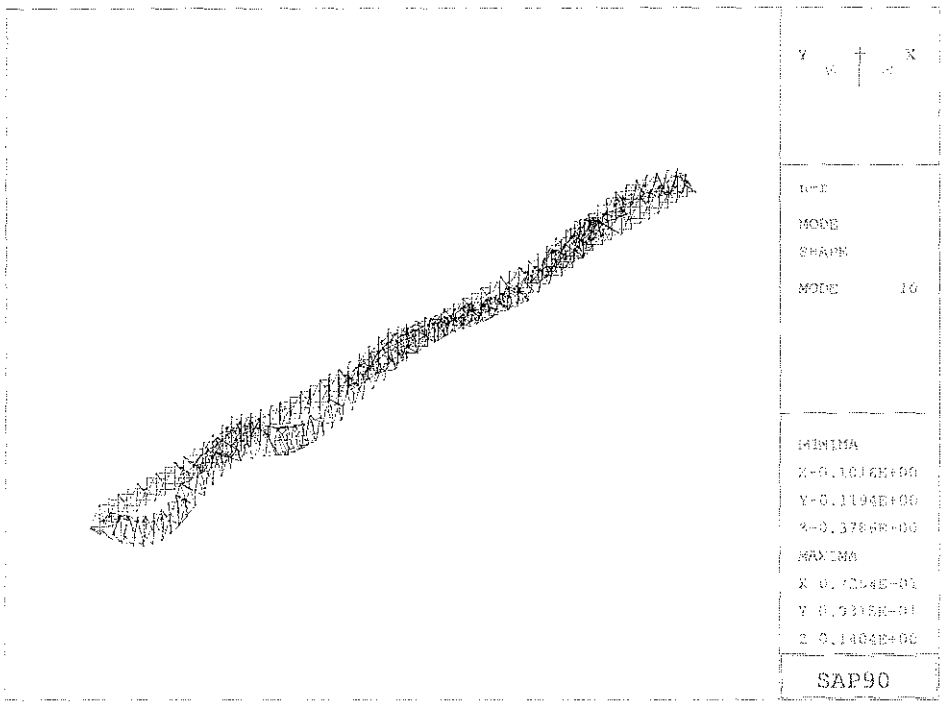

(a)

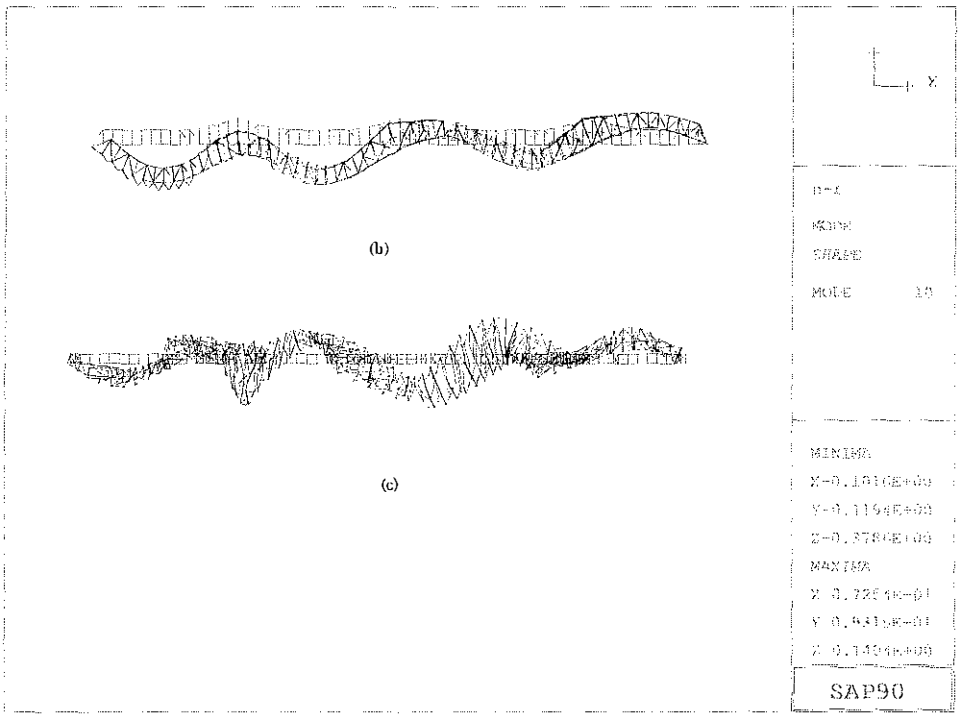

Figure 4.11 Mode Shape of the Tenth Natural Frequency (1.375 Hz)
(a) Isometric View, (b) Elevation View, and (c) Plan View

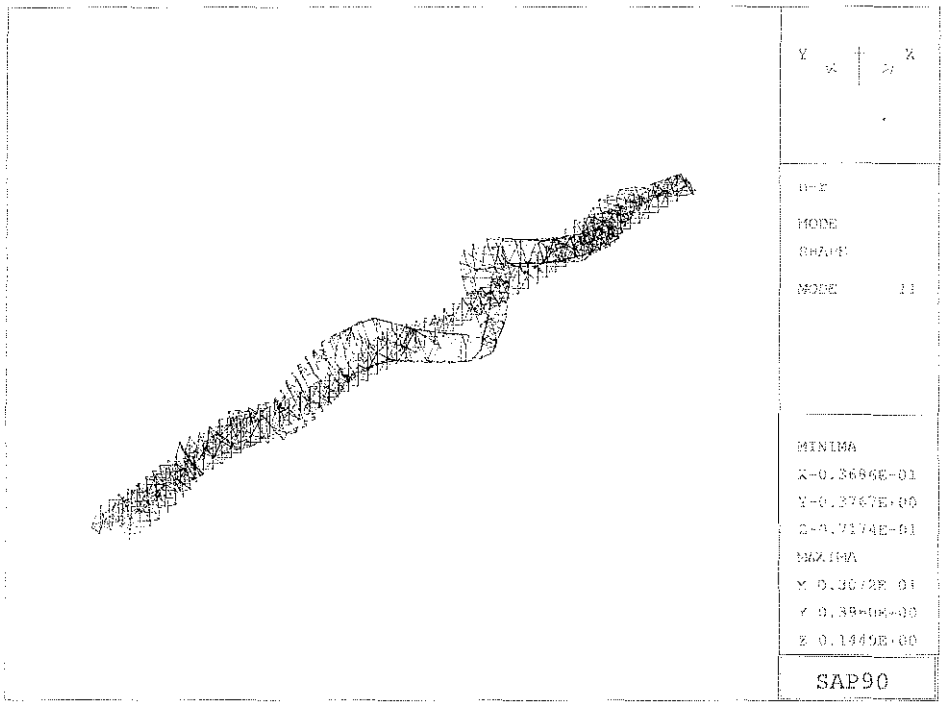

(a)

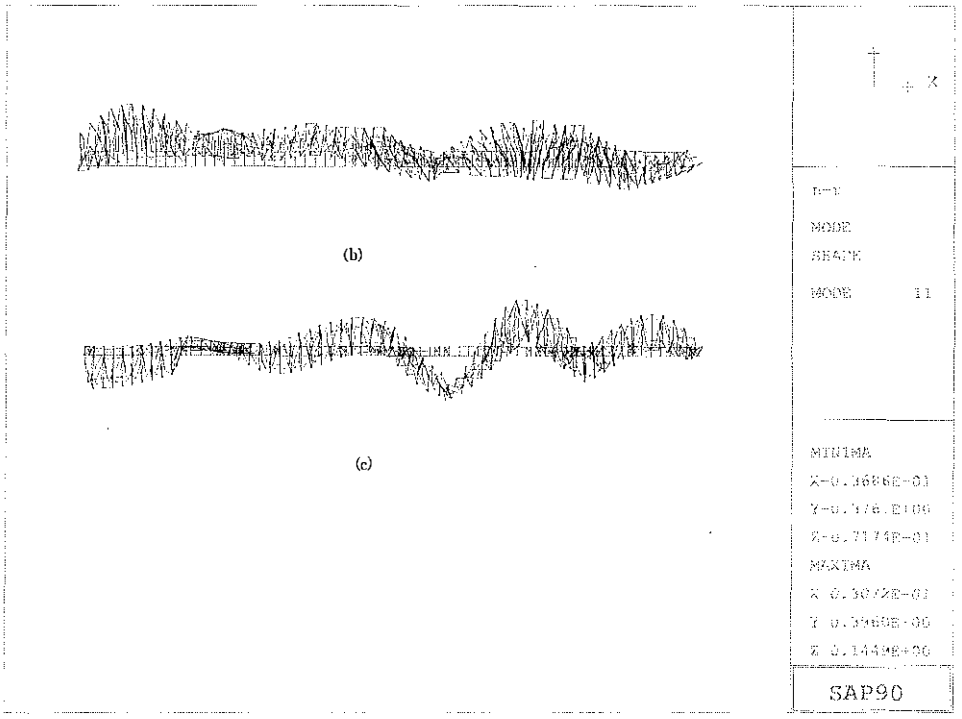

Figure 4.12 Mode Shape of the Eleventh Natural Frequency (1.456 Hz)
(a) Isometric View, (b) Elevation View and (c) Plan View

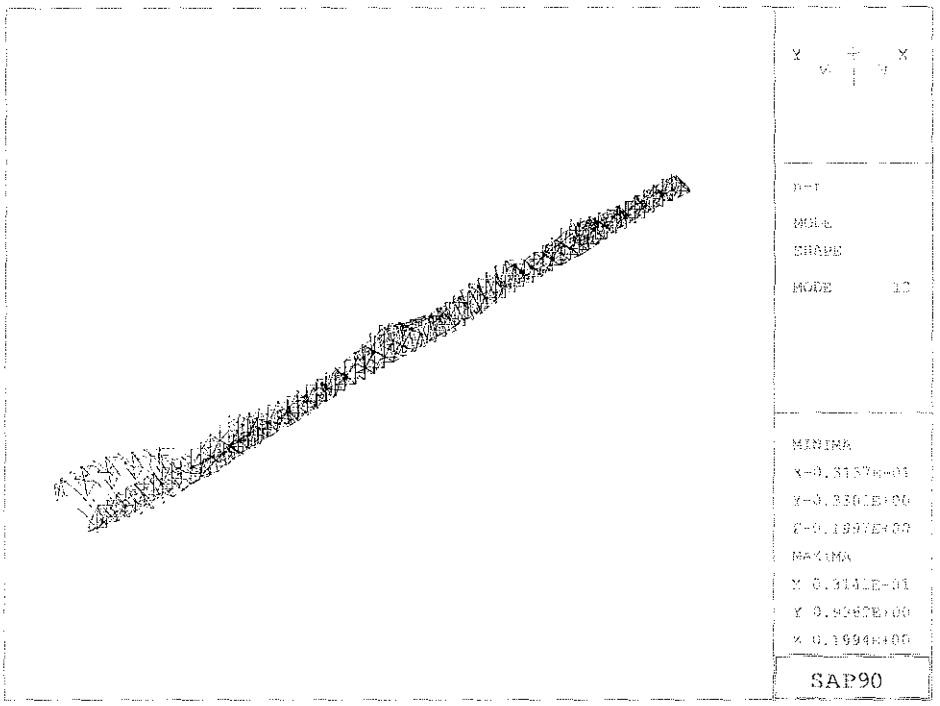

(a)

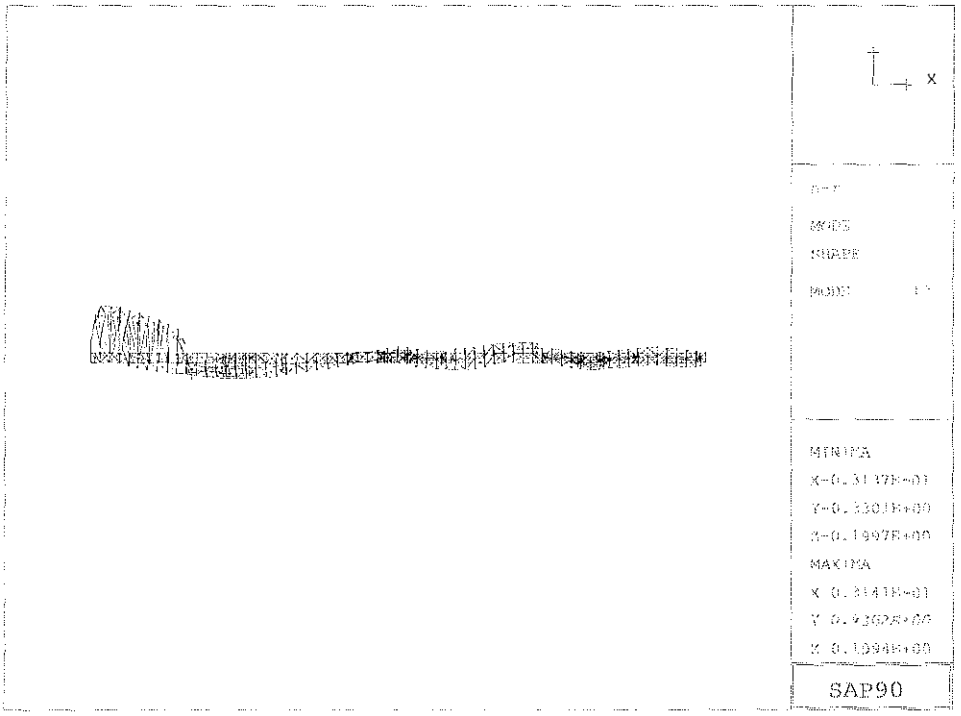

(b)

Figure 4.13 Mode Shape of the 12th Natural Frequency (1.539 Hz)
(a) Isometric View and (b) Plan View

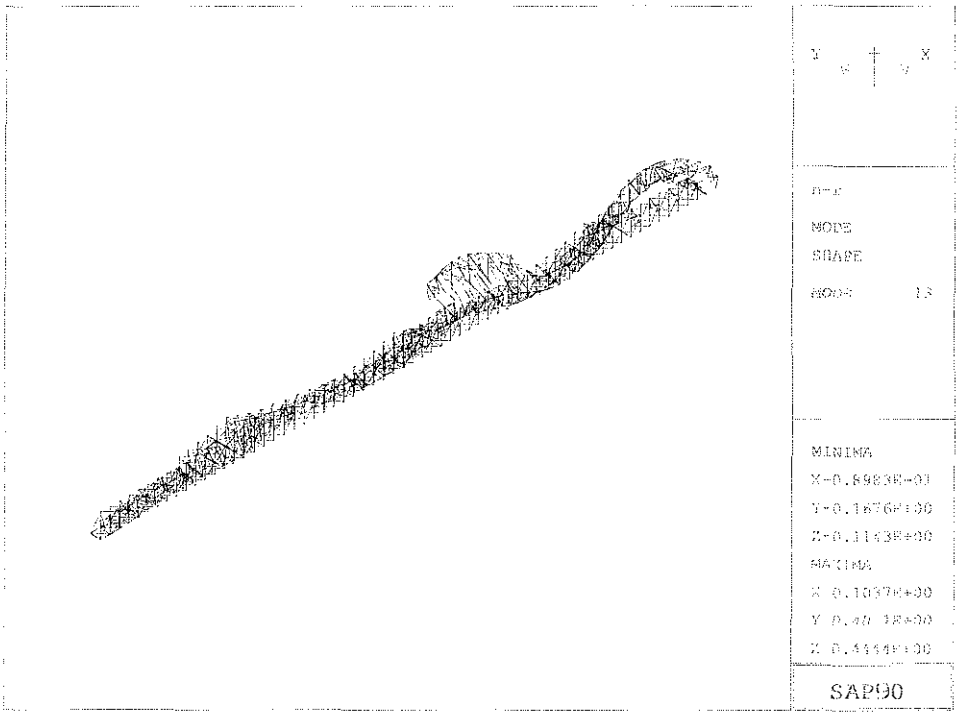

(a)

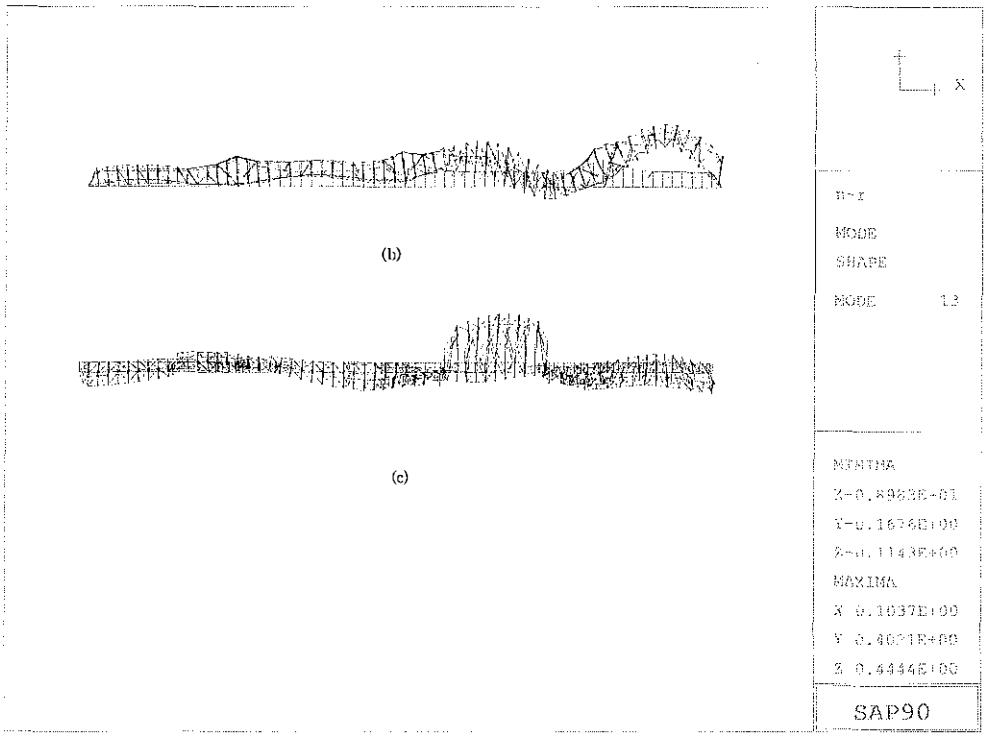

Figure 4.14 Mode Shape of the 13th Natural Frequency (1.637 Hz)
(a) Isometric View, (b) Elevation View and (c) Plan View

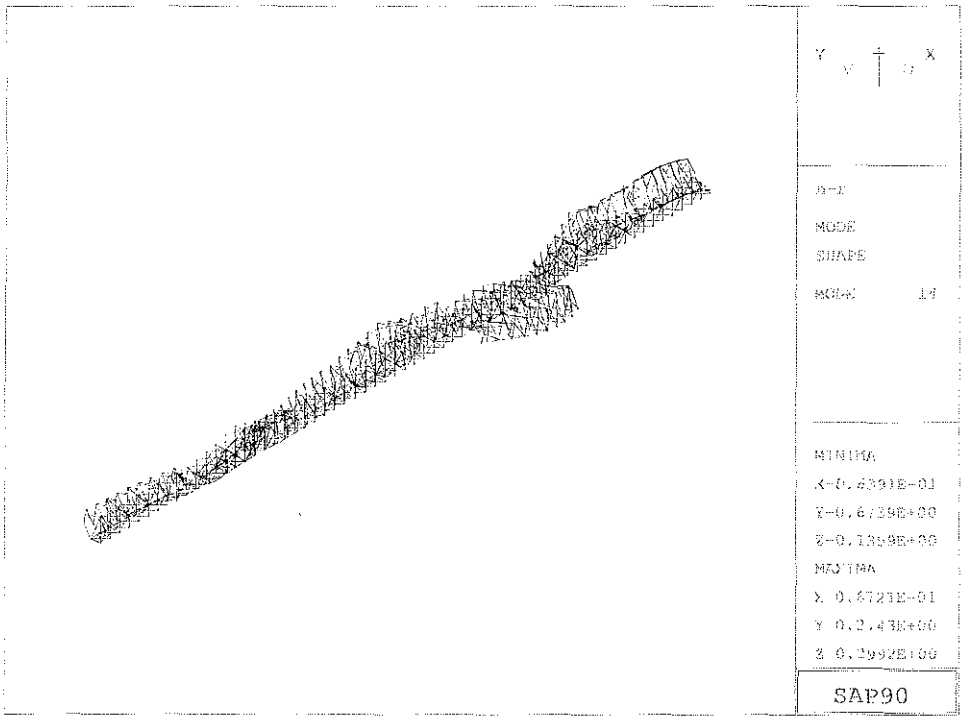

(a)

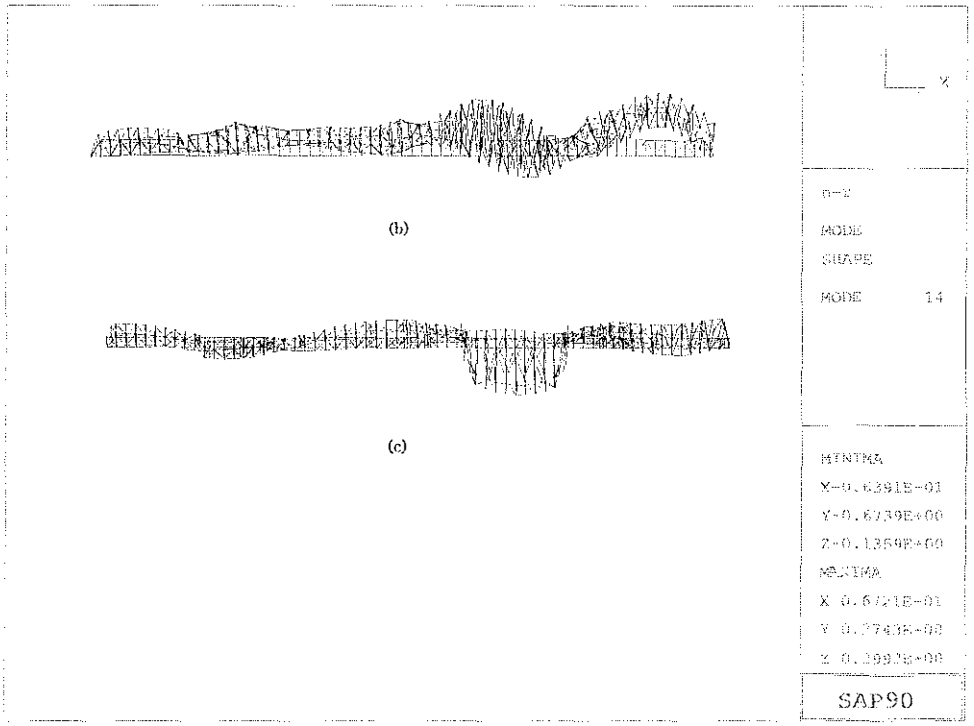

Figure 4.15 Mode Shape of the 14th Natural Frequency (1.64 Hz)
(a) Isometric View, (b) Elevation View and (c) Plan View

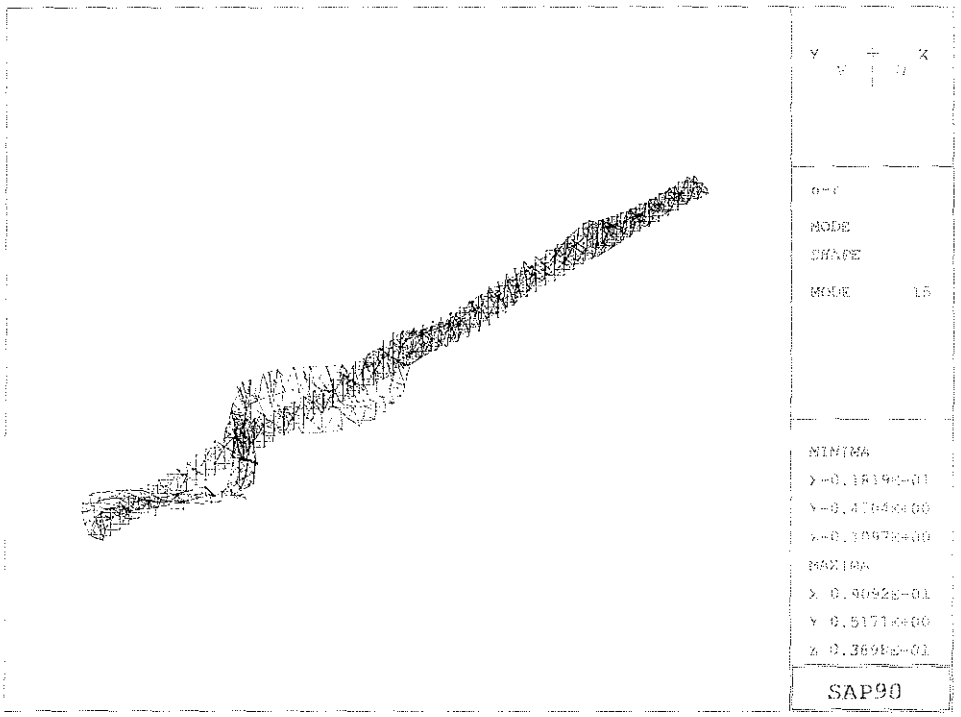

(a)

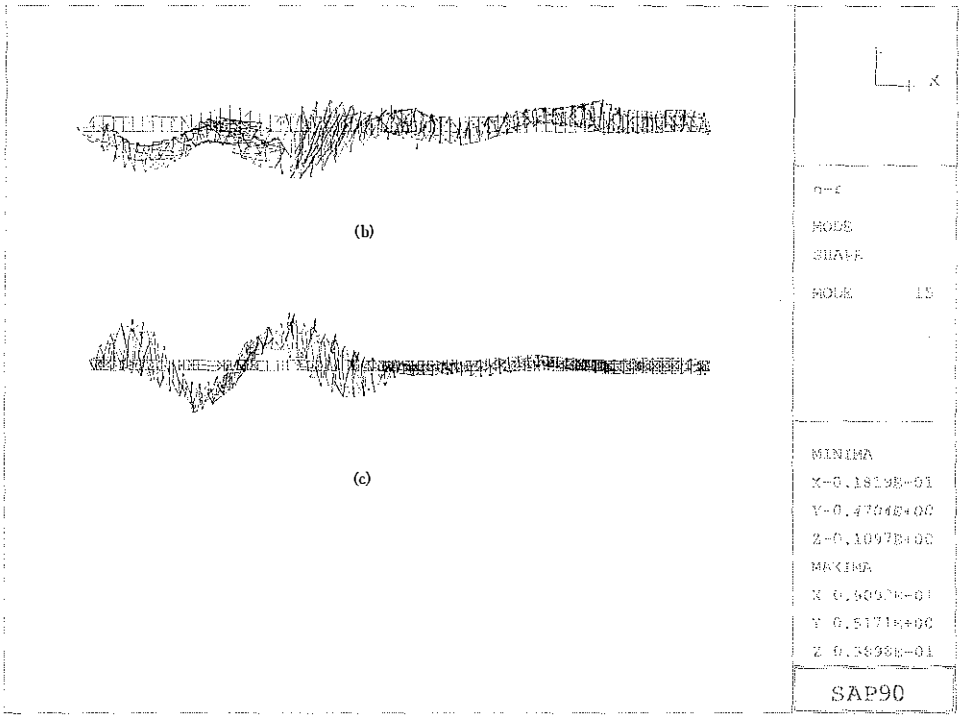

Figure 4.16 Mode Shape of the 15th Natural Frequency (1.751 Hz)
(a) Isometric View, (b) Elevation View, and (c) Plan View

Figure 5.1 Time-history and Response spectra identification map for the Commonwealth of Kentucky

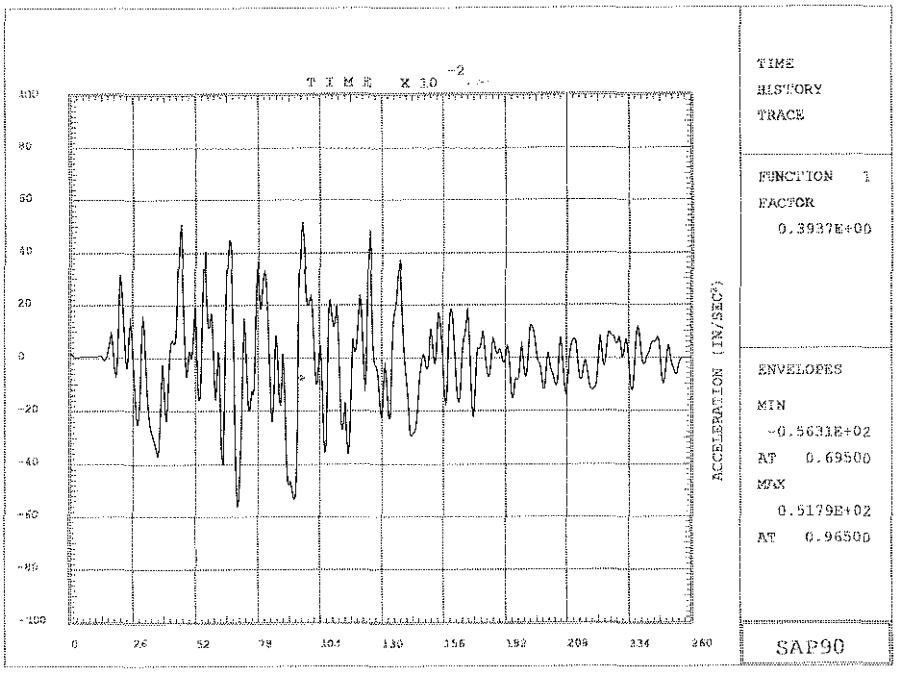

Figure 5.2 Acceleration-Time History of Horizontal Component of the 50-year Earthquake

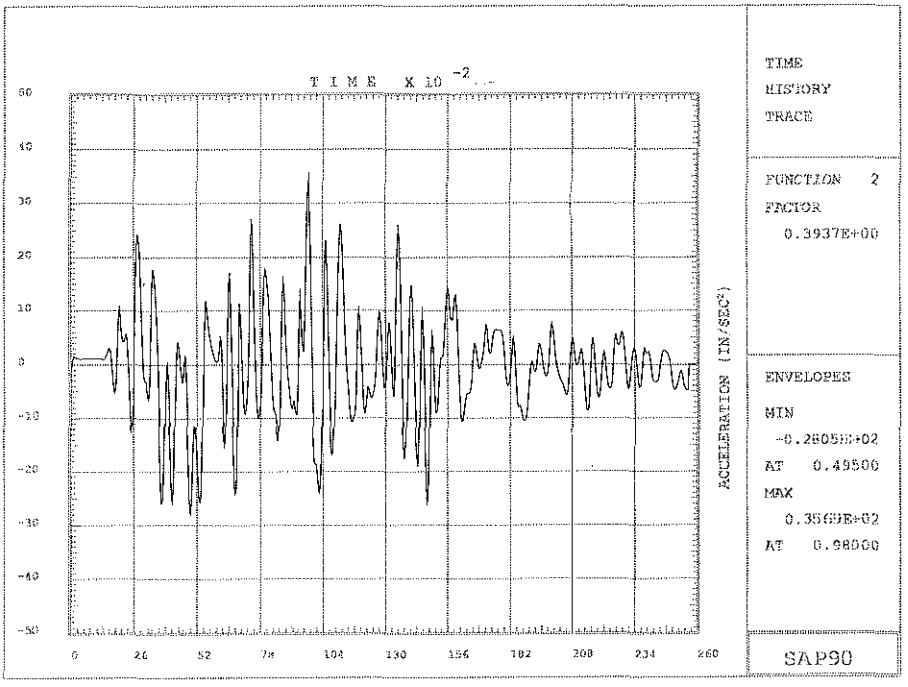

Figure 5.3 Acceleration-Time History of the Vertical Component of the 50-year Earthquake

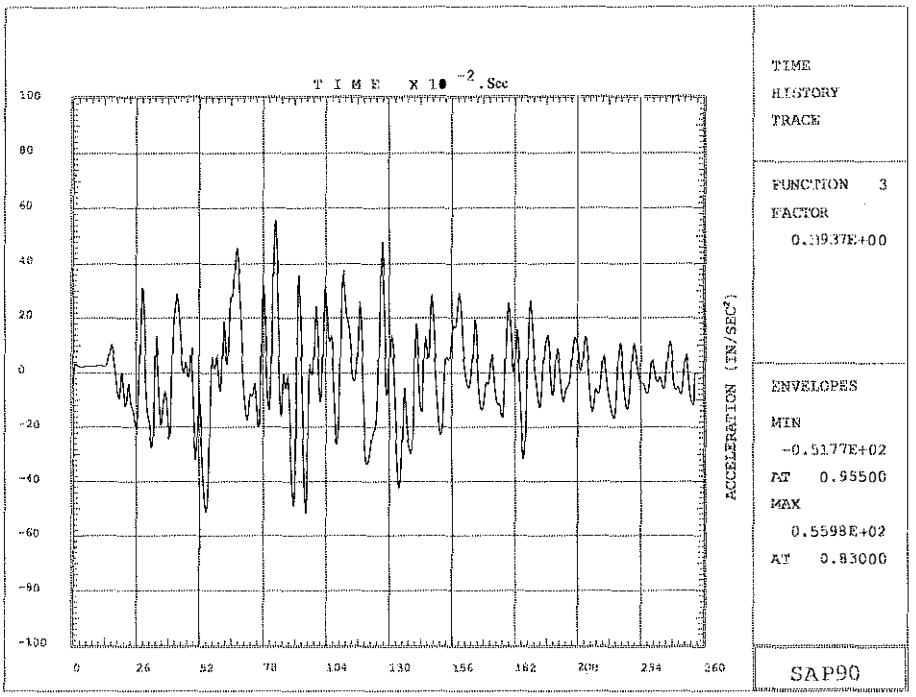

Figure 5.4 Acceleration-Time History of the Transverse Component of the 50-year Earthquake

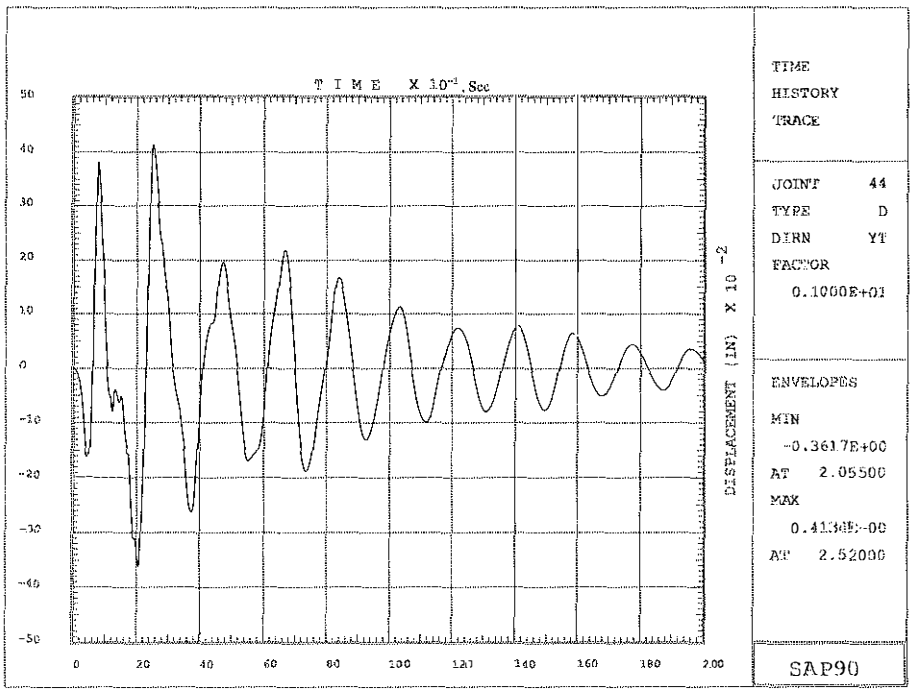

Figure 5.5 Displacement-Time History in the Transverse Direction at Node 44 under the L1T2V3 Excitation Case

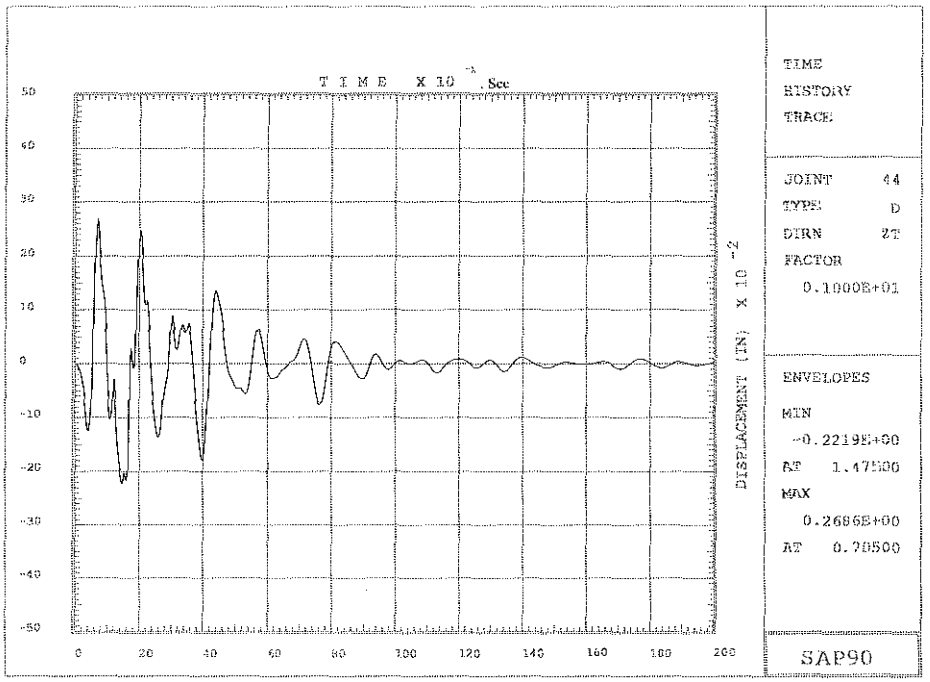

Figure 5.6 Displacement-Time History in the Vertical Direction at Node 44 under the L1T2V3 Excitation Case

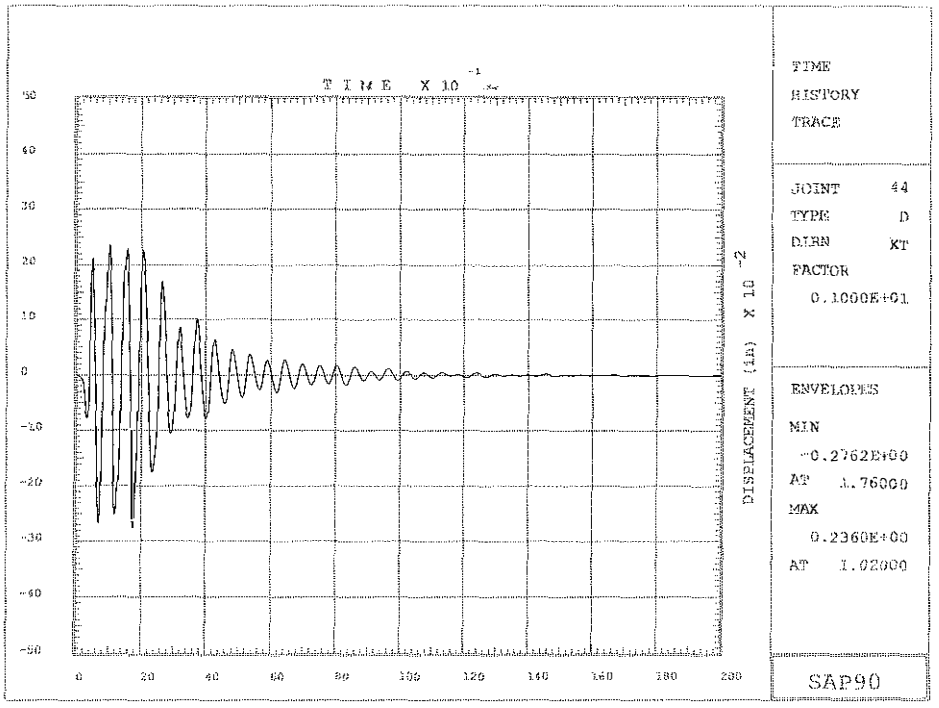

Figure 5.7 Displacement-Time History in the Longitudinal Direction at Node 44 under L1T2V3 Excitation Case

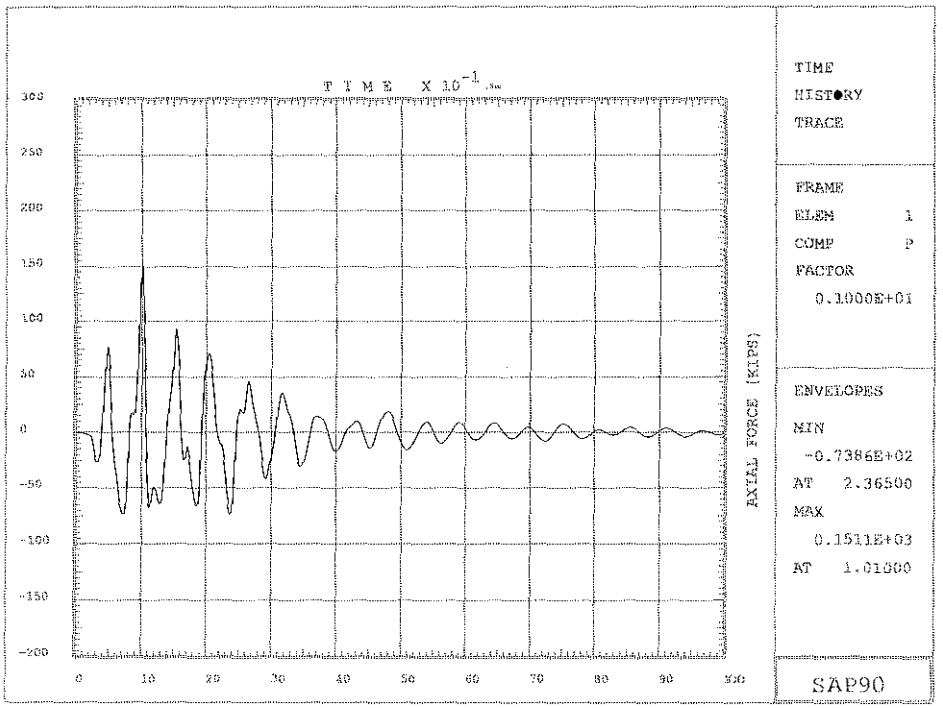

Figure 5.8 Axial Force-Time History of Member 1 under L1T2V3 Excitation Case

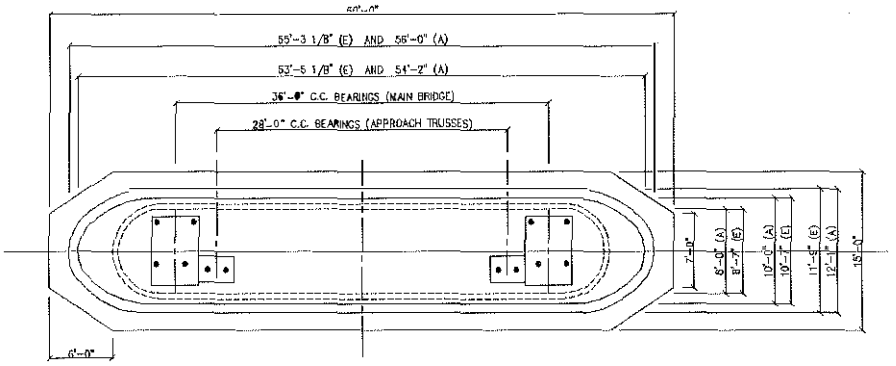

Note: 1. Minimum additional capacity of anchor bolts required = 2180 kips

2. Alternate retrofit would be to replace the existing bearings with seismic isolation bearings

Figure 5.9 Minimum Required Shear Capacity (V_{req}) to be Provided by Additional Anchor Bolts at Bearings of the Pier A on the US41 Northbound Main Bridge

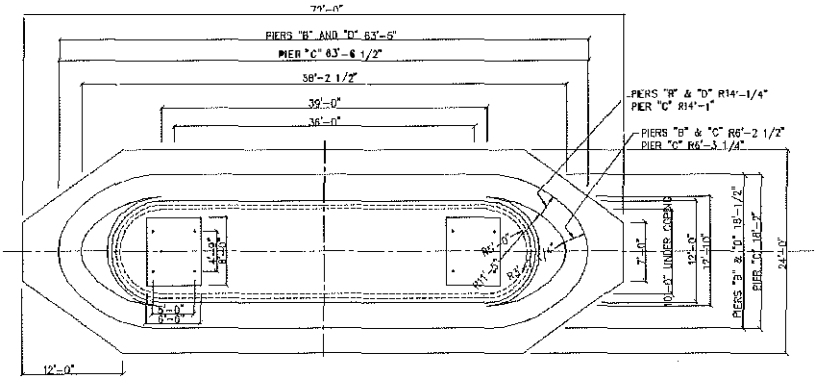

Note: 1. Minimum additional capacity of anchor bolts required = 1315 kips

2. Alternate retrofit would be to replace the existing bearings with seismic isolation bearings

Figure 5.10 Minimum Required Shear Capacity (V_{req}) to be Provided by Additional Anchor Bolts at Bearings of the Pier B on the US41 Northbound Main Bridge

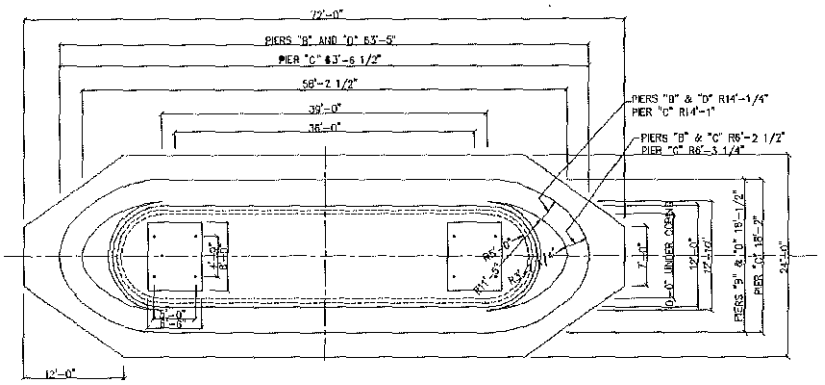

Note: **1. Minimum additional capacity of anchor bolts required = 1815 kips**

2. Alternate retrofit would be to replace the existing bearings with seismic isolation bearings

Figure 5.11 Minimum Required Shear Capacity (V_{req}) to be Provided by Additional Anchor Bolts at Bearings of the Pier C on the US41 Northbound Main Bridge

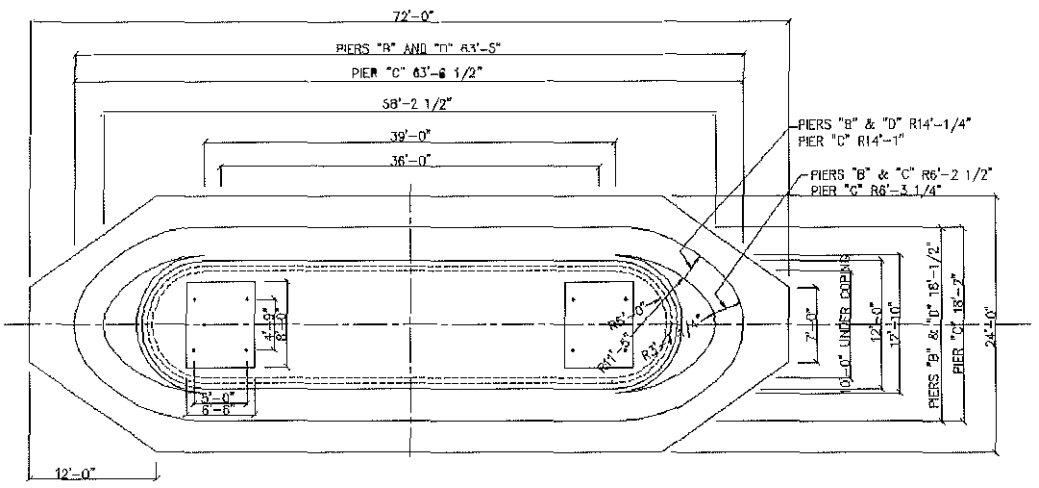

Note: **1. Minimum additional capacity of anchor bolts required = 1065 kips**

2. Alternate retrofit would be to replace the existing bearings with seismic isolation bearings

Figure 5.12 Minimum Required Shear Capacity (V_{req}) to be Provided by Additional Anchor Bolts at Bearings of the Pier D on the US41 Northbound Main Bridge

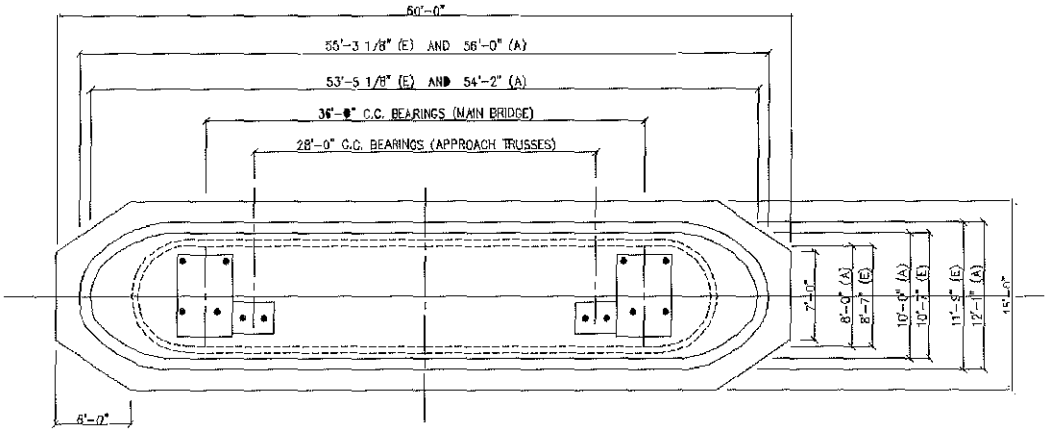

Note: **1. Mini** **mum additional capacity of anchor bolts required = 1860 kips**

2. Alternate retrofit would be to replace the existing bearings with seismic isolation bearings

Figure 5.13 Minimum Required Shear Capacity (V_{req}) to be Provided by Additional Anchor Bolts at Bearings of the Pier E on the US41 Northbound Main Bridge

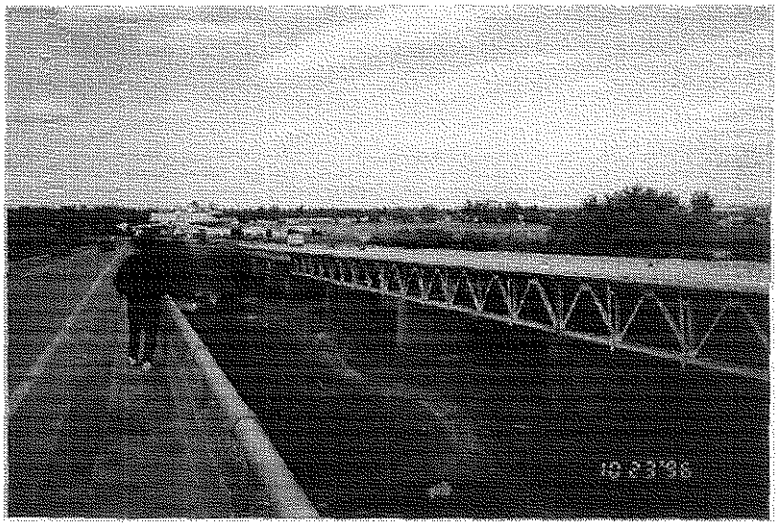

Figure 6.1a Truss Spans in Evansville, IN
Approach Bridge

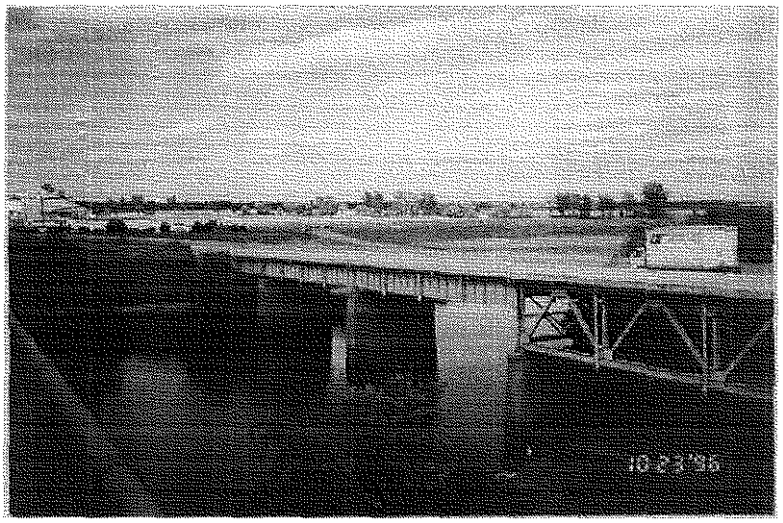

Figure 6.1b Girder Spans in Evansville, IN
Approach Bridge

Figure 6.1c View of Evansville, IN Approach Bridge

Figure 6.1d View of Henderson, KY Approach Bridge

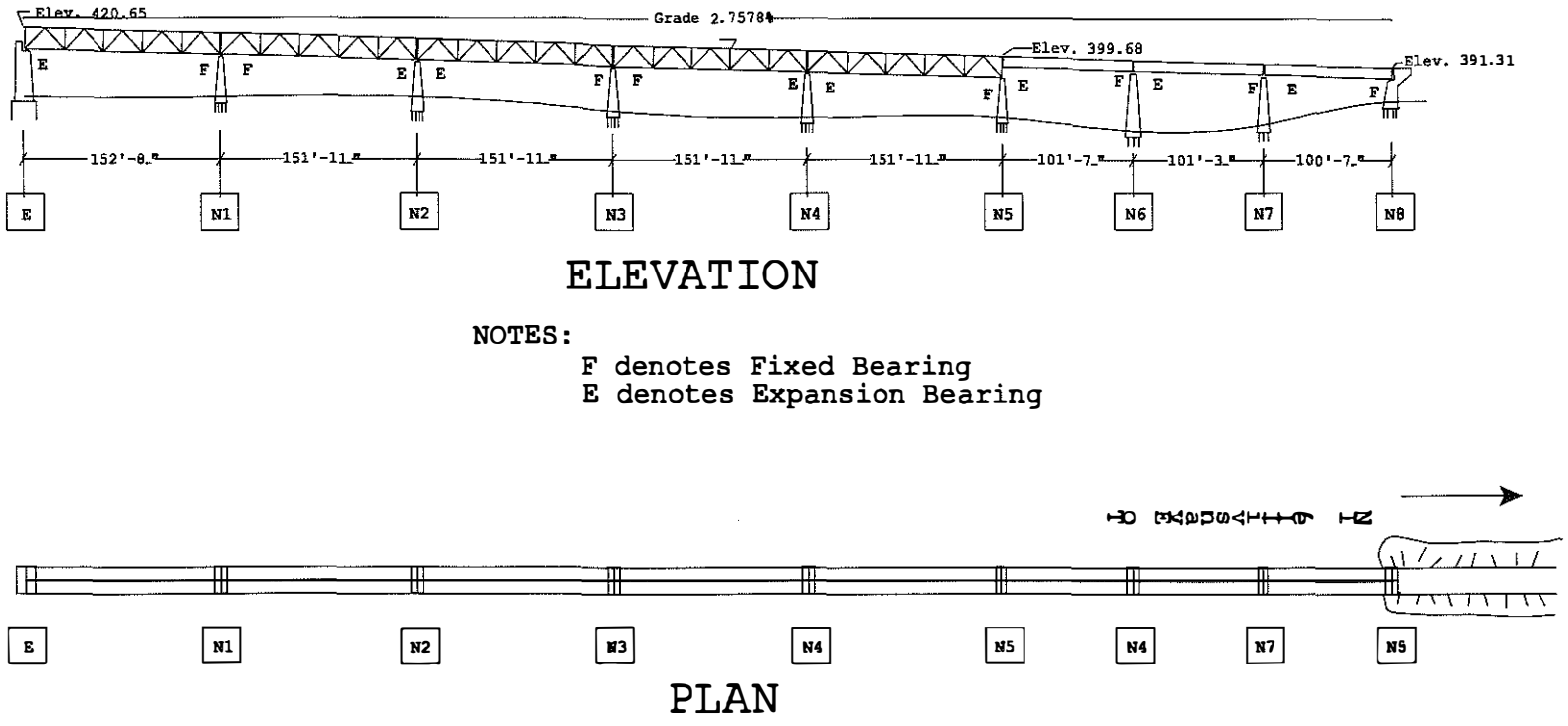

Figure 6.2 Plan and Elevation Views of Evansville, IN Approach on US41 Northbound Bridge

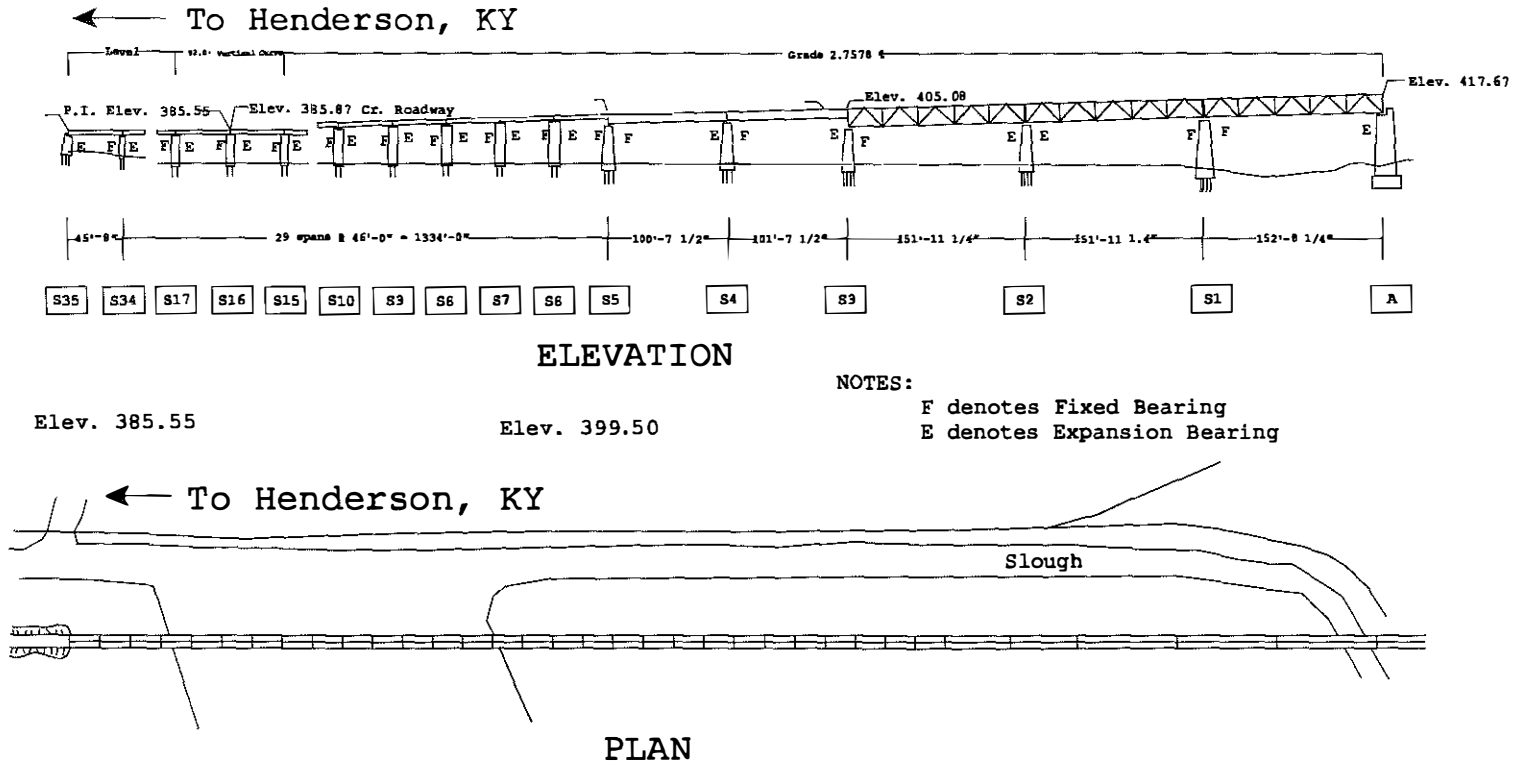

Figure 6.3 Plan and Elevation Views of Henderson, KY Approach on US41 Northbound Bridge

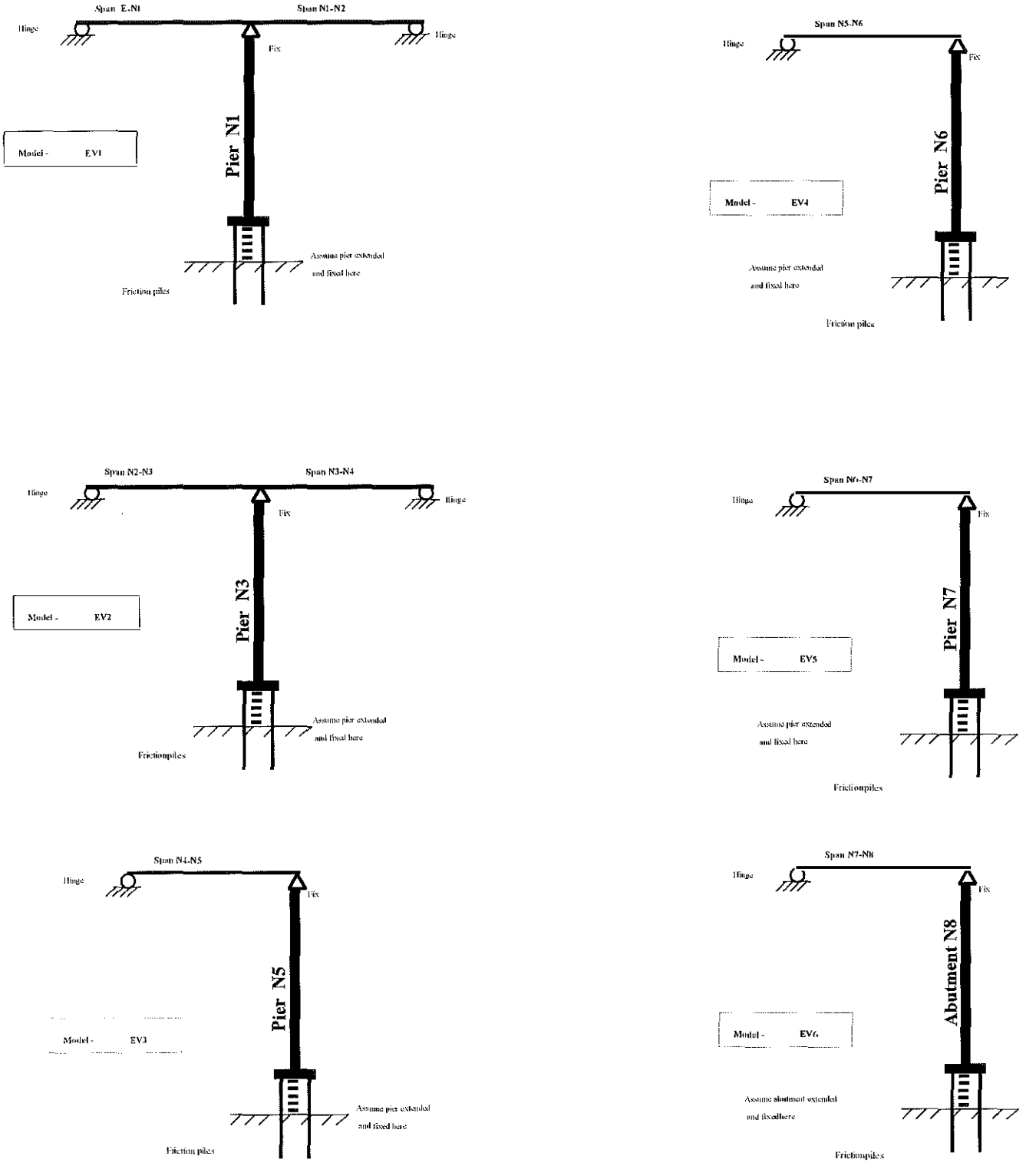

Figure 6.4 Single Degree of Freedom System Models for Evansville, IN Approach

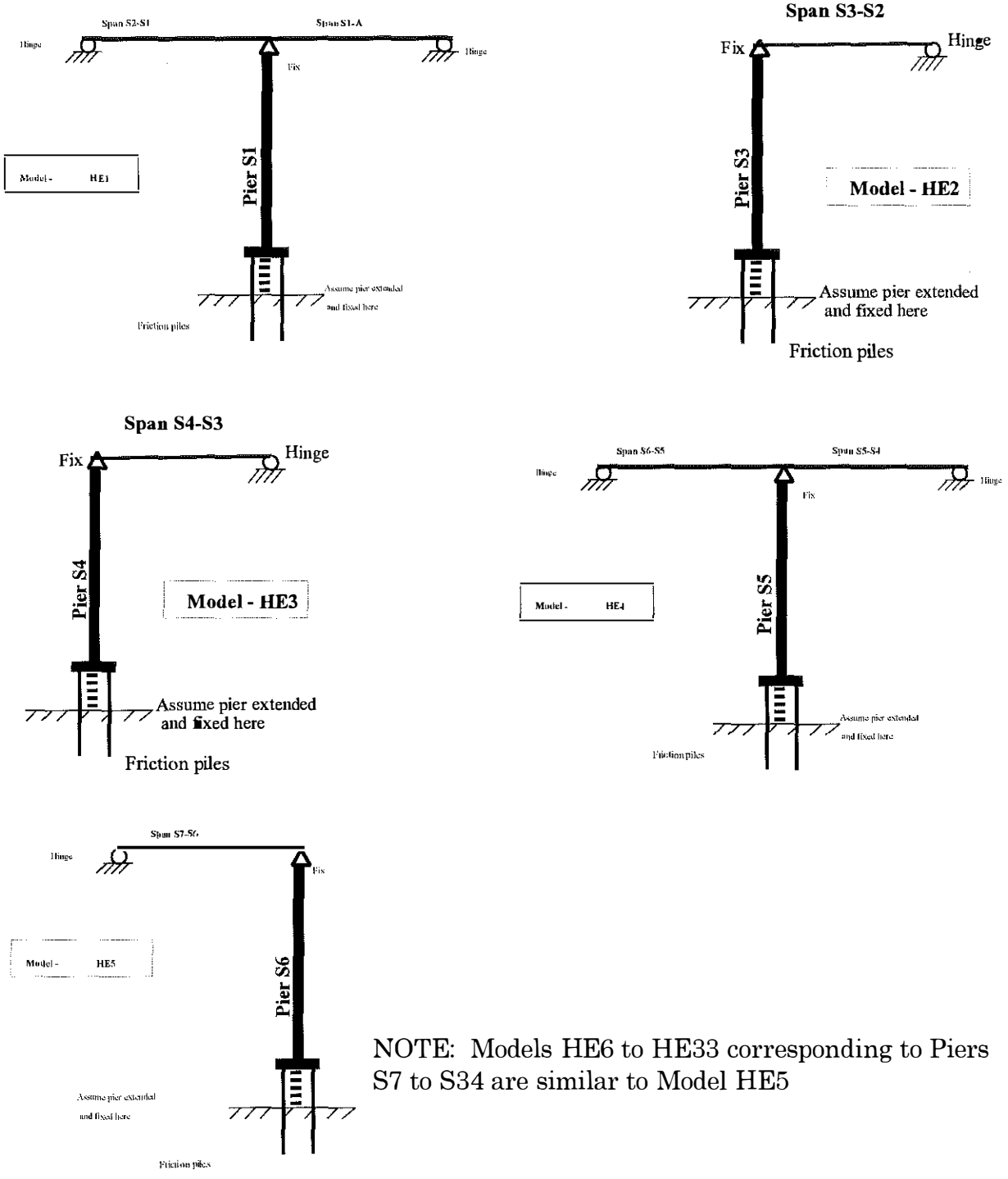

NOTE: Models HE6 to HE33 corresponding to Piers S7 to S34 are similar to Model HE5

Figure 6.5 Single Degree of Freedom System Models for Henderson, KY Approach

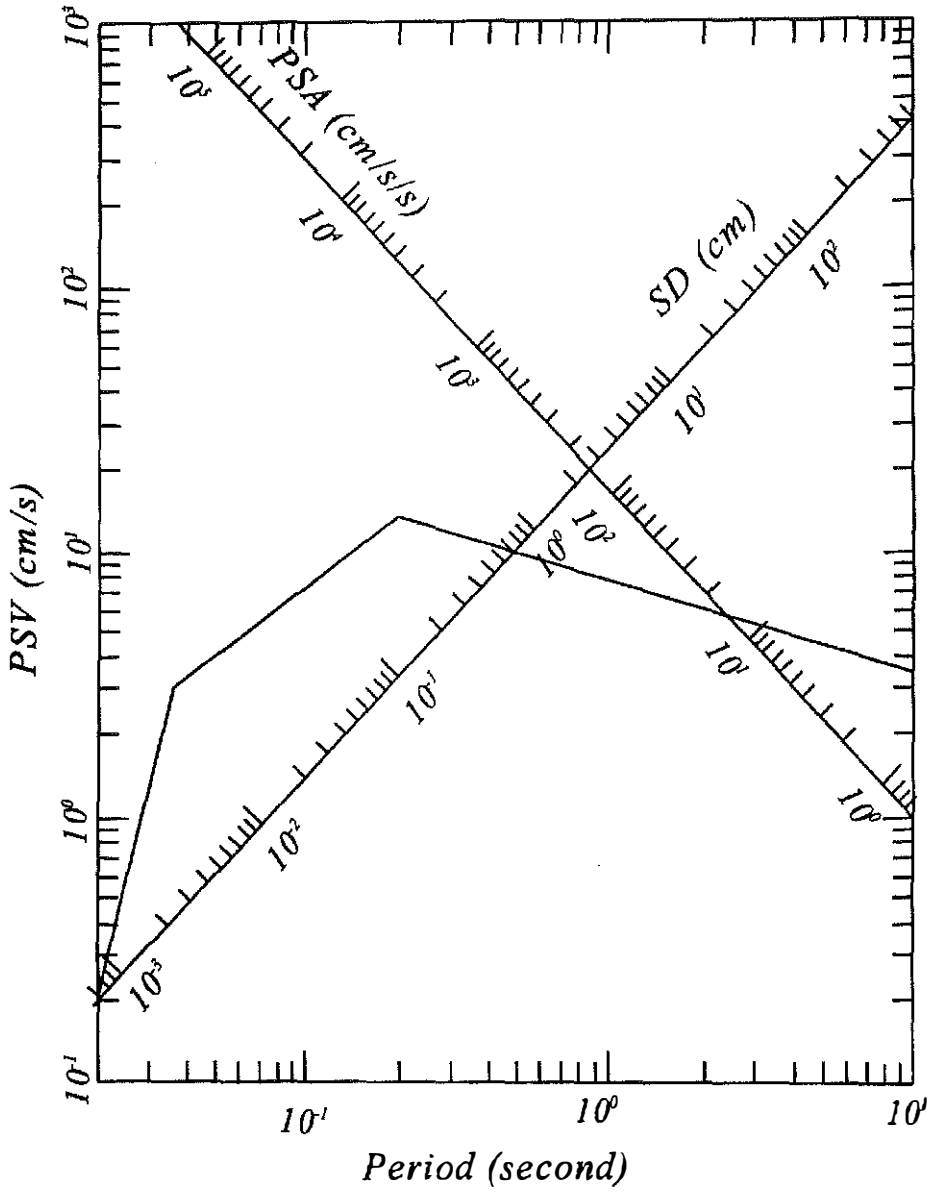

Figure 6.6 Response Spectra for the 50-year Event for Henderson, KY (0.15g-2 from Fig. 5.1); Damping ratio = 0.05

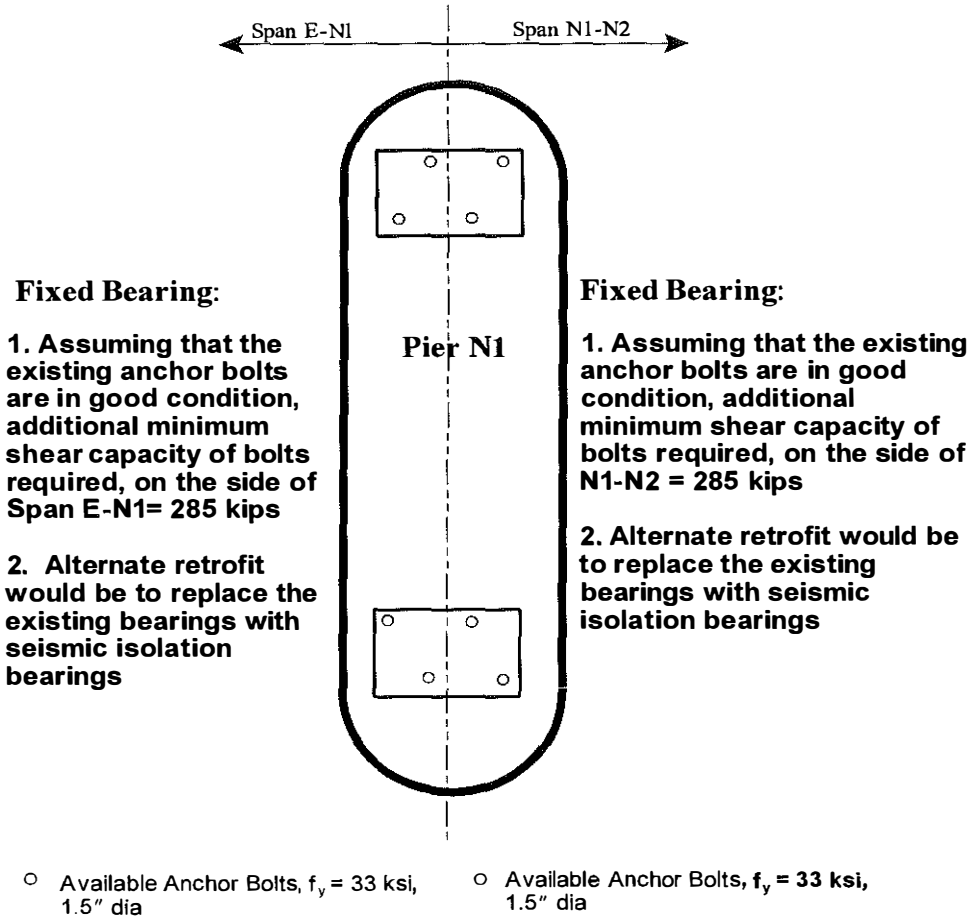

Figure 6.7 Minimum Required Shear Capacity (V_{req}) to be Provided by Additional Anchor Bolts at Bearings of Pier N1 on the Evansville, IN Approach of the US41 Northbound Bridge

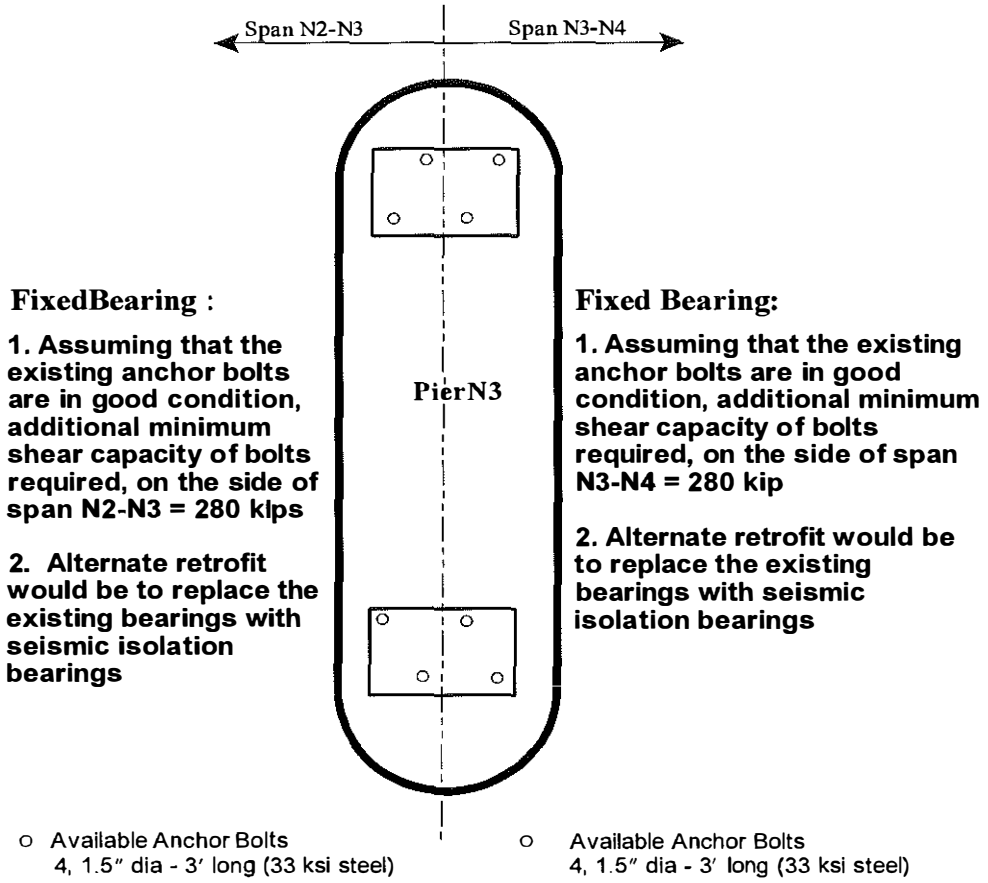

Figure 6.8 Minimum Required Shear Capacity (V_{req}) to be Provided by Additional Anchor Bolts at Bearings of Pier N3 on the Evansville, IN Approach on the US41 Northbound Bridge

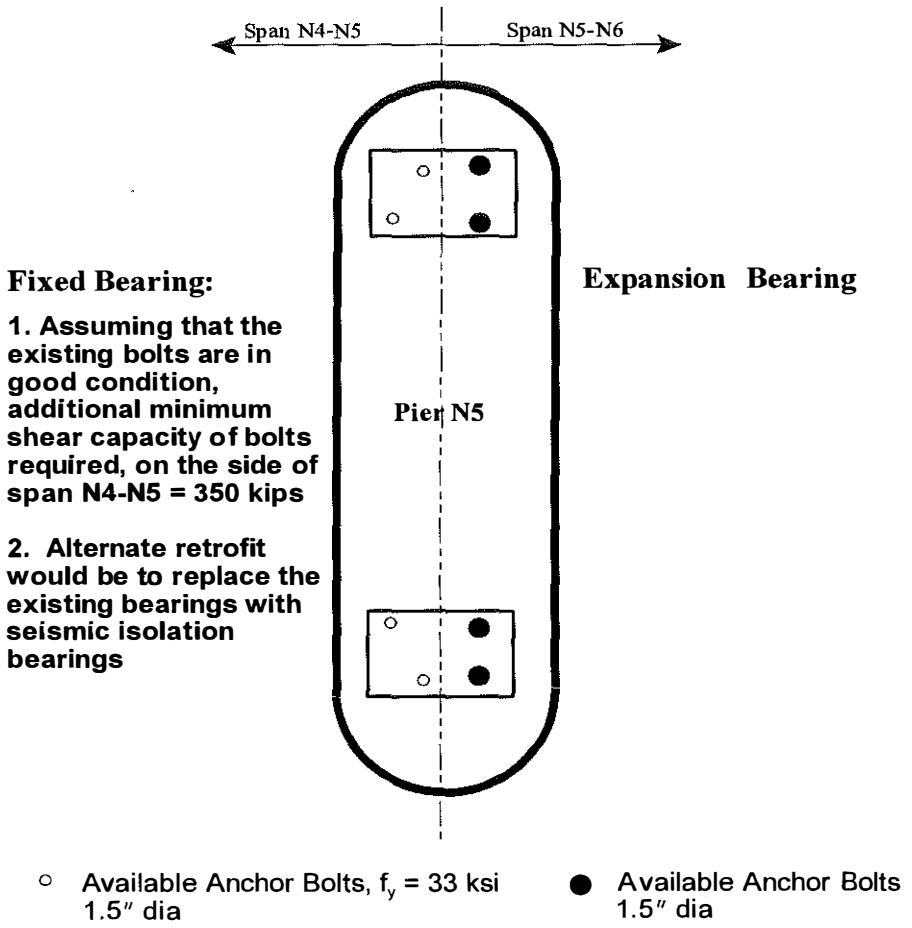

Figure 6.9 Minimum Required Shear Capacity (V_{req}) to be Provided by Additional Anchor Bolts at Bearings of Pier N5 on the Evansville, IN Approach of the US41 Northbound Bridge

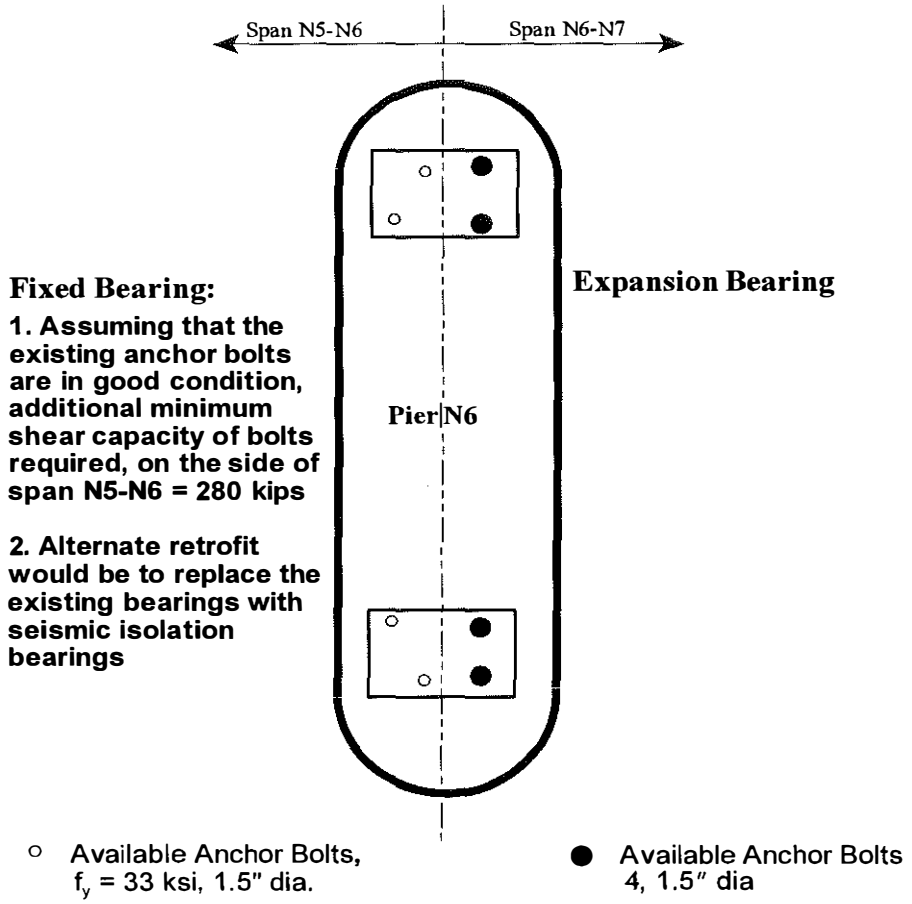

Figure 6.10 Minimum Required Shear Capacity (V_{req}) to be Provided by Additional Anchor Bolts at Bearings of Pier N6 on the Evansville, IN Approach of the US41 Northbound Bridge

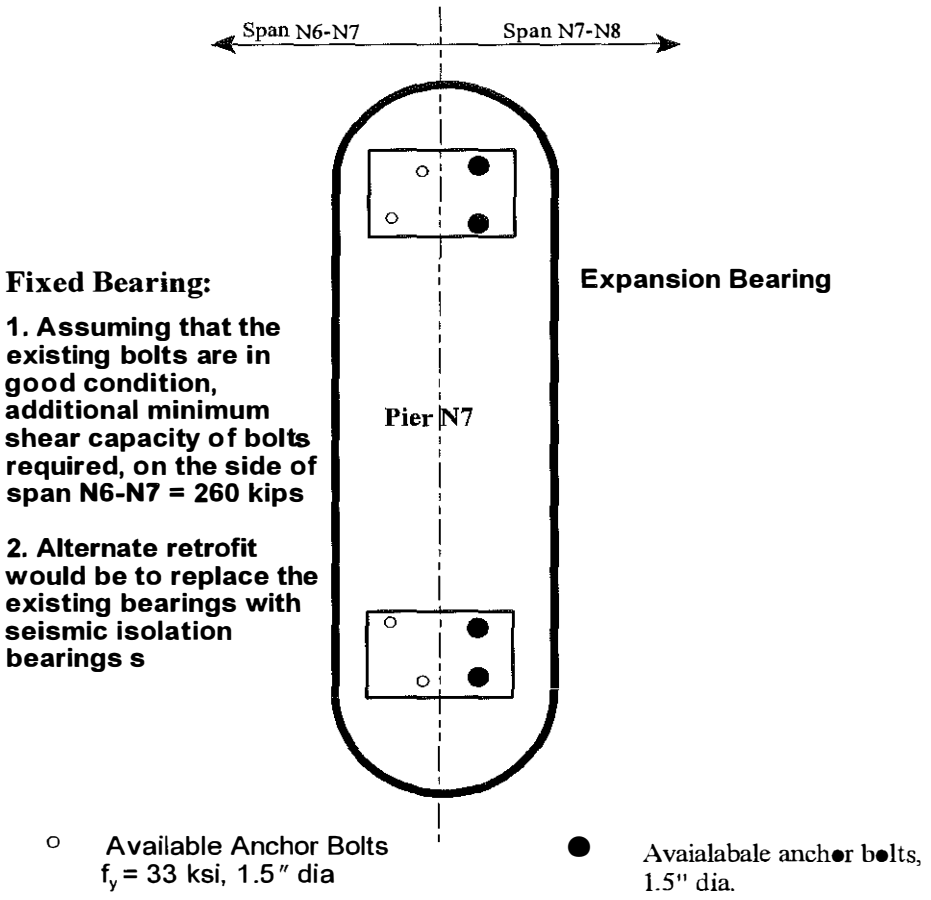

Figure 6.11 Minimum Required Shear Capacity (V_{req}) to be Provided by Additional Anchor Bolts at Bearings of Pier N7 on the Evansville, IN Approach of the US41 Northbound Bridge

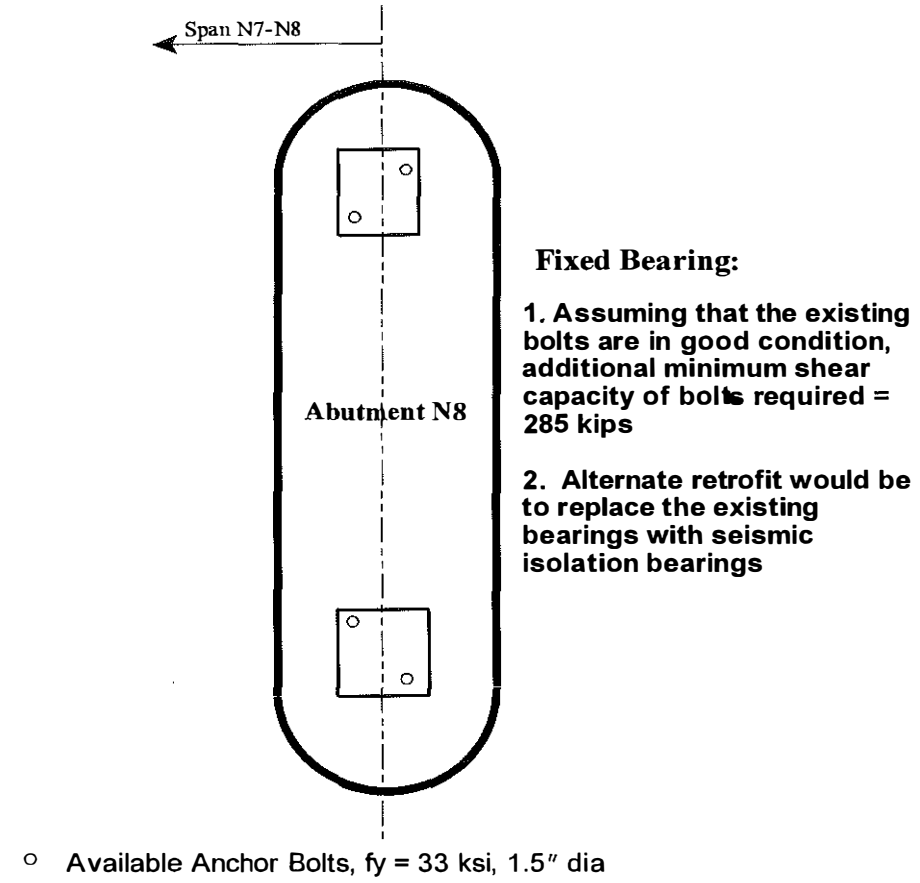

Figure 6.12 Minimum Required Shear Capacity (V_{req}) to be Provided by Additional Anchor Bolts at Bearings of Pier N8 on the Evansville, IN Approach of the US41 Northbound Bridge

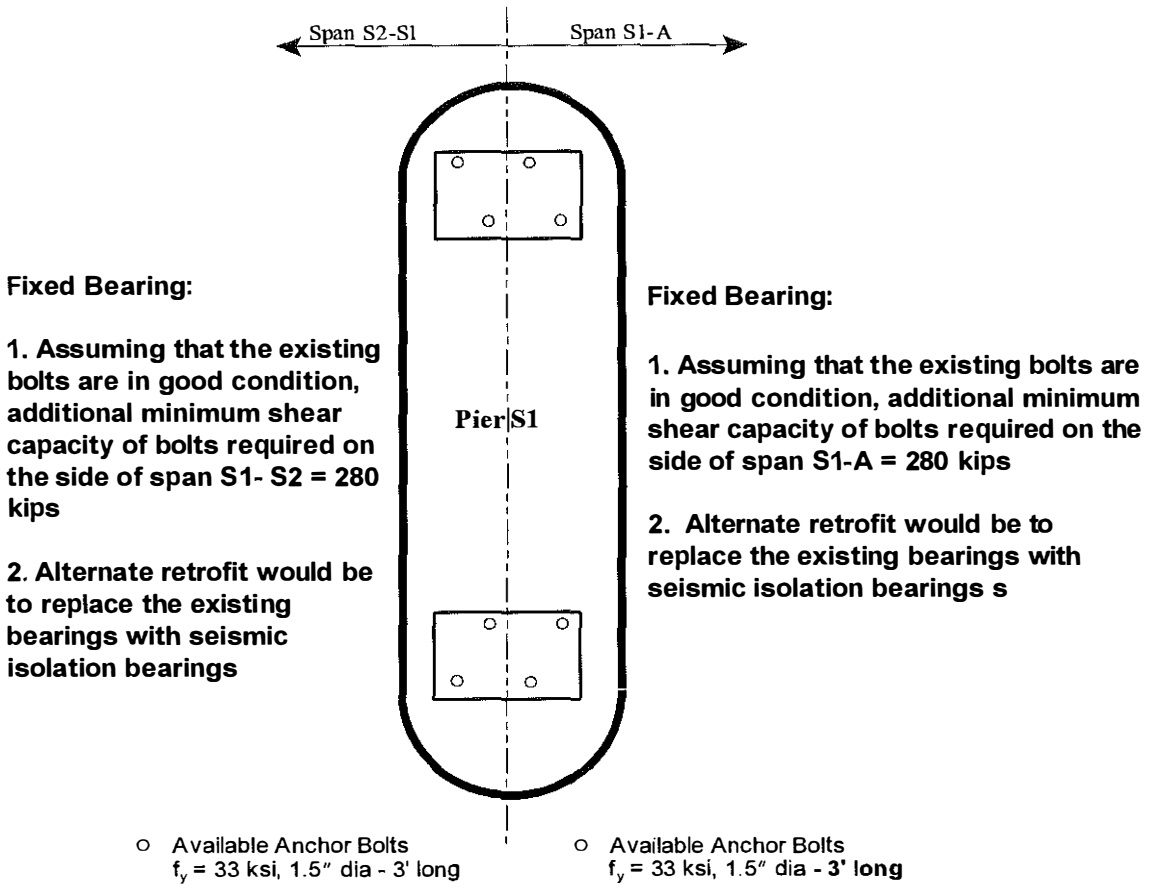

Figure 6.13 Minimum Required Shear Capacity (V_{req}) to be Provided by Additional Anchor Bolts at Bearings of Pier S1 on the Henderson, KY Approach of the US41 Northbound Bridge

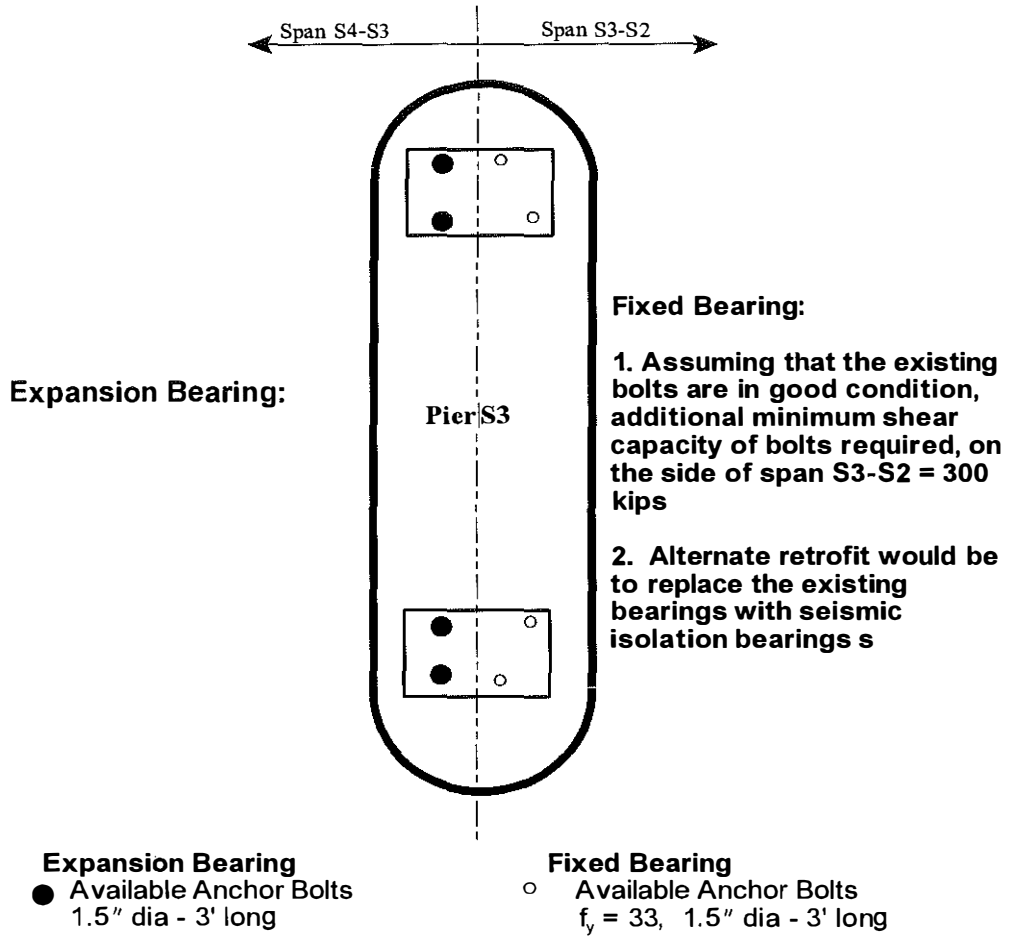

Figure 6.14 Minimum Required Shear Capacity (V_{req}) to be Provided by Additional Anchor Bolts at Bearings of Pier S3 on the Henderson, KY Approach of the US41 Northbound Bridge

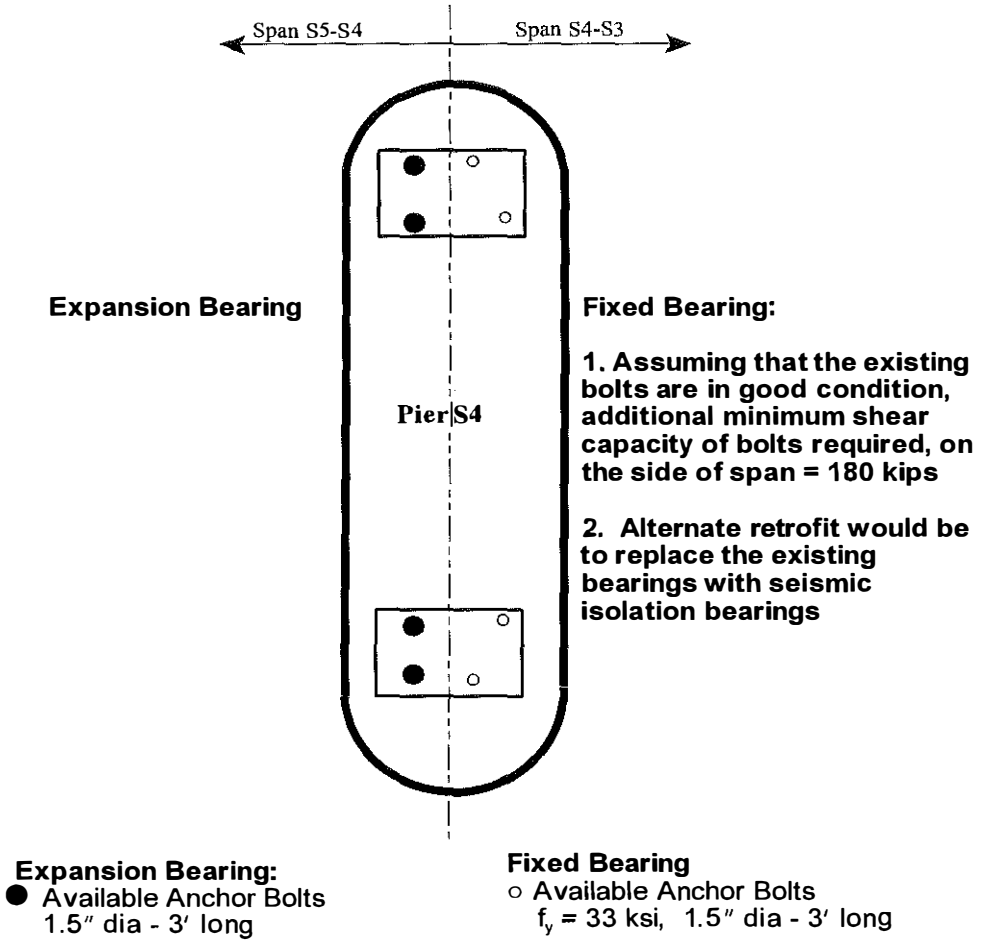

Figure 6.15 Minimum Required Shear Capacity (V_{req}) to be Provided by Additional Anchor Bolts at Bearings of Pier S4 on the Henderson, KY Approach of the US41 Northbound Bridge

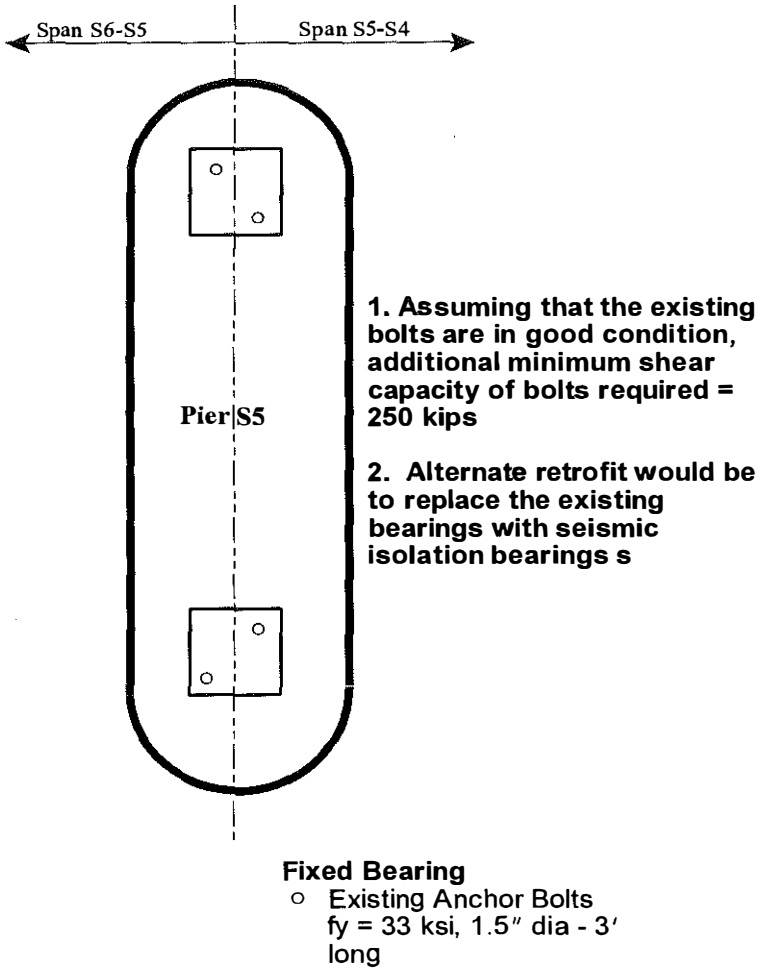

Figure 6.16 Minimum Required Shear Capacity (V_{req}) to be Provided by Additional Anchor Bolts at Bearings of Pier S5 on the Henderson, KY Approach of the US41 Northbound Bridge